Department of Radio Science and Engineering

Electromagnetic Characterization of Metasurfaces

Mohammad Albooyeh

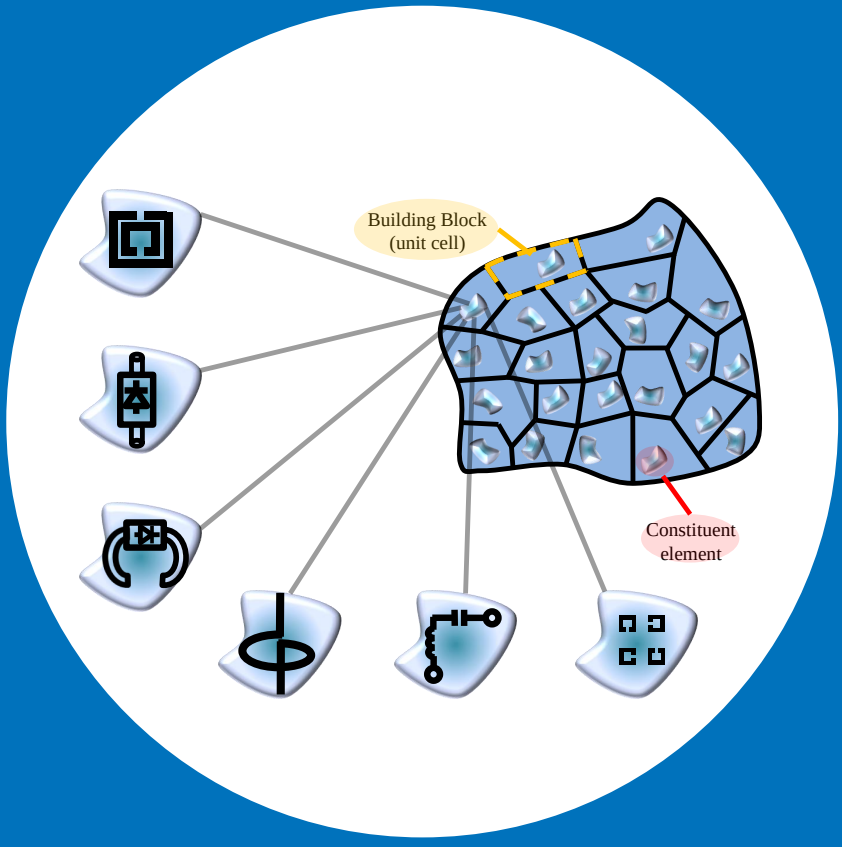

Aalto University

DOCTORAL
DISSERTATIONS

Aalto University publication series
DOCTORAL DISSERTATIONS 70/2015

Electromagnetic Characterization of Metasurfaces

Mohammad Albooyeh

A doctoral dissertation completed for the degree of Doctor of Science (Technology) to be defended, with the permission of the Aalto University School of Electrical Engineering, at a public examination held at the lecture hall S1 of the school on 1 June 2015 at 13:00.

Aalto University
School of Electrical Engineering
Department of Radio Science and Engineering
Theoretical and Applied Electromagnetics of Complex Media

Supervising professor
Constantin Simovski

Preliminary examiners
Prof. Andrei Lavrinenko, Technical University of Denmark, Lyngby, Denmark
Prof. George Goussetis, Heriot-Watt University, Scotland, United Kingdom

Opponent
Prof. Mario Silveirinha, University of Coimbra, Portugal

Aalto University publication series
DOCTORAL DISSERTATIONS 70/2015

ISBN 978-952-60-6210-5 (printed)
ISBN 978-952-60-6209-9 (pdf)
ISSN-L 1799-4934
ISSN 1799-4934 (printed)
ISSN 1799-4942 (pdf)
http://urn.fi/URN:ISBN:978-952-60-6209-9

Unigrafia Oy
Helsinki 2015

Finland

Publication orders (printed book):
Otakaari 5, School of Electrical Engineering, Department of Radio Science and Engineering

441 697
Printed matter

Aalto University

Abstract

Aalto University, P.O. Box 11000, FI-00076 Aalto www.aalto.fi

Author
Mohammad Albooyeh

Name of the doctoral dissertation
Electromagnetic Characterization of Metasurfaces

Publisher School of Electrical Engineering

Unit Department of Radio Science and Engineering

Series Aalto University publication series DOCTORAL DISSERTATIONS 70/2015

Field of research Theoretical and Applied Electromagnetics of Complex Media

Manuscript submitted 5 March 2015 **Date of the defence** 1 June 2015

Permission to publish granted (date) 26 March 2015 **Language** English

☐ **Monograph** ☒ **Article dissertation (summary + original articles)**

Abstract

Electromagnetic characterization of metasurfaces (MSs), electrically/optically thin sheet metamaterials (MMs), is the subject of the current study. Briefly, a MM is a composite material with unusual electromagnetic properties offered by specific response of its constituents and their arrangement. The main goal in this work is to attribute some macroscopic characteristic parameters to MSs.

We first discuss the definitions and present a brief review of the electromagnetic characterization of MMs and MSs. We explain the failures of the traditional characterization approach when applied to MSs. We discuss two known approaches especially suggested for the characterization of MSs in 1990s-2000s.

We continue to introduce a heuristic homogenization model of MSs located on a dielectric interface. Indeed, we derive the general boundary conditions invariant on the polarization of the excitation field. Then, we present the most general algorithm to retrieve the characteristic macroscopic parameters through two-dimensional reflection and transmission dyadics.

We next present two explicit examples of MSs in order to prove the applicability of our theory. The first one is a periodic array of plasmonic nano-spheres while the second one is an array of coupled plasmonic nano-patches positioned in a disordered fashion on a flat surface. We show that our approach works for for both random and periodic MSs. Indeed, the restriction of our theory is a sufficiently small electrical/optical size of a unit cell (area per one particle).

We finally present the main results of the thesis through functional MSs. We theoretically reveal and discuss novel physical effects and various functionalities. We present some discussions on the intrinsically bianisotropic and intrinsically magnetic MSs operating in the visible range. We also discuss the microscopic effect of *substrate-induced* bianisotropy for a substrated array of plasmonic nano-spheres. Moreover, we reveal the magnetic response within the framework of our homogenization model; i.e., retrieving some magnetic parameters. Furthermore, we obtain the perfect absorbance conditions for different topologies and discuss them in this chapter. Finally, we present a model which explains the different behavior of electric and magnetic resonant modes of MSs in transition from periodic to amorphous arrangements.

Keywords metamaterials, metasurfaces, electromagnetic characterization, amorphous arrays, substrate-induced bianisotropy

ISBN (printed) 978-952-60-6210-5 **ISBN (pdf)** 978-952-60-6209-9

ISSN-L 1799-4934 **ISSN (printed)** 1799-4934 **ISSN (pdf)** 1799-4942

Location of publisher Helsinki **Location of printing** Helsinki **Year** 2015

Pages 170 **urn** http://urn.fi/URN:ISBN:978-952-60-6209-9

Preface

The present work is carried out in the Department of Radio Science and Engineering at Aalto University, School of Electrical Engineering.

First of all, I wish to express my sincere thanks to my supervisor and friend, Prof. Constantin Simovski, for providing me with all the necessary tools for the research. You were not only a supervisor but also a kind friend whose helps cannot be mentioned by only thankful words. I would also like to thank Prof. Sergei Tretyakov, for his scientific supports and especially for his constructive and invaluable comments he made on my dissertation. I could never distinguish between Constantin and you, since you always have also been like a generous supervisor for me.

Next, I take this opportunity to express my gratitude to all of the group members from the beginning of my career in our group: Dr. Igor Nefedov, Dr. Pekka Alitalo, Dr, Vladimir Podlozny, Dr. Antti Karilainen, Dr. Dmitri Morits, Mr. Joni Vehmas, Mr. Younes Radi, Mr. Victor Asadchy, Mr. Mohammad S. Mirmoosa, Mr. Mikhail Omelyanovich, and Mr. Sergei Kosulnikov. I always remember all unforgettable moments we spent together during our weekly seminars and daily coffee breaks.

I would also like to thank my collaborators and friends in Jena and Canberra: Prof. Carsten Rockstuhl, Prof. Yuri Kivshar, Dr. Cristoph Menzel, Mr. Sergey kruk, and Mr. Rasoul Alaee. I received many lessons from you during our joint works, particularly in the academic writing. I would like to specially thank my friend, Rasoul, for our scientific discussions which were not fruitful without you.

My dearest friends: Ghazaleh, Arsham, Javad, Ali N., Vahid, Sara,

Maral, Nima, Ali A., and Pegah. Thank you for being with me during these wonderful years. I greatly enjoyed being with you, abundantly learned from you, and unlimitedly spent a lot of money with you. ◡̈

My dearest friends: Mohammad S. Mahani, Mojtaba Shobeiri, Hamed Modaghegh, Majid Nosoohi, Morteza Shahpari, and Majid Daryabak. I will never forget the moments we spent together: all hard, joyful, and unforgettable times we shared. Live long and stay friend with me.

There are also much more friends which I should thank. However, there is not enough space for all to put their names. I would like to thank you all for spending such pleasant moments during my doctoral studies together.

My parents and their unconditional love have spiritually helped me during my life so far. They have always been trying to make an independent person out of me. Their presence have always been like a sun behind the clouds for me: Although I do not see them directly, I cannot live without them. I gratefully and sincerely thank them for their always supportive presence.

The last but not least is my wife and also my closest friend whose presence is the air I breathe. I would like to thank you, Ghazaleh, for being unconditionally supportive and patient during my studies. I would like to say, I just love you!

Espoo, May 7, 2015,

Mohammad Albooyeh

Contents

List of Publications

This thesis consists of an overview and of the following publications which are referred to in the text by their Roman numerals.

I M. Albooyeh, D. Morits, C.R. Simovski. Electromagnetic characterization of substrated metasurfaces. *Metamaterials*, 5, issue, 178-205, August 2011.

II M. Albooyeh and C. R. Simovski. Substrate-induced bianisotropy in plasmonic grids. *Journal of Optics*, 13, issue, 105102 (1-10), September 2011.

III M. Albooyeh, D. Morits, and S. A. Tretyakov. Effective electric and magnetic properties of metasurfaces in transition from crystalline to amorphous state. *Physical Review B*, 85, issue, 205110 (1-7), May 2012.

IV M. Albooyeh and C. R. Simovski. Huge local field enhancement in perfect plasmonic absorbers. *Optics Express*, 20, 20, 21888-21895, September 2012.

V M. Albooyeh, Y. Ra'di, M. Q. Adil, and C. R. Simovski. Revised transmission line model for electromagnetic characterization of metasurfaces. *Physical Review B*, 88, issue, 085435 (1-6), August 2013.

VI M. Albooyeh, C. Menzel, C. Helgert, M. Kroll, A. Krysinski, M. Decker, S. Kruk, D. N. Neshev, Y. S. Kivshar, T. Pertsch, C. Etrich, C. Rockstuhl, and C. R. Simovski. Electromagnetic response of resonant metasurfaces

at the oblique incidence: From periodic to amorphous structures. *Scientific Reports*, 4, issue, 4484 (1-7), March 2014.

Author's Contribution

Publication I: "Electromagnetic characterization of substrated metasurfaces"

The author has derived formulas for the reflection and transmission coefficients in the TE-case starting from the boundary conditions which he had obtained. The author also revised already derived formulas for the TM-case by C. Simovski as well. The author did most of the simulations while some simulations was done by D. Morits. The author has obtained analytical formulas for the effective susceptibilities at the presence of a substrate as a function of the reflection and transmission coefficients. The introduction, history, and formulation parts were written by C. Simovski while the other parts were mainly written by the author.

Publication II: "Substrate-induced bianisotropy in plasmonic grids"

The author has recalculated the reflection and transmission coefficients from the theory introduced by Yamaguchi *et al*. He has proven that the Yamaguchi's model is inadequate in the case of resonant plasmonic absorbers. The author has also revealed a bianisotropy effect which is induced by the presence of the substrate. The author has used the results of the extracted formulas from the previous paper to achieve the results in this paper. The author has also proven the energy conservation for the normally incident illumination of an array located on top of a substrate. This paper has been thoroughly revised by the author.

Publication III: "Effective electric and magnetic properties of metasurfaces in transition from crystalline to amorphous state"

The author has derived all formulas and has made required simulations. Some discussions and simulations has been done by D. Morits to improve the quality of the paper. The introduction has been mainly written by S. Tretyakov while a part of it was written by D. Morits. The main body of the paper has been written by the author.

Publication IV: "Huge local field enhancement in perfect plasmonic absorbers"

The derivations of all formulas, simulations and writing of the paper was mainly done by the author.

Publication V: "Revised transmission line model for electromagnetic characterization of metasurfaces"

The author has derived all formulas presented in the paper while Y. Ra'di also derived similar formulas to the author's in a different way and the results were in perfect match. The simulations and writing of the paper draft were also done by the author.

Publication VI: "Electromagnetic response of resonant metasurfaces at the oblique incidence: From periodic to amorphous structures"

The author was responsible for writing the paper and derivation of formulas. C. Helgert and S. Kruk did the measurements while C. Menzel and T. Pertsch did numerical simulations of the work. Other authors were either partly contributing in the revision of the paper text and/or in the measurements.

List of Abbreviations

Au	gold
GSTC	generalized sheet transition condition
HK	Holloway-Kuester approach
MgO	Magnesium Oxide
MM	metamaterial
MS	metasurface
SRR	split-ring resonator
ST	Simovski-Tretyakov approach
TE	transverse electric
TM	transverse magnetic

List of Symbols

A	absorption
a	unit cell period [m]
D	sphere diameter [m]
d	metasurface thickness [m]
dv	volume element [m^3]
$\mathbf{E}$	electric field [Vm^{-1}]
$\mathbf{E}^{ave}$	average electric field [Vm^{-1}]
$\mathbf{E}^{i}$	incident electric field [Vm^{-1}]
$\mathbf{E}^{loc}$	local electric field [Vm^{-1}]
E_n	normal component of the electric field [Vm^{-1}]
$\mathbf{E}_t$	transversal component of the electric field [Vm^{-1}]
E_n^i	normal component of the incident electric field [Vm^{-1}]
$\mathbf{E}_t^i$	transversal component of the incident electric field [Vm^{-1}]
E_n^r	normal component of the reflected electric field [Vm^{-1}]
$\mathbf{E}_t^r$	transversal component of the reflected electric field [Vm^{-1}]
E_n^t	normal component of the transmitted electric field [Vm^{-1}]
$\mathbf{E}_t^t$	transversal component of the transmitted electric field [Vm^{-1}]
f_{e}	electric mode resonance frequency [s^{-1}]
f_{m}	magnetic mode resonance frequency [s^{-1}]
$f(.)$	function
g	gap [m]
$g(.)$	function
$\mathbf{H}$	magnetic field [Am^{-1}]
$\mathbf{H}^{ave}$	average magnetic field [Am^{-1}]
$\mathbf{H}^{i}$	incident magnetic field [Am^{-1}]
$\mathbf{H}^{loc}$	local magnetic field [Am^{-1}]
H_n	normal component of the magnetic field [Am^{-1}]
$\mathbf{H}_t$	transversal component of the magnetic field [Am^{-1}]
H_n^i	normal component of the incident magnetic field [Am^{-1}]

$\mathbf{H}_t^i$	transversal component of the incident magnetic field [Am^{-1}]
H_n^r	normal component of the reflected magnetic field [Am^{-1}]
$\mathbf{H}_t^r$	transversal component of the reflected magnetic field [Am^{-1}]
H_n^t	normal component of the transmitted magnetic field [Am^{-1}]
$\mathbf{H}_t^t$	transversal component of the transmitted magnetic field [Am^{-1}]
$h(.)$	function
$h^{-1}(.)$	inverse function
$\bar{\bar{I}}$	three-dimensional unit dyadic
$\bar{\bar{I}}_t$	two-dimensional unit dyadic
i	imaginary unit
$\mathbf{J_e}$	electric polarization current [Am^{-1}]
$\mathbf{J_m}$	magnetic polarization current [Vm^{-1}]
$\mathbf{J}(\mathbf{r})$	induced current density [Am^{-2}]
j	imaginary unit
k	wave number [m^{-1}]
k_n	propagation constant of eigenwaves in the normal direction [m^{-1}]
$\mathbf{k}_t$	tangential wave vector[m^{-1}]
k_t	tangential wave number [m^{-1}]
L	length [m]
L_{patch}	patch length [m]
L_{SRR}	split-ring length [m]
$\mathbf{M}$	magnetic bulk polarization [$\mathrm{Vm}^{-2}\mathrm{s}$]
$\bar{\mathcal{M}}$	magnetic surface polarization [$\mathrm{Vm}^{-1}\mathrm{s}$]
M_n	normal component of the electric bulk polarization [$\mathrm{Vm}^{-2}\mathrm{s}$]
$\mathcal{M}_n$	normal component of the electric surface polarization [$\mathrm{Vm}^{-1}\mathrm{s}$]
$\mathbf{M}_t$	transversal component of the electric bulk polarization [$\mathrm{Vm}^{-2}\mathrm{s}$]
$\mathcal{M}_t$	transversal component of the electric surface polarization [$\mathrm{Vm}^{-1}\mathrm{s}$]
$\mathbf{m}$	magnetic dipole moment [Vms]
$\bar{\mathbf{n}}$	normal vector to the metasurface
n	refractive index
$\mathbf{P}$	electric bulk polarization [$\mathrm{Am}^{-2}\mathrm{s}$]
$\bar{\mathcal{P}}$	electric surface polarization [$\mathrm{Am}^{-1}\mathrm{s}$]
P_n	normal component of the electric bulk polarization [$\mathrm{Am}^{-2}\mathrm{s}$]
$\mathcal{P}_n$	normal component of the electric surface polarization [$\mathrm{Am}^{-1}\mathrm{s}$]
$\mathbf{P}_t$	transversal component of the electric bulk polarization [$\mathrm{Am}^{-2}\mathrm{m}$]
$\mathcal{P}_t$	transversal component of the electric surface polarization [$\mathrm{Am}^{-1}\mathrm{m}$]
$\mathbf{p}$	electric dipole moment [Ams]
$\mathbf{r}$	position vector [m]

r_{e}	partial reflection coefficient created by induced electric current
r_{m}	partial reflection coefficient created by induced magnetic current
r_n	disorder parameter
r_0	reflection coefficient at normal incidence
$\bar{\bar{r}}$	reflection dyadic
r_θ	reflection coefficient at $\theta_i = \theta$
r_+	reflection coefficient for forward illumination direction
r_-	reflection coefficient for backward illumination direction
t	patch or split-ring thickness [m]
t_0	transmission coefficient at normal incidence
$\bar{\bar{t}}$	transmission dyadic
t_θ	transmission coefficient at $\theta_i = \theta$
t_+	transmission coefficient for forward illumination direction
t_-	transmission coefficient for backward illumination direction
V	unit cell volume [m^3]
W	patch width [m]
W_1	patch width [m]
W_2	patch width [m]
$\overline{\overline{Z}}$	dyadic characteristic impedance [Ω]
Z^{TE}	characteristic impedance of the transverse electric mode [Ω]
Z^{TM}	characteristic impedance of the transverse magnetic mode [Ω]
$\bar{\bar{\alpha}}^{\mathrm{ee}}$	individual electric polarizability tensor [AsV^{-1}]
$\hat{\bar{\bar{\alpha}}}^{\mathrm{ee}}$	effective (collective) electric polarizability tensor [AsV^{-1}]
$\bar{\bar{\alpha}}^{\mathrm{em}}$	individual electro-magnetic polarizability tensor [s]
$\hat{\bar{\bar{\alpha}}}^{\mathrm{em}}$	effective (collective) electro-magnetic polarizability tensor [s]
$\bar{\bar{\alpha}}^{\mathrm{me}}$	individual magneto-electric polarizability tensor [s]
$\hat{\bar{\bar{\alpha}}}^{\mathrm{me}}$	effective (collective) magneto-electric polarizability tensor [s]
$\bar{\bar{\alpha}}^{\mathrm{mm}}$	individual magnetic polarizability tensor [$\mathrm{A}^{-1}\mathrm{sV}$]
$\hat{\bar{\bar{\alpha}}}^{\mathrm{mm}}$	effective (collective) magnetic polarizability tensor [$\mathrm{A}^{-1}\mathrm{sV}$]
$\hat{\bar{\alpha}}_{nn}$	normal component of the effective (collective) polarizability tensor
$\hat{\bar{\alpha}}_{nt}$	effective (collective) polarizability vector
$\hat{\bar{\alpha}}_{tn}$	effective (collective) polarizability vector
$\hat{\bar{\bar{\alpha}}}_{tt}$	two-dimensional tangential effective (collective) polarizability dyadic
β	interaction constant
β_{amorph}	interaction constant for amorphous arrays
β^{ee}	electric interaction constant
β^{mm}	magnetic interaction constant
$\beta_{\mathrm{periodic}}$	interaction constant for periodic arrays

Γ_{e}	dissipation loss corresponding to the electric mode [s^{-1}]
Γ_{m}	dissipation loss corresponding to the magnetic mode [s^{-1}]
$\Delta\omega_{\mathrm{e\ amorph}}$	electric resonant curve width for amorphous arrays [s^{-1}]
$\Delta\omega_{\mathrm{e\ periodic}}$	electric resonant curve width for periodic arrays [s^{-1}]
$\Delta\omega_{\mathrm{m\ amorph}}$	magnetic resonant curve width for amorphous arrays [s^{-1}]
$\Delta\omega_{\mathrm{m\ periodic}}$	magnetic resonant curve width for periodic arrays [s^{-1}]
ϵ	permittivity [$\mathrm{Asm}^{-1}\mathrm{V}^{-1}$]
ϵ_r	substrate relative permittivity
η	characteristic impedance [Ω]
θ	incident angle [radian]
θ_i	incident angle [radian]
λ	wavelength [m]
λ_0	free space wavelength [m]
μ	permeability [$\mathrm{A}^{-1}\mathrm{m}^{-1}\mathrm{sV}$]
$\rho(\mathbf{r})$	induced charge density [CC^{-3}]
$\hat{\bar{\bar{\chi}}}_{\mathrm{asym}}$	antisymmetric part of effective susceptibility dyadic
$\hat{\bar{\bar{\chi}}}_{\mathrm{sym}}$	symmetric part of effective susceptibility dyadic
$\bar{\bar{\chi}}^{\mathrm{ee}}$	individual electric susceptibility tensor [AsV^{-1}]
$\hat{\bar{\bar{\chi}}}^{\mathrm{ee}}$	effective electric susceptibility tensor [AsV^{-1}]
$\bar{\bar{\chi}}^{\mathrm{em}}$	individual electro-magnetic susceptibility tensor [s]
$\hat{\bar{\bar{\chi}}}^{\mathrm{em}}$	effective electro-magnetic susceptibility tensor [s]
$\bar{\bar{\chi}}^{\mathrm{me}}$	individual magneto-electric susceptibility tensor [s]
$\hat{\bar{\bar{\chi}}}^{\mathrm{me}}$	effective magneto-electric susceptibility tensor [s]
$\bar{\bar{\chi}}^{\mathrm{mm}}$	individual magnetic susceptibility tensor [$\mathrm{A}^{-1}\mathrm{sV}$]
$\hat{\bar{\bar{\chi}}}^{\mathrm{mm}}$	effective magnetic susceptibility tensor [$\mathrm{A}^{-1}\mathrm{sV}$]
$\omega_{0\mathrm{e}}$	angular resonant frequency for the electric mode [s^{-1}]
$\omega_{0\mathrm{m}}$	angular resonant frequency for the magnetic mode [s^{-1}]
$\tilde{\omega}_0$	resonant frequency shift due to the interactions [s^{-1}]
∇	nabla operator [m^{-1}]
∇_t	transversal component of the nabla operator [m^{-1}]
$\frac{\partial}{\partial z}$	normal component of the nabla operator [m^{-1}]

1. Introduction

Characterization, when applied in the materials science implies the use of external techniques to probe into the internal structure and properties of a material (see e.g. in [1]). Electromagnetic characterization of metamaterials (MMs) has been the focus of many studies since the origination of MMs in 2000-2001 in works [2, 3]. In the current study, by electromagnetic characterization of any material including a MM, we mean finding some macroscopic parameters that can be used to predict the response of a material sample (e.g. a layer) to the electromagnetic waves. The definition of MMs is discussed below. However, we can briefly define a MM as a composite material with unusual electromagnetic properties offered by specific response of its constituents and their arrangement (see e.g. in [4, 5, 6, 7]). Though the MM literature body has been growing since 2000, recently, the priority on the bulk MMs' studies started to be shifted to their optically thin counterparts called metasurfaces (MSs), reviewed e.g. in [8, 9]. MSs as well as bulk MMs, in the fields of plane electromagnetic waves, behave as effectively homogeneous structures. Therefore, it is reasonable to perform the characterization of an optically dense MS within the framework of a homogenization model; that is, a model describing the electromagnetic response of a MS in a condensed form. Indeed, we should be able to assign some macroscopic parameters to the MS in order to predict its behavior in response to an external electromagnetic wave.

These parameters, firstly, must be measurable experimentally or calculable numerically/analytically using available methods. Secondly, they should not depend on the polarization of the incident wave (this is the condition of the homogeneity). Moreover, these parameters would depend on the topology of the constituents and their arrangement in the MS. Furthermore, they may be frequency dependent and this dependence is, as a rule, resonant. Of course, not all MSs can satisfy the second condition. It

is clear that optically sparse planar arrays definitely do not belong to this category [10]. As to optically dense arrays, those with resonant multipolar response are also not effectively homogeneous (at least we are not familiar with opposite examples). On the other hand, optically dense arrays with electric and magnetic dipole responses may be homogenized, being regular, aperiodic, random or even amorphous (see below). Therefore, we concentrate on such – dipolar – MSs.

By taking the advantage of electromagnetic characterization, one may predict the behavior of an array, consisting of many (theoretically of infinite number of) inclusions, in response to the electromagnetic fields independent of the complexity of each individual element and on their arrangement. This way, within a reasonable accuracy, we drastically reduce the calculation time and resources. It is especially important on the stage of the optimization of a prospective MS.

In Chapter 2, we discuss the definitions and present a brief review of the electromagnetic characterization of MMs and MSs. We explain the failures of the traditional characterization approach when applied to MSs. We discuss two known approaches especially suggested for the characterization of MSs in 1990s-2000s and select one of them (though the alternative approach is also involved). We conclude this chapter by claiming the novelty of the current study.

The third chapter is devoted to the theoretical mainstay of the present study. We start with the heuristic homogenization model of a metasurface located on a dielectric interface. After the rather special boundary conditions obtained for some MSs and separately for the transverse electric (TE) and transverse magnetic (TM) incident cases, we derive the general boundary conditions invariant on the polarization of the excitation field. Next, we introduce relations between the surface polarizations and the incident (one approach) or averaged (another approach) fields. In one case, we perform the characterization in terms of so-called collective polarizability dyadics. In another case, we deal with the surface susceptibility dyadics. Then, we present the most general algorithm to retrieve the characteristic parameters through two-dimensional reflection and transmission dyadics.

In Chapter 4, we present two explicit examples of theoretically investigated MSs in the previous chapter. The first one is a periodic array of plasmonic nano-spheres. We retrieve its effective susceptibilities and show their potential for predicting the reflection/transmission coefficients. The

second one is an array of coupled plasmonic nano-patches positioned in a disordered fashion on a flat surface. We show that our retrieval approach for this random MS is as powerful as for a periodic MS. The restriction of our theory is a sufficiently small optical size of a unit cell (area per one particle).

We present the main results of the thesis in Chapter 5. This chapter is dedicated to functional metasurfaces. Here, we theoretically reveal and discuss novel physical effects and various functionalities. We present some discussions on the intrinsically bianisotropic and intrinsically magnetic MSs operating in the visible range. We then discuss the microscopic effect of *substrate-induced bianisotropy* for a substrated array of plasmonic nano-spheres. Indeed, this effect results in magnetic response of a substrated MS which is neither bianisotropic nor magnetic when located in a uniform host medium. We reveal the magnetic response within the framework of our homogenization model; i.e., retrieving some magnetic parameters. We also obtain the perfect absorbance conditions for different topologies and discuss them in this chapter. Finally, with an investigation of random and amorphous metasurfaces, we conclude our study. Here, we present a model which explains the different behavior of electric and magnetic resonant modes of MSs in transition from periodic to amorphous arrangements.

In Conclusions we summarize our main results.

2. Electromagnetic Characterization of Metamaterials: A General Overview

2.1 Definitions, importance, and some notes

Before the historical investigation on the "*electromagnetic characterization of metamaterials*", we would like to first introduce and/or define each word of the phrase separately. After that, we may have a better intuition and understanding of what we are exactly seeking for and looking at. We also draw your attention to the point that all definitions are in the context of electromagnetic science which deals with the interactions of electromagnetic waves with matter[1]. Therefore, we exclude other branches of science such as chemistry, mechanics, etc., from our consideration. Nevertheless, we know that all these branches may somehow be interconnected. As a result, when we talk about "metamaterials", we restrict ourselves to "electromagnetic metamaterials" and present a brief historical overview of their electromagnetic characterization. For other types of metamaterials, e.g., mechanical metamaterials, one may refer to [11, 12, 13, 14, 15].

2.1.1 Definition: *metamaterials*

The main word in the title of this section is "*metamaterials*" which is composed of two sub-words; i.e., "*meta*" and "*materials*". First, the Greek prefix "*meta*"–"$\mu\epsilon\tau\acute{\alpha}$" means after, beyond and also of higher kind [16]. Second, "*materials*" according to the definition presented on the title page of the famous journal of *Nature Materials* are substances in the condensed states – solids (crystalline and amorphus media) and liquids (pure liq-

[1]The common classical definition of matter is anything that has mass and volume (occupies space) [17] and exists in four fundamental states: solid, liquid, gas, and plasma.

uids, solutions, suspensions and colloids[2]) – designed or manipulated for technological ends. Indeed, materials themselves composed of constituent elements (atoms and/or molecules) which are put together with a specific arrangement. Therefore, the properties of each element together with the manner in which they are arranged are responsible for characteristics of the material. With these definitions in hand, we may expect that "*metamaterials*" should have a meaning composed of its two sub-words; i.e., "higher kind of ordinary materials". However, it would be very premature to conclude with this very general meaning. This terminology was introduced in the group of D. R. Smith at the beginning of the twenty-first century [2, 3, 18] in order to share out so-called Veselago's or doubly-negative media from other *engineered materials* usually called *composites*. The Veselago's media if created in the optical range have promised an exciting effect of the so-called perfect lens [19]. The development of their microwave analogue in works [2, 3, 18] gave birth to the whole research direction of metamaterials. Since that time, the definition of metamaterials has undergone many variations. In order to have a complete overview of various definitions for this term one may refer to [20]. According to [20], metamaterials should exhibit two essential properties common in all definitions; i.e.,

- not observed in natural materials, e.g. in materials of their constitutive elements;

- effectively homogeneous in their electromageric response.

After all, the most recent definition for the term "metamaterial" may be given[3] as following.

Metamaterial is an electromagnetically homogenous arrangement of artificial structural elements, designed to achieve advantageous and unusual electromagnetic properties.

To conclude, *metamaterials* generally are composed of smaller structural elements which are preferably assembled together. These elements, in-

[2]A colloid is a substance in which microscopically dispersed insoluble particles are suspended throughout another substance [21].

[3]According to the Virtual Institute for Artificial Electromagnetic Materials and Metamaterials (METAMORPHOSE VI AISBL [22]) which is concentrating on the research, study, and the promotion of artificial electromagnetic materials and metamaterials.

deed, play the same role as atoms and/or molecules do in ordinary matter. However, the position and properties of each element may be desirably engineered to fulfill a specific goal not usually met in nature. The concept of a metamaterial prototype is illustrated in Fig. 2.1.

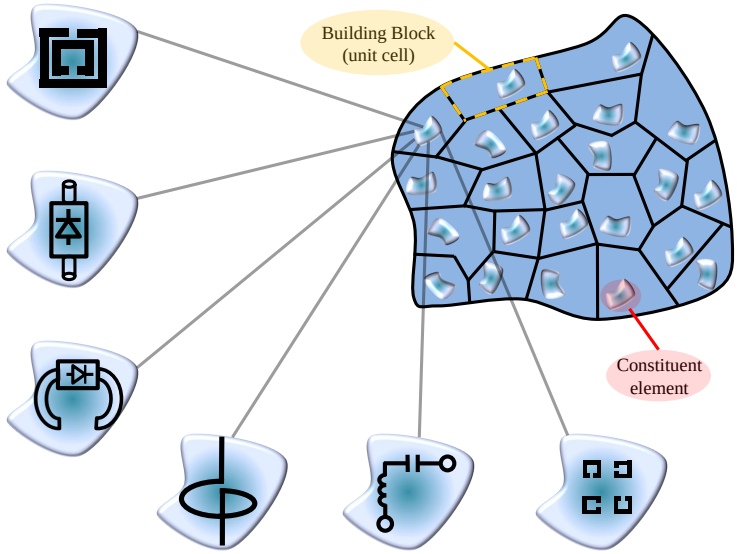

Figure 2.1. The concept of metamaterial, building block, and constituent element. The elements may generally be arranged amorphously. Also, the constituent elements may be any kind of electrical circuit or any other type of inclusions such as split-ring resonator, chiral particle, active element, etc. [23, 24]. Average size a of a building block may be defined as the cubic root of its volume V; i.e., $a = \sqrt[3]{V}$.

2.1.2 Definition: *electromagnetic characterization*

The next term in the title is "*electromagnetic characterization*". Characterization is the way materials scientists examine the structure of a material in order to describe its properties. In chemistry and physics, for example, characterization depends on the molecular structural level we are dealing with. These characteristics may refer to the melting point, boiling point, tension, hardness, volumetric mass density, transparency, crystallinity (a degree of structural order in a solid medium [25]), type of atoms that materials are composed of, number of electrons of each atom, etc. In electromagnetics, however, these characteristics either refer to the constitutive (material) parameters or to macroscopic wave parameters. Two most important macroscopic wave parameters are the wave impedance relating the amplitudes of the electric and magnetic fields and the refractive index relating the phase velocity of the wave in the

medium to the vacuum speed of light c. Material parameters are also macroscopic values, and may be introduced only for effectively homogeneous media (materials). They relate the electric and magnetic fields to the corresponding polarization densities. These parameters for bulk materials are usually two tensors: permittivity and permeability. In some materials called bianisotropic ones, there are two additional material tensors; that is magneto-electric and electro-magnetic coupling tensors. For reciprocal bianisotropic media these two parameters reduce to one tensor which is usually split onto two simpler tensors; that is the so-called chirality and so-called omega-coupling tensors. A comprehensive overview of bianisotropic media can be found in [26].

We have stayed at this point because a significant portion of this dissertation is dedicated to bianisotropic surface metamaterials (metasurfaces). Natural surface materials except recently synthesized graphene[4] are not known. However, surface metamaterials represent an important group of metamaterials. To characterize them, one introduces either surface susceptibilities or surface impedances [9, 27, 28, 29].

2.1.3 Why are *metamaterials* and their *characterization* important?

As it was implicitly mentioned earlier, there are different aspects which make metamaterials beneficial. First, they are artificial and therefore may be favorably engineered for a specific purpose using different constituents and/or arrangements. Second, the arranging processes of structural elements is much easier on the element's level in metamaterials compared to natural atoms and molecules arranged in chemically synthesized materials. Finally, the analysis of metamaterial performances is easier and more precise, since the need for quantum calculations (which are so difficult to combine with calculations of macroscopic fields) in their structural level is alleviated. To know more about the advantages of metamaterials one may refer to [20, 23, 24, 30]. These works also present research directions, classification of metamaterials, and their applications.

The importance of the *electromagnetic characterization* of materials, in general, and metamaterials, in particular, is that once we have found their characteristic parameters, we can predict the behavior of the proposed material in response to an arbitrary electromagnetic wave. That is, we may identify how fast, with which power level, and in which direction an

[4]This thesis does not concern the electromagnetic characterization of graphene.

electromagnetic wave propagates in the presence of the target material in response to an incident wave.

2.1.4 Preliminary notes

There are some points regarding to the concept of metamaterials which should be considered before the historical overview on their characterization. The first point is associated with the length scale in metamaterials. As we have discussed before, a natural material or an engineered metamaterial is composed of many tiny constituent elements which are particularly positioned in a host medium. Notice, each constituent element may in turn be composed of many other sub-elements (see Fig. 2.1). However, the constituent elements and their arrangements determine the properties of the composite metamaterial. The size of each building block[5] generally determines weather the material under study could belong to the metamaterial category or not. Briefly saying, the building block size "a" must be sufficiently smaller than the operational wavelength "λ" in the host medium, however, not incomparably smaller. The idea is that the resonance of an individual element manifests in the macroscopic electromagnetic response without the violation of the material homogeneity. Of course, such materials should be characterized with dispersive effective parameters. At low frequencies, where the response of the building block is not resonant, the dispersion of the electromagnetic response of the whole material does not differ from that of the natural medium forming the building blocks. Most often, the dispersion of the constituent materials in this range is negligible. Such artificial media refer to the non-dispersive composite materials. These materials may be effectively characterized using classical homogenization methods [see e. g. in [31]]. The frequency region where a composite of resonant inclusions behaves as an ordinary composite (is not a metamaterial), is called the quasi-static region. On the other side of the resonance band, the size of the building blocks is in the order of the operational wavelengths (e.g. half-wavelength or larger). Therefore, the electromagnetic response of the lattice can be described using the well-known Floquet-Bloch mode expansion. Furthermore, the resonances of this response are related to the lattice unit cell dimensions [32]. Photonic crystals also called photonic (in optics) or elec-

[5] In periodic arrangements, each element together with its local surrounding medium is called unit cell. It is called building block in a general arrangement (periodic, aperiodic, or amorphous arrangements), see Fig. 2.1 [see e.g. in [23]].

tromagnetic (in radio science) band-gap structures (PBG/EBG) belong to this category. Finally, in the range of the building block resonances, the same structure is a metamaterial. Therefore, the same regular array of resonant building blocks may be treated as three different types of media operating in three different frequency regions. More details on this treatment may be found in [23, 32]. Figure 2.2 shows the classification of regular artificial materials in term of the wavelength scale. Notice, in both optics and radio engineering, one often uses composites of non-resonant inclusions, which are also consistent with Figure 2.2 since these materials are only applied in the lowest frequency region. Similarly, intrinsic PBG/EBG structures of non-resonant inclusions are only applied in the upper frequency region, and their existence also does not change the scheme. For non-regular matematerials the scheme changes: in the upper frequency range, these metamaterials become turbid media and practically do not transmit the electromagnetic waves.

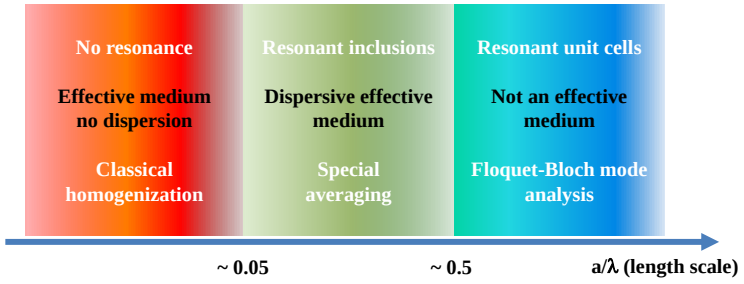

Figure 2.2. Composite materials in electromagnetics versus wave length scale: relation between the materials' terminology and length scale of their unit cells.

Surface metamaterials or briefly metasurfaces (see e.g. in [8, 9]) is the next point. As it was already mentioned, metasurfaces are very thin[6] sheets rather than bulk three-dimensional structures. In Figure 2.3, different categories of metasurfaces – metafilms and metascreens – are schematically depicted. The metafilm name has been coined to a surface array of isolated elements ("cermet" topology shown in Fig. 2.3) while the metascreen name has been assigned to a homogeneous sheet with isolated apertures ("fishnet" topology shown in Fig. 2.3). Notice, there may be metasurfaces with a mixture of these two extreme types [32]. In the present dissertation, following to Refs. [8, 9], we refer to thin sheet meta-

[6]In the whole dissertation when we refer to the thickness we mean the optical thickness – that normalized to the operational wavelength of the wave propagating in the surrounding medium. We will otherwise specify.

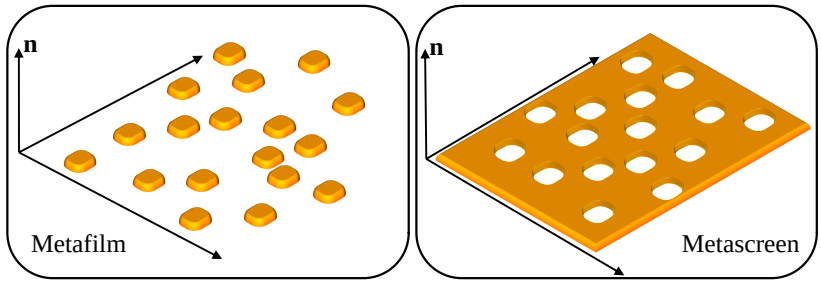

Figure 2.3. General concept of metsasurfaces: metafilms and metascreens as two extreme subcategories of metasurfaces. Notice, the inclusions and/or holes may be periodically or amorphously arranged on/in a planar or curved surface and **n** is the normal vector to the surface.

materials as "*metasurfaces*" while we mainly analyze the metafilm category of metasurfaces. In order to see how our study is related to metamaterial composites and how metamaterials are connected with ordinary materials one may refer to Fig. 2.4.

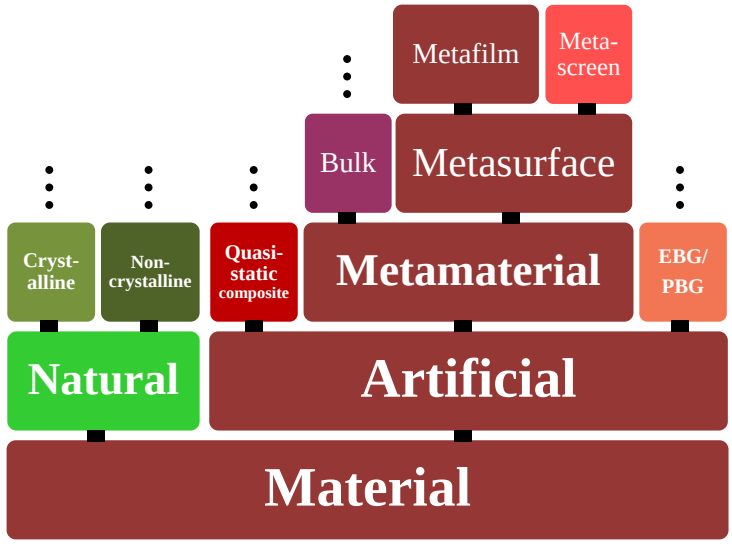

Figure 2.4. Metafilm as a type of metamaterial. Metamaterial is here shared from intrinsically quasi-static composites and EPBG/PBG lattices on the basis of its resonant constitutive elements. The dark brown color of some blocks show how metafilm connects to general material.

This Figure demonstrates different material categories in the basis of the arrangement of their constituent elements in various levels. Indeed, it shows the connection between different classes of natural and artificial materials.

With these notes, we are ready to start the discussion of the history of electromagnetic characterization of metametarials related to their *ho-*

mogenization models.

2.2 History: material/metamaterial characterization

Electromagnetic characterization of *materials*; i.e., measuring/calculating their constitutive parameters dates back to the first half of twentieth century. Prof. Hippel [33] in 1954, with the help of twenty-two contributors, has collected a plethora of different methods for measuring permittivity and permeability of various materials for a diverse frequency range, all covering radio frequencies (below millimeter waves). He has divided the measurement techniques into two categories; that is, techniques based on *lumped circuits* comprising the materials under characterization for the frequency range lower than 200 MHz and *distributed circuits* – for higher frequencies. After that, in 1970s and with the advent of the computer and automatic test equipments, Nicolson, Ross, and Weir (NRW) have developed time-domain and frequency-domain techniques for the measurement of complex constitutive parameters. Their techniques are now between the two most cited works [34, 35]. These traditional methods, in the beginning of the twenty-first century, become the backbone of the initial approach for characterization of *metamaterials* in terms of their effective constitutive parameters. This simplistic approach was first applied for metamaterials in work [27] by Smith *et al*.

According to this approach, one uses the reflection and transmission data of a metamaterial slab (in which its thickness is only known) in order to determine its effective permittivity and permeability as if it was a uniformly homogeneous bulk layer. Although this approach was appropriate and successful for ordinary *materials*, for *metamaterials* it was subjected to ambiguities related to the correct definition of the front and rear surfaces of the sample. While some methods have been used to resolve these ambiguities [28], none of them were general. Indeed, they resulted in non-physical frequency dispersion and wrong sign of the imaginary part of some retrieved material parameters (see e.g. in [7]). Moreover, this approach resulted in unique electromagnetic material parameters only for a sufficiently bulk metamaterial layer (five or more unit cells across its thickness). When applied for thin metamaterial slabs, the NRW approach fully failed; that is, the extracted material parameters strongly depended on the thickness of the test slab [9, 27, 28, 29]. Since the popularity of metasurfaces have grown due to their lower optical losses and easier

manufacturing compared to their bulk counterparts, the lack of physically sound characterization techniques urged the specialists to search novel ways.

The joint team guided by Profs. Holloway and Kuester was the first group who did it. In work [9], they have shown the inapplicability of the NRW approach to metasurfaces. First, they showed that the dependence of the retrieved material parameters on the physical sample thickness is conceptually related to cutoff modes excited at the junction of two different waveguides; i.e., the physical thickness of the metasurafce is irrelevant for its characterization. They stated in [32] that: "The effective bulk material properties, which are determined from the same modified NRW approach used to analyze the bulk three-dimensional metamaterials, are not uniquely defined for metasurfaces. While the geometry of scatterers and the lattice constant (unit cell size) are uniquely defined, the thickness of the equivalent layer is obviously not."

They then suggested an alternative characterization approach initially inspired by a classical work [36] which was the first known paper treating the reflection and transmission of an incident plane wave for a crystalline or liquid half-space in terms of both bulk polarization of the medium and its surface polarization. In the review [8], the group of Holloway and Kuester presents many further attempts towards the response of polarizable surfaces to incident waves. Even more detailed overview on the history of this problem may be found in Publication I and Publication II.

In works by Holloway-Kuester's team published during a decade (2003-2013) [8, 9], a systematic analysis of a metasurface formed by resonant electrically and magnetically polarizable dipole scatterers resulted in a correct characterization technique. A magneto-dielectric metasurface was described via Generalized Sheet Transition Conditions (GSTCs) earlier introduced by Senior and Volakis [37, 38]. The presentation of metasurfaces using GSTCs are more physical than an effective-bulk-medium model. Therefore, the metasurface after its homogenization in terms of surface polarizations (electric and magnetic) acts as an infinitesimally thin sheet of polarization currents which causes amplitude and phase changes in the macroscopic electric and magnetic fields. As a result, the electric and magnetic surface susceptibilities (polarizabilities per unit area) that appear in the GSTCs were uniquely defined. These parameters could serve as characteristic metasurface parameters since they were obtained independent of the metasurface physical thickness. Moreover,

these retrieved characteristic parameters turn out to be independent of the polarization of the external excitation [8].

In our interpretation, metasurfaces can be electromagnetically homogenized via the averaging over each unit cell (Fig. 2.1), assumed to be sufficiently small compared to the operational wavelength. Meanwhile, the whole planar array is assumed to be extended enough in order to be treated as an infinite metasurface. this way, its characteristic parameters do not depend on the transversal sizes of the array.

Notice, even earlier than Holloway-Kuester's group that started to develop their characterization technique, in works of another joint team, namely guided by Profs. Tretyakov and Simovski, an alternative model of metasurfaces has been developing since 1997 [39, 40, 41, 42, 43, 44, 45]. This homogenization model was even more general than Holloway-Kuester's one since it took into account the possible bianisotropy of scatterers. It was based on the concept of so-called collective polarizabilities of scattering particles. These polarizabilities relate the electric and magnetic polarization of the unit cell with the *incident* electric and magnetic fields taken in the plane of the array. These polarizabilities, like the *surface susceptibilities* entering the GSTCs, can be retrieved from the reflection and transmission coefficients. Also, these polarizabilities were related with the surface impedances [44, 45]. Unfortunately, this model of metasurfaces was not sufficiently developed up to 2013; i.e., no feasible and robust retrieval algorithm was created based on it. Below, for brevity we refer this homogenization model as the ST model (described in works of the group guided by Simovski and Tretyakov), whereas the model described in works of the group guided by Holloway and Kuester will be referred as the HK model.

In the following chapters, we are going to present the theory and results of the electromagnetic characterization of metasurfaces. Basically, we generalize the HK model, though the ST model is also inspected, and we discuss the difference between these two approaches in what concerns the characterization of metasurfaces. The novelty of our theory compared to the HK model results from:

1. The bianisotropy of metasurfaces under characterization;

2. The presence of the high-contrast substrate on which the scatterers are located;

3. The two-side incidence of plane waves (important for bianisotropic metasurfaces when the reflected and/or transmitted fields are not necessarily the same for the illumination from different directions [[46], Publication I]);

4. The possible randomness of the metasurface.

The novelty of our theory compared to the ST model results from:

1. The rather simple and reliable algorithm of characterization;

2. The presence of the high-contrast substrate;

3. The possible randomness of the metasurface.

In summary, in our theory, two significant drawbacks of both HK and ST models, neglecting the influence of the substrate and the restriction to only periodical arrangements of scatterers, are overcome. Moreover, we show that the ST and HK models represent two mathematically equivalent descriptions of the metasurface.

We start the next chapter from the general problem formulation and methodology. We then obtain the boundary conditions for a general plane wave excitation. We continue with the representation of the reflected and transmitted fields in term of the incident (ST approach) or average fields (HK approach) using Maxwell's equations. We eventually establish a general algorithm to retrieve the effective parameters of the metasurface through the reflection and transmission coefficients. Finally, we study functional metasurfaces and reveal a new physical effect; i.e., *substrate-induced bianisotropy* which exists at both microsopic and macroscopic levels.

3. Theory

3.1 Problem formulation

The problem is to characterize an optically dense planar array of resonant elements, with electric and perhaps magnetic dipole response to an electromagnetic field, with some macroscopic parameters. The array is supported by a semi-infinite dielectric substrate and after its homogenization is considered as a metasurface. The macroscopic parameters should be independent of the external excitation. They should only depend on the frequency and physical parameters of the metasurface. These physical parameters e.g., the unit cell size and shape, the geometry of elements, and the materials of the elements and of the top (superstrate, $z > 0$ in Fig. 3.2) and bottom (substrate, $z < 0$ in Fig. 3.2) media, determine the frequency dispersion of the electromagnetic response. However, this model should be unique; i.e., independent on the excitation, for a homogeneous metasurface. The top medium for brevity is, in below, treated as free space, however, in our derivations we keep its wave impedance η_+ and refractive index n_+ and it is easy to apply our results for two arbitrary isotropic media on top and bottom of the metasurface.

Figure 3.1 shows a dense planar array of resonant particles which are randomly arranged in the general case. The arrangement may be periodic in the special case, however, as we will see below our characterization model keeps valid even for amorphous (fully random) arrangements of constituents. The metasurface is excited by an electromagnetic plane wave which may impinge from either free space or substrate. With an external excitation through an electromagnetic wave, we may induce currents on each element of the metasurface. Each element, therefore, may re-radiate as a pair of electric and/or magnetic dipoles. Each dipole scat-

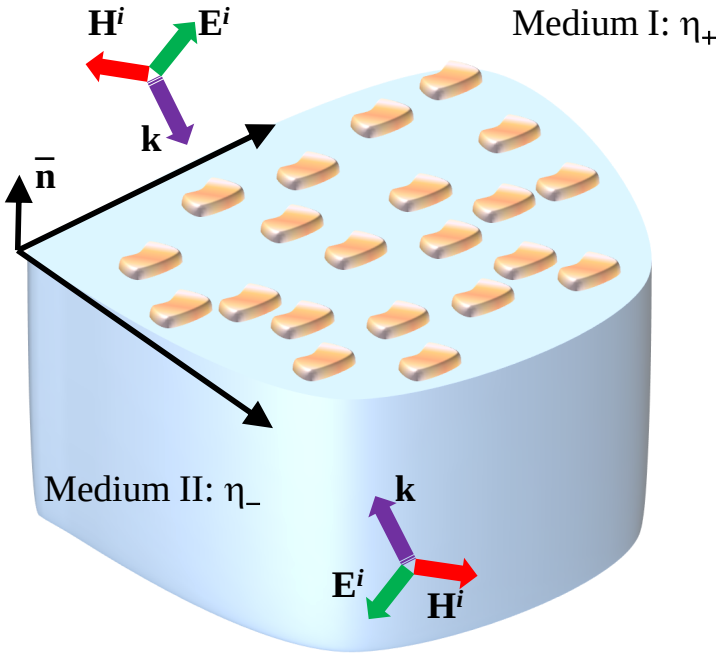

Figure 3.1. Geometry of a metasurface composed of a dens planar array with an amorphous arrangement of its constituent elements which are located on top of a substrate with the characteristic impedances "η_-". The free space characteristic impedance is assumed to be: η_+. Normalized vector $\bar{\mathbf{n}}$ is the normal vector to the metasurface.

terer may interact with the other dipoles of the metasurface. According to [8, 10], we replace the array by a homogenous sheet with an electric and a magnetic surface polarization $\bar{\mathcal{P}}$ and $\bar{\mathcal{M}}$. Indeed, they represent the metasurface response to the external excitation. As a consequence, we have surface currents which cause the field discontinuity across the plane $z = 0$.

In the next section, we derive the boundary conditions for such a metasurface. Indeed, we demonstrate how the fields are related to each other, through the surface polarizations, on both sides of the surface $z = 0$. The derivations are done for an arbitrary polarized electromagnetic wave. The specific derivations for a transverse electric and/or a transverse magnetic polarization of the incident field can be found in Publication I.

3.2 Boundary Conditions

The metasurface is considered as a homogenized thin sheet of an electric surface polarization (vector "$\bar{\mathcal{P}}$") and a magnetic surface polarization

(vector "$\bar{\mathcal{M}}$") which is located at the interface of two half spaces with characteristic impedances $\eta_+ = \sqrt{\mu_+/\epsilon_+}$ (upper half space in Fig. 3.2) and $\eta_- = \sqrt{\mu_-/\epsilon_-}$ (lower half space in Fig. 3.2). Here, $\epsilon_\pm$ and $\mu_\pm$ are the permittivity and permeability of the corresponding media. First, the meta-

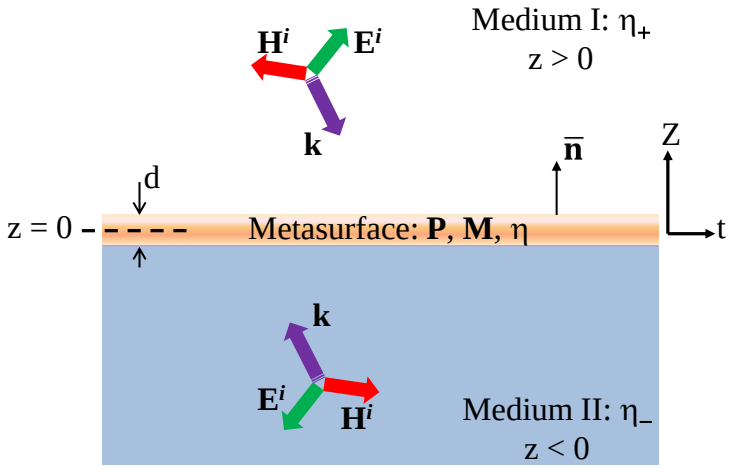

Figure 3.2. Two-dimensional homogenized representation of the metasurface shown in Fig. 3.1. The homogenization model is assumed to be a sheet with the electric "**P**" and magnetic "**M**" polarizations and characteristic impedance η. Its thickness is assumed to be at zero limit; i.e., $d \longrightarrow 0$. The metasurface is located at the interface of two different media with characteristic impedances η_+ and η_-. The sheet may be illuminated from forward ($z > 0$) or backward ($z < 0$) direction. While $\bar{\mathbf{n}}$ is the normal vector to the metasurface, t is the tangent to the same surface of the metasurface.

surface is assumed to have the finite thickness d which further vanishes: $d \longrightarrow 0$. In order to make this assumption, the constituent elements of the metasurface as well as the unit cell size (Fig. 2.1) need to be sufficiently smaller than the operational wavelength.

We assume that the elements of the metasurface are located in a host medium with the permittivity and permeability ϵ and μ, respectively. These ϵ and μ are, in general, different from the upper and lower permittivities ($\epsilon_\pm$) and permeabilities ($\mu_\pm$), however, may be either material parameters of the top medium if the elements lie on the substrate or material parameters of the substrate if they are submerged.

Following to the procedure introduced in [10], we start from Maxwell's equations for total electric and magnetic fields and bulk electric and magnetic polarizations inside the homogeneous slab of thickness d:

$$\nabla \times \mathbf{E} = -j\omega\mu \left(\mathbf{H} + \frac{\mathbf{M}}{\mu} \right) \tag{3.1}$$

$$\nabla \times \mathbf{H} = j\omega\epsilon \left(\mathbf{E} + \frac{\mathbf{P}}{\epsilon} \right) \tag{3.2}$$

$$\nabla \cdot (\epsilon \mathbf{E} + \mathbf{P}) = 0 \tag{3.3}$$

$$\nabla \cdot (\mu \mathbf{H} + \mathbf{M}) = 0 \tag{3.4}$$

Here, **E**, **H**, **P** and **M** are, respectively, the electric and magnetic fields and bulk polarizations inside the slab, averaged over the unit cell area. Notice, the time dependence in (3.1)–(3.4) is assumed to be $\exp(j\omega t)$. Also note the contribution of the electric and magnetic polarization terms **P** and **M** which we have added to the Maxwell's equations in comparison with [10].

Now, we decompose the fields and polarizations into the normal and transversal components in order to find the relation between the tangential electric and magnetic fields on two sides of the slab. We first define the following relations between the transversal (t) and normal (n) components of the fields (**E**, **H**) and polarizations (**P**, **M**):

$$\begin{aligned} \mathbf{E} &= \mathbf{E}_t + \bar{\mathbf{n}} E_n, \qquad & \mathbf{H} &= \mathbf{H}_t + \bar{\mathbf{n}} H_n, \\ \mathbf{P} &= \mathbf{P}_t + \bar{\mathbf{n}} P_n, \qquad & \mathbf{M} &= \mathbf{M}_t + \bar{\mathbf{n}} M_n, \end{aligned} \tag{3.5}$$

and also the nabla operator ∇ [10]:

$$\nabla = \nabla_t + \frac{\partial}{\partial z} \bar{\mathbf{n}}. \tag{3.6}$$

In (3.6), without loosing generality, we have assumed that the normal direction is along the z axis. Now we may decompose (3.1) and (3.2) using the definitions in (3.5) and (3.6). After simplifications, the Maxwell's equations reduce into two sets:

$$\nabla_t \times \bar{\mathbf{n}} E_n + \frac{\partial}{\partial z} (\bar{\mathbf{n}} \times \mathbf{E}_t) = -j\omega\mu \mathbf{H}_t - j\omega \mathbf{M}_t, \tag{3.7a}$$

$$\nabla_t \times \bar{\mathbf{n}} H_n + \frac{\partial}{\partial z} (\bar{\mathbf{n}} \times \mathbf{H}_t) = j\omega\epsilon \mathbf{E}_t + j\omega \mathbf{P}_t, \tag{3.7b}$$

with the transversal components of the polarizations and:

$$\bar{\mathbf{n}} E_n = \frac{1}{j\omega\epsilon} \nabla_t \times \mathbf{H}_t - \bar{\mathbf{n}} \frac{P_n}{\epsilon}, \tag{3.8a}$$

$$\bar{\mathbf{n}} H_n = -\frac{1}{j\omega\mu} \nabla_t \times \mathbf{E}_t - \bar{\mathbf{n}} \frac{M_n}{\mu}. \tag{3.8b}$$

with their normal components. Now, substituting $\bar{\mathbf{n}} E_n$ and $\bar{\mathbf{n}} H_n$ from (3.8) into (3.7) we obtain the following equations:

$$\frac{\partial}{\partial z} (\bar{\mathbf{n}} \times \mathbf{E}_t) = -j\omega\mu \mathbf{H}_t - \frac{1}{j\omega\epsilon} \nabla_t \times \nabla_t \times \mathbf{H}_t - j\omega \mathbf{M}_t + \nabla_t \times \bar{\mathbf{n}} \frac{P_n}{\epsilon}, \tag{3.9a}$$

$$\frac{\partial}{\partial z} (\bar{\mathbf{n}} \times \mathbf{H}_t) = j\omega\epsilon \mathbf{E}_t + \frac{1}{j\omega\mu} \nabla_t \times \nabla_t \times \mathbf{E}_t + j\omega \mathbf{P}_t + \nabla_t \times \bar{\mathbf{n}} \frac{M_n}{\mu}. \tag{3.9b}$$

We next cross-multiply (3.9a) by $(-\bar{\mathbf{n}})$ to find the following set of equations:

$$\frac{\partial}{\partial z}\mathbf{E}_t = j\omega\mu\left[\bar{\bar{I}}_t + \frac{\nabla_t\nabla_t}{k^2}\right]\cdot(\bar{\mathbf{n}}\times\mathbf{H}_t) + j\omega\,(\bar{\mathbf{n}}\times\mathbf{M}_t) - \nabla_t\frac{P_n}{\epsilon}, \tag{3.10a}$$

$$\frac{\partial}{\partial z}\,(\bar{\mathbf{n}}\times\mathbf{H}_t) = j\omega\epsilon\left[\bar{\bar{I}}_t + \frac{(\bar{\mathbf{n}}\times\nabla_t)\,(\bar{\mathbf{n}}\times\nabla_t)}{k^2}\right]\cdot\mathbf{E}_t + j\omega\mathbf{P}_t + \nabla_t\times\bar{\mathbf{n}}\frac{M_n}{\mu}. \tag{3.10b}$$

Here $\bar{\bar{I}}_t$ is the two-dimensional unit dyadic; i.e., $\bar{\bar{I}}_t = \bar{\bar{I}} - \bar{\mathbf{n}}\bar{\mathbf{n}}$, and k is the wave number inside the slab; i.e., $k = \omega\sqrt{\mu\epsilon}$. Also, $\nabla_t\nabla_t$ and $(\bar{\mathbf{n}}\times\nabla_t)(\bar{\mathbf{n}}\times\nabla_t)$ are two-dimensional dyadics with the following representations:

$$\nabla_t\nabla_t = \begin{pmatrix}\frac{\partial}{\partial x}\\ \frac{\partial}{\partial y}\end{pmatrix}\begin{pmatrix}\frac{\partial}{\partial x} & \frac{\partial}{\partial y}\end{pmatrix} = \begin{pmatrix}\frac{\partial}{\partial x}\frac{\partial}{\partial x} & \frac{\partial}{\partial x}\frac{\partial}{\partial y}\\ \frac{\partial}{\partial y}\frac{\partial}{\partial x} & \frac{\partial}{\partial y}\frac{\partial}{\partial y}\end{pmatrix},$$

and

$$(\bar{\mathbf{n}}\times\nabla_t)(\bar{\mathbf{n}}\times\nabla_t) = \begin{pmatrix}-\frac{\partial}{\partial y}\\ \frac{\partial}{\partial x}\end{pmatrix}\begin{pmatrix}-\frac{\partial}{\partial y} & \frac{\partial}{\partial x}\end{pmatrix} = \begin{pmatrix}\frac{\partial}{\partial y}\frac{\partial}{\partial y} & -\frac{\partial}{\partial y}\frac{\partial}{\partial x}\\ -\frac{\partial}{\partial x}\frac{\partial}{\partial y} & \frac{\partial}{\partial x}\frac{\partial}{\partial x}\end{pmatrix}.$$

Notice, for a plane wave solution, the dependence is exponential; that is, $\exp(-j\mathbf{k}_t\cdot\mathbf{r})$, and therefore we have $\nabla_t = -j\mathbf{k}_t$ where $\mathbf{k}_t$ is the tangential wave vector. In the next step, we define

$$\langle\mathbf{E}_t\rangle = \frac{1}{d}\int_0^d \mathbf{E}_t dz, \qquad \langle\mathbf{H}_t\rangle = \frac{1}{d}\int_0^d \mathbf{H}_t dz. \tag{3.11}$$

Now, we integrate equations (3.10) over the surface thickness assuming that the field distributions inside the slab are locally quasi-static in the the normal direction z (see e.g. [10]) which is true if the thickness of the slab is electrically very small compared to the wavelength. On this stage we introduce the surface polarizations:

$$\bar{\mathcal{P}} = \langle\mathbf{P}\rangle d, \qquad \bar{\mathcal{M}} = \langle\mathbf{M}\rangle d, \tag{3.12}$$

In (3.12) it is denoted,

$$\langle\mathbf{P}\rangle = \frac{1}{d}\int_0^d \mathbf{P}dz, \qquad \langle\mathbf{M}\rangle = \frac{1}{d}\int_0^d \mathbf{M}dz.$$

After the integration of equations (3.10) and tending the slab thickness to zero ($d \longrightarrow 0$) we obtain the following vectorial forms of the generalized sheet boundary conditions:

$$\mathbf{E}_t^+ - \mathbf{E}_t^- = j\omega\bar{\mathbf{n}}\times\bar{\mathcal{M}}_t - \nabla_t\frac{\mathcal{P}_n}{\epsilon}, \tag{3.13a}$$

$$\bar{\mathbf{n}}\times\mathbf{H}_t^+ - \bar{\mathbf{n}}\times\mathbf{H}_t^- = j\omega\bar{\mathcal{P}}_t + \nabla_t\times\bar{\mathbf{n}}\frac{\mathcal{M}_n}{\mu}. \tag{3.13b}$$

In the above equations it is denoted:

$$\bar{\mathcal{P}} = \bar{\mathcal{P}}_t + \bar{\mathbf{n}}\mathcal{P}_n, \qquad \bar{\mathcal{M}} = \bar{\mathcal{M}}_t + \bar{\mathbf{n}}\mathcal{M}_n, \tag{3.14}$$

and $\bar{\mathcal{P}}$ and $\bar{\mathcal{M}}$ have been defined in (3.12). Equations (3.13), relating the jumps of transversal electric ($\mathbf{E}_t^{\pm}$) and magnetic ($\mathbf{H}_t^{\pm}$) fields across the sheet to the surface electric ($\bar{\mathcal{P}}$) and magnetic ($\bar{\mathcal{M}}$) polarizations, do not differ from the previously known GSTCs obtained in [8]. However, we have not only proven them for the case of the optical contrast $\eta_- \neq \eta_+$, we have also clarified the role of the substrate for the normal polarizations. If the particles of the metasurface lie on top of the substrate, this component of the polarizations enters the GSTCs in the same form as in the conventional HK model. If the particles are submerged, this component is additionally divided by the relative permittivity (electric polarization) and permeability (magnetic one) of the substrate. If particles are encapsulated by an optically thin layer of the third medium with material parameters ϵ and μ, these components of the electric and magnetic polarizations are divisible by these parameters, respectively. As to tangential polarizations, they enters the GSTCs in the same way for all three cases (particles are on top, submerged, or encapsulated). More importantly, in Section 3.4, we show how the normal and tangential components of the surface polarizations are related to the tangential average fields.

At this step, we are ready to search for the reflected and transmitted fields in terms of these surface polarizations.

3.3 Transverse components of the reflected and transmitted waves

Let us now illuminate a metasurface that is functionalized of being electrically and magnetically polarized with surface polarizations $\mathcal{P}$ and $\mathcal{M}$, by a plane electromagnetic wave ($\nabla_t = -j\mathbf{k}_t$). We consider two cases: a) illumination from the forward direction which is denoted by the upper half space ($z > 0$) in Fig. 3.2 and b) illumination from the backward direction which is denoted by the lower half space ($z < 0$) in the same figure. The upper half space has the characteristic impedance η_+ (by default, free space) while for the lower half space we have η_- (by default, a dielectric substrate). It is known from [10] that for a plane wave we have:

$$\bar{\mathbf{n}} \times \mathbf{H}_t = \mp \overline{\overline{Z}}_{\pm}^{-1} \cdot \mathbf{E}_t, \tag{3.15}$$

where the $\begin{matrix}\text{top}\\ \text{bottom}\end{matrix}$ sign denotes the waves traveling in the direction $\pm z$. In (3.15), $\bar{\bar{Z}}_{\pm}$ is the dyadic impedance of the corresponding media and denoted by [10]:

$$\bar{\bar{Z}}_{\pm} = Z_{\pm}^{TM}\frac{\mathbf{k}_t\mathbf{k}_t}{k_{t,\pm}^2} + Z_{\pm}^{TE}\frac{(\bar{\mathbf{n}}\times\mathbf{k}_t)(\bar{\mathbf{n}}\times\mathbf{k}_t)}{k_{t,\pm}^2}, \tag{3.16}$$

and

$$Z_{\pm}^{TM} = \eta_{\pm}\sqrt{1-\frac{k_{t,\pm}^2}{k_{\pm}^2}}, \quad Z_{\pm}^{TE} = \frac{\eta_{\pm}}{\sqrt{1-\frac{k_{t,\pm}^2}{k_{\pm}^2}}}, \tag{3.17}$$

where

$$k_{n,\pm} = \sqrt{k_{\pm}^2 - k_{t,\pm}^2}, \tag{3.18}$$

is the propagation constant of eigenwaves in the normal direction $\bar{\mathbf{n}}$, and $k_{t,\pm}$ is the tangential wave number, and $k_{\pm} = \omega\sqrt{\mu_{\pm}\epsilon_{\pm}}$.

Let us now decompose the incident, reflected, and transmitted electric/magnetic fields into their transversal ($\mathbf{E}_t^i/\mathbf{H}_t^i$, $\mathbf{E}_t^r/\mathbf{H}_t^r$, $\mathbf{E}_t^t/\mathbf{H}_t^t$) and normal ($E_n^i/H_n^i$, E_n^r/H_n^r, E_n^t/H_n^t) components as following:

$$\mathbf{E}^i = \mathbf{E}_t^i + \bar{\mathbf{n}}E_n^i, \qquad \mathbf{E}^r = \mathbf{E}_t^r + \bar{\mathbf{n}}E_n^r, \qquad \mathbf{E}^t = \mathbf{E}_t^t + \bar{\mathbf{n}}E_n^t, \tag{3.19}$$

$$\mathbf{H}^i = \mathbf{H}_t^i + \bar{\mathbf{n}}H_n^i, \qquad \mathbf{H}^r = \mathbf{H}_t^r + \bar{\mathbf{n}}H_n^r, \qquad \mathbf{H}^t = \mathbf{H}_t^t + \bar{\mathbf{n}}H_n^t, \tag{3.20}$$

Then, for the transversal components, in the case of illumination from top (forward direction), we have:

$$\mathbf{E}_t^+ = \mathbf{E}_t^i + \mathbf{E}_t^r, \qquad \mathbf{E}_t^- = \mathbf{E}_t^t, \tag{3.21a}$$

$$\mathbf{H}_t^+ = \mathbf{H}_t^i + \mathbf{H}_t^r, \qquad \mathbf{H}_t^- = \mathbf{H}_t^t, \tag{3.21b}$$

while, for the illumination from the bottom (backward direction), we have:

$$\mathbf{E}_t^+ = \mathbf{E}_t^t, \qquad \mathbf{E}_t^- = \mathbf{E}_t^i + \mathbf{E}_t^r, \tag{3.22a}$$

$$\mathbf{H}_t^+ = \mathbf{H}_t^t, \qquad \mathbf{H}_t^- = \mathbf{H}_t^i + \mathbf{H}_t^r. \tag{3.22b}$$

Using (3.15) in (3.21) and (3.22) and then substituting $\mathbf{E}_t^{\pm}$ and $\mathbf{H}_t^{\pm}$ in the transversal boundary conditions (3.13) one may find the following two sets for the illumination from forward direction:

$$\mathbf{E}_t^i + \mathbf{E}_t^r - \mathbf{E}_t^t = j\omega\bar{\mathbf{n}}\times\bar{\mathcal{M}}_t + j\mathbf{k}_t\frac{\mathcal{P}_n}{\epsilon}, \tag{3.23a}$$

$$\bar{\bar{Z}}_+^{-1}\cdot\mathbf{E}_t^i - \bar{\bar{Z}}_+^{-1}\cdot\mathbf{E}_t^r - \bar{\bar{Z}}_-^{-1}\cdot\mathbf{E}_t^t = j\omega\bar{\mathcal{P}}_t - j\mathbf{k}_t\times\bar{\mathbf{n}}\frac{\mathcal{M}_n}{\mu}, \tag{3.23b}$$

and from backward direction:

$$\mathbf{E}_t^t - \mathbf{E}_t^i - \mathbf{E}_t^r = j\omega\bar{\mathbf{n}} \times \bar{\mathcal{M}}_t + j\mathbf{k}_t \frac{\mathcal{P}_n}{\epsilon}, \tag{3.24a}$$

$$-\overline{\overline{Z}}_+^{-1} \cdot \mathbf{E}_t^t + \overline{\overline{Z}}_- \cdot \mathbf{E}_t^i - \overline{\overline{Z}}_-^{-1} \cdot \mathbf{E}_t^r = j\omega\bar{\mathcal{P}}_t - j\mathbf{k}_t \times \bar{\mathbf{n}} \frac{\mathcal{M}_n}{\mu}, \tag{3.24b}$$

respectively.

The final step for finding the transversal components of the reflected $\mathbf{E}_t^r$ and transmitted $\mathbf{E}_t^t$ waves is to separately solve two sets of equations (3.23) and (3.24). Therefore, the results for the transversal components of the reflected $\mathbf{E}_t^r$ and transmitted $\mathbf{E}_t^t$ electric fields read as:

$$\begin{aligned}\mathbf{E}_t^r = &-\left(\bar{\bar{I}}_t + \overline{\overline{Z}}_\mp \overline{\overline{Z}}_\pm^{-1}\right)^{-1} \left(\bar{\bar{I}}_t - \overline{\overline{Z}}_\mp \overline{\overline{Z}}_\pm^{-1}\right) \cdot \mathbf{E}_t^i \\ &- \left(\bar{\bar{I}}_t + \overline{\overline{Z}}_\mp \overline{\overline{Z}}_\pm^{-1}\right)^{-1} \cdot \Big[j\omega \left(\overline{\overline{Z}}_\mp \cdot \mathcal{P}_t \mp \bar{\mathbf{n}} \times \mathcal{M}_t\right) \\ &\qquad \mp j \left(\mathbf{k}_t \frac{\mathcal{P}_n}{\epsilon} \pm \overline{\overline{Z}}_\pm \cdot (\bar{\mathbf{n}} \times \mathbf{k}_t) \frac{\mathcal{M}_n}{\mu}\right)\Big],\end{aligned} \tag{3.25}$$

and

$$\begin{aligned}\mathbf{E}_t^t = &\ 2\left(\bar{\bar{I}}_t + \overline{\overline{Z}}_\mp \overline{\overline{Z}}_\pm^{-1}\right)^{-1} \cdot \mathbf{E}_t^i \\ &- \left(\bar{\bar{I}}_t + \overline{\overline{Z}}_\mp \overline{\overline{Z}}_\pm^{-1}\right)^{-1} \cdot \Big[j\omega \left(\overline{\overline{Z}}_\pm \cdot \mathcal{P}_t \pm \bar{\mathbf{n}} \times \mathcal{M}_t\right) \\ &\qquad \pm j \left(\mathbf{k}_t \frac{\mathcal{P}_n}{\epsilon} \mp \overline{\overline{Z}}_\mp \cdot (\bar{\mathbf{n}} \times \mathbf{k}_t) \frac{\mathcal{M}_n}{\mu}\right)\Big],\end{aligned} \tag{3.26}$$

where $\substack{\text{top}\\\text{bottom}}$ sign denotes for the illumination from $\substack{\text{forward}\\\text{backward}}$ direction. In a special case, when $\overline{\overline{Z}}_+ = \overline{\overline{Z}}_- = \overline{\overline{Z}}$, we have:

$$\mathbf{E}_t^r = -\frac{1}{2}\left[j\omega \left(\overline{\overline{Z}} \cdot \mathcal{P}_t \mp \bar{\mathbf{n}} \times \mathcal{M}_t\right) \mp j \left(\mathbf{k}_t \frac{\mathcal{P}_n}{\epsilon} \pm \overline{\overline{Z}} \cdot (\bar{\mathbf{n}} \times \mathbf{k}_t) \frac{\mathcal{M}_n}{\mu}\right)\right], \tag{3.27}$$

and

$$\mathbf{E}_t^t = \mathbf{E}_t^i - \frac{1}{2}\left[j\omega \left(\overline{\overline{Z}} \cdot \mathcal{P}_t \pm \bar{\mathbf{n}} \times \mathcal{M}_t\right) \pm j \left(\mathbf{k}_t \frac{\mathcal{P}_n}{\epsilon} \mp \overline{\overline{Z}} \cdot (\bar{\mathbf{n}} \times \mathbf{k}_t) \frac{\mathcal{M}_n}{\mu}\right)\right]. \tag{3.28}$$

Notice, the equations (3.25), (3.26), (3.27), and (3.28) that present the reflected and transmitted fields in terms of the surface polarizations, are general. They may be applied for any special case of incidences; for example, TE or TM incidence or a superposition of these two. More importantly, as we show later, all of these surface polarizations may be expressed in terms of the transversal electric field $\mathbf{E}_t$.

In the next section, we are going to present the relations between the surface polarizations $\bar{\mathcal{P}}$ and $\bar{\mathcal{M}}$ with the electromagnetic fields $\mathbf{E}$ and $\mathbf{H}$. Two different relations can be obtained: one corresponds to the HK approach, another – to the ST approach.

3.4 Effective polarizability/susceptibility tensors: characteristic parameters of metasurfaces

The parameters which relate the fields to the surface polarizations are called polarizabilities or susceptibilities depending on the definition of the fields associated to the relations. Really, they are the constitutive parameters which do not change with different conditions of the external excitation and they only depend on the physical parameters of the metasurface; i.e., the shapes and sizes of the metasurface elements and unit cells. In the HK model, we use the total fields whose different values on two sides of the metasurface are averaged. In the ST model, we use the incident field in the constitutive relations. Therefore, we may write the following constitutive relations between the fields and polarizations in the ST approach:

$$\bar{\mathcal{P}} = \bar{\bar{\alpha}}^{\mathrm{ee}} \cdot \mathbf{E}^i + \bar{\bar{\alpha}}^{\mathrm{em}} \cdot \mathbf{H}^i, \tag{3.29a}$$

$$\bar{\mathcal{M}} = \bar{\bar{\alpha}}^{\mathrm{me}} \cdot \mathbf{E}^i + \bar{\bar{\alpha}}^{\mathrm{mm}} \cdot \mathbf{H}^i, \tag{3.29b}$$

where $\bar{\bar{\alpha}}^{\mathrm{ee}}$,$\bar{\bar{\alpha}}^{\mathrm{em}}$,$\bar{\bar{\alpha}}^{\mathrm{em}}$, and $\bar{\bar{\alpha}}^{\mathrm{mm}}$ are called *collective polarizability* tensors: electric, magneto-electric, electro-magnetic, and magnetic ones, respectively. They, indeed, relate the incident fields to the same surface polarizations as we introduced above. We may alternatively define another set of characteristic parameters (the HK approach):

$$\bar{\mathcal{P}} = \bar{\bar{\chi}}^{\mathrm{ee}} \cdot \mathbf{E}^{ave} + \bar{\bar{\chi}}^{\mathrm{em}} \cdot \mathbf{H}^{ave}, \tag{3.30a}$$

$$\bar{\mathcal{M}} = \bar{\bar{\chi}}^{\mathrm{me}} \cdot \mathbf{E}^{ave} + \bar{\bar{\chi}}^{\mathrm{mm}} \cdot \mathbf{H}^{ave}. \tag{3.30b}$$

Here, $\bar{\bar{\chi}}$ denotes *surface susceptibility* tensors. In (3.30), all vectors in the form of $\mathbf{A}^{ave}$ refer to the *average* fields, calculated as

$$\mathbf{A}^{ave} = \frac{\mathbf{A}^i + \mathbf{A}^r + \mathbf{A}^t}{2}, \tag{3.31}$$

where superscripts i, r, and t correspond to the incident, reflected, and transmitted wave fields, respectively (all taken at $z = 0$). Notice, the normal components of the average fields can be expressed in terms of their transversal components. Therefore, we are indeed performing the averaging in the tangential direction.

At this point, we have all tools to calculate the two-dimensional reflection and transmission dyadics $\bar{\bar{r}}$ and $\bar{\bar{t}}$ as functions of effective polarizability/susceptibility tensors; where $\mathbf{E}_t^r = \bar{\bar{r}} \cdot \mathbf{E}_t^i$ and $\mathbf{E}_t^t = \bar{\bar{t}} \cdot \mathbf{E}_t^i$. One may substitute the relations (3.29) into equations (3.25) and (3.26) to find the

reflection and transmission dyadics as functions of the effective polarizability tensors. Notice, when using (3.30) as constitutive relations, it is easier to substitute them into the boundary conditions (3.23) and (3.24) and then solve these equations for $\bar{\bar{r}}$ and $\bar{\bar{t}}$, to find them as functions of the effective susceptibility tensors.

Before presenting a general approach and algorithm, we draw your attention to some important points related to calculations of the reflection and transmission dyadics from the obtained boundary conditions. In the presented equations (3.25) and (3.26), we need to find $\bar{\mathcal{P}}_t$ and $\bar{\mathcal{M}}_t$ in term of the incident/average field $\mathbf{E}^i$/$\mathbf{E}^{ave}$. Let us first consider an arbitrary three-dimensional dyadic $\bar{\bar{A}}$ as following:

$$\bar{\bar{A}} = \begin{pmatrix} A_{xx} & A_{xy} & A_{xz} \\ A_{yx} & A_{yy} & A_{yz} \\ A_{zx} & A_{zy} & A_{zz} \end{pmatrix}. \tag{3.32}$$

If we define the following dyadics, vectors, and scalar $\bar{\bar{A}}_{tt}$, $\bar{A}_{tn}$, $\bar{A}_{nt}$, and A_{nn} from the initial dyadic $\bar{\bar{A}}$ as following:

$$\bar{\bar{A}}_{tt} = \begin{pmatrix} A_{xx} & A_{xy} \\ A_{yx} & A_{yy} \end{pmatrix}, \quad \bar{A}_{tn} = \begin{pmatrix} A_{xz} \\ A_{yz} \end{pmatrix}, \quad \bar{A}_{nt} = \begin{pmatrix} A_{zx} & A_{zy} \end{pmatrix}, \quad A_{nn} = A_{zz}, \tag{3.33}$$

then we may present any three-dimensional dyadics $\bar{\bar{A}}$ as a mixture of a two-dimensional dyadic $\bar{\bar{A}}_{tt}$, two two-component vectors $\bar{A}_{tn}$ and $\bar{A}_{nt}$, and a scalar value A_{nn}; that is,

$$\bar{\bar{A}} = \begin{pmatrix} \bar{\bar{A}}_{tt} & \bar{A}_{tn} \\ \bar{A}_{nt} & A_{nn} \end{pmatrix}. \tag{3.34}$$

Now, using the definitions in (3.33) for effective polarizability tensors and the definitions in (3.5) and (3.14) we may write the following relations for the tangential and normal components of surface polarizations $\bar{\mathcal{P}}$ and $\bar{\mathcal{M}}$ from (3.29):

$$\begin{aligned} \bar{\mathcal{P}}_t = {} & \hat{\bar{\alpha}}^{\mathrm{ee}}_{tt} \cdot \mathbf{E}_t \mp \frac{1}{\omega\epsilon_\pm} \hat{\alpha}^{\mathrm{ee}}_{tn} \mathbf{k}_t \cdot \left(\bar{\bar{Z}}^{-1}_\pm \cdot \mathbf{E}_t \right) \\ & \pm \hat{\bar{\alpha}}^{\mathrm{em}}_{tt} \cdot \left[\bar{\mathbf{n}} \times \left(\bar{\bar{Z}}^{-1}_\pm \cdot \mathbf{E}_t \right) \right] - \frac{1}{k_{n,\pm}} \hat{\alpha}^{\mathrm{em}}_{tn} \mathbf{k}_t \cdot \left[\bar{\mathbf{n}} \times \left(\bar{\bar{Z}}^{-1}_\pm \cdot \mathbf{E}_t \right) \right], \end{aligned} \tag{3.35}$$

$$\begin{aligned} \mathcal{P}_n = {} & \hat{\alpha}^{\mathrm{ee}}_{nt} \cdot \mathbf{E}_t \mp \frac{1}{\omega\epsilon_\pm} \hat{\alpha}^{\mathrm{ee}}_{nn} \mathbf{k}_t \cdot \left(\bar{\bar{Z}}^{-1}_\pm \cdot \mathbf{E}_t \right) \\ & \pm \hat{\alpha}^{\mathrm{em}}_{nt} \cdot \left[\bar{\mathbf{n}} \times \left(\bar{\bar{Z}}^{-1}_\pm \cdot \mathbf{E}_t \right) \right] - \frac{1}{k_{n,\pm}} \hat{\alpha}^{\mathrm{em}}_{nn} \mathbf{k}_t \cdot \left[\bar{\mathbf{n}} \times \left(\bar{\bar{Z}}^{-1}_\pm \cdot \mathbf{E}_t \right) \right], \end{aligned} \tag{3.36}$$

$$\begin{aligned}\bar{\mathcal{M}}_t = &\hat{\bar{\bar{\alpha}}}_{tt}^{\mathrm{me}} \cdot \mathbf{E}_t \mp \frac{1}{\omega\epsilon_\pm}\hat{\alpha}_{tn}^{\mathrm{me}}\mathbf{k}_t \cdot \left(\overline{\overline{Z}}_\pm^{-1} \cdot \mathbf{E}_t\right) \\ &\pm \hat{\bar{\bar{\alpha}}}_{tt}^{\mathrm{mm}} \cdot \left[\bar{\mathbf{n}} \times \left(\overline{\overline{Z}}_\pm^{-1} \cdot \mathbf{E}_t\right)\right] - \frac{1}{k_{n,\pm}}\hat{\alpha}_{tn}^{\mathrm{mm}}\mathbf{k}_t \cdot \left[\bar{\mathbf{n}} \times \left(\overline{\overline{Z}}_\pm^{-1} \cdot \mathbf{E}_t\right)\right],\end{aligned} \tag{3.37}$$

$$\begin{aligned}\mathcal{M}_n = &\hat{\alpha}_{nt}^{\mathrm{me}} \cdot \mathbf{E}_t \mp \frac{1}{\omega\epsilon_\pm}\hat{\alpha}_{nn}^{\mathrm{me}}\mathbf{k}_t \cdot \left(\overline{\overline{Z}}_\pm^{-1} \cdot \mathbf{E}_t\right) \\ &\pm \hat{\alpha}_{nt}^{\mathrm{mm}} \cdot \left[\bar{\mathbf{n}} \times \left(\overline{\overline{Z}}_\pm^{-1} \cdot \mathbf{E}_t\right)\right] - \frac{1}{k_{n,\pm}}\hat{\alpha}_{nn}^{\mathrm{mm}}\mathbf{k}_t \cdot \left[\bar{\mathbf{n}} \times \left(\overline{\overline{Z}}_\pm^{-1} \cdot \mathbf{E}_t\right)\right],\end{aligned} \tag{3.38}$$

or we may express them in a simplified compact representation:

$$\bar{\mathcal{P}}_t = \left[\hat{\bar{\bar{\alpha}}}_{tt}^{\mathrm{ee}}\overline{\overline{Z}}_\pm \mp \frac{1}{\omega\epsilon_\pm}\hat{\alpha}_{tn}^{\mathrm{ee}}\mathbf{k}_t\right] \cdot \left(\overline{\overline{Z}}_\pm^{-1} \cdot \mathbf{E}_t\right) \pm \left[\hat{\bar{\bar{\alpha}}}_{tt}^{\mathrm{em}} \mp \frac{1}{k_{n,\pm}}\hat{\alpha}_{tn}^{\mathrm{em}}\mathbf{k}_t\right] \cdot \left[\bar{\mathbf{n}} \times \left(\overline{\overline{Z}}_\pm^{-1} \cdot \mathbf{E}_t\right)\right], \tag{3.39a}$$

$$\mathcal{P}_n = \left[\hat{\alpha}_{nt}^{\mathrm{ee}}\overline{\overline{Z}}_\pm \mp \frac{1}{\omega\epsilon_\pm}\hat{\alpha}_{nn}^{\mathrm{ee}}\mathbf{k}_t\right] \cdot \left(\overline{\overline{Z}}_\pm^{-1} \cdot \mathbf{E}_t\right) \pm \left[\hat{\alpha}_{nt}^{\mathrm{em}} \mp \frac{1}{k_{n,\pm}}\hat{\alpha}_{nn}^{\mathrm{em}}\mathbf{k}_t\right] \cdot \left[\bar{\mathbf{n}} \times \left(\overline{\overline{Z}}_\pm^{-1} \cdot \mathbf{E}_t\right)\right], \tag{3.39b}$$

$$\bar{\mathcal{M}}_t = \left[\hat{\bar{\bar{\alpha}}}_{tt}^{\mathrm{me}}\overline{\overline{Z}}_\pm \mp \frac{1}{\omega\epsilon_\pm}\hat{\alpha}_{tn}^{\mathrm{me}}\mathbf{k}_t\right] \cdot \left(\overline{\overline{Z}}_\pm^{-1} \cdot \mathbf{E}_t\right) \pm \left[\hat{\bar{\bar{\alpha}}}_{tt}^{\mathrm{mm}} \mp \frac{1}{k_{n,\pm}}\hat{\alpha}_{tn}^{\mathrm{mm}}\mathbf{k}_t\right] \cdot \left[\bar{\mathbf{n}} \times \left(\overline{\overline{Z}}_\pm^{-1} \cdot \mathbf{E}_t\right)\right], \tag{3.39c}$$

$$\mathcal{M}_n = \left[\hat{\alpha}_{nt}^{\mathrm{me}}\overline{\overline{Z}}_\pm \mp \frac{1}{\omega\epsilon_\pm}\hat{\alpha}_{nn}^{\mathrm{me}}\mathbf{k}_t\right] \cdot \left(\overline{\overline{Z}}_\pm^{-1} \cdot \mathbf{E}_t\right) \pm \left[\hat{\alpha}_{nt}^{\mathrm{mm}} \mp \frac{1}{k_{n,\pm}}\hat{\alpha}_{nn}^{\mathrm{mm}}\mathbf{k}_t\right] \cdot \left[\bar{\mathbf{n}} \times \left(\overline{\overline{Z}}_\pm^{-1} \cdot \mathbf{E}_t\right)\right]. \tag{3.39d}$$

In the transition from (3.35)–(3.38) to (3.39), one should be careful about the vector and tensor products. Here, following to (3.33) all three dimensional effective polarizability dyadics $\hat{\bar{\bar{\alpha}}}$ are defined as:

$$\hat{\bar{\bar{\alpha}}} = \begin{pmatrix} \hat{\bar{\bar{\alpha}}}_{tt} & \hat{\alpha}_{tn} \\ \hat{\alpha}_{nt} & \hat{\alpha}_{nn} \end{pmatrix}. \tag{3.40}$$

Again, in the above equations, the $\begin{smallmatrix}\text{top}\\ \text{bottom}\end{smallmatrix}$ sign corresponds to the illumination from $\begin{smallmatrix}\text{top}\\ \text{bottom}\end{smallmatrix}$ at $\begin{smallmatrix}z>0\\ z<0\end{smallmatrix}$.

In equations (3.35)–(3.39d), we have applied the following relations to represent the normal electric, normal magnetic, and transversal magnetic fields E_n, H_n, and $\mathbf{H}_t$ in terms of the transversal electric field component ($\mathbf{E}_t$); i.e.,

$$E_n = \mp\frac{1}{\omega\epsilon_\pm}\mathbf{k}_t \cdot \left(\overline{\overline{Z}}_\pm^{-1} \cdot \mathbf{E}_t\right), \tag{3.41a}$$

$$H_n = -\frac{1}{k_{n,\pm}}\mathbf{k}_t \cdot \left[\bar{\mathbf{n}} \times \left(\overline{\overline{Z}}_\pm^{-1} \cdot \mathbf{E}_t\right)\right], \tag{3.41b}$$

$$\mathbf{H}_t = \pm\bar{\mathbf{n}} \times \left(\overline{\overline{Z}}_\pm^{-1} \cdot \mathbf{E}_t\right). \tag{3.41c}$$

Where $\overline{\overline{Z}}_\pm$ and $k_{n,\pm}$ are defined in (3.16) and (3.18), respectively. This formalism makes the calculation of the reflected and transmitted electric

fields general and compact. Moreover, all components of the surface polarizations including the normal ones are presented in terms of the transversal electric field $\mathbf{E}_t$. In equations (3.35)–(3.39d), the transverse electric field $\mathbf{E}_t$ may be replaced by the incident field ($\mathbf{E}_t \equiv \mathbf{E}_t^i$) for the ST model. If we use the HK approach instead of the ST approach, we simply imply dyadics $\bar{\bar{\alpha}} \equiv \bar{\bar{\chi}}$, and replace $\mathbf{E}_t$ by the tangential average field; i.e., $\mathbf{E}_t \equiv (\mathbf{E}_t^i + \mathbf{E}_t^t + \mathbf{E}_t^r)/2$.

The final step is to find the reflection and transmission dyadics relating $\mathbf{E}_t^r$ and $\mathbf{E}_t^t$ to $\mathbf{E}_t^i$. This can be done by substitution of the surface polarizations found in (3.35)–(3.39d) into the formulas for the reflected (3.25) and transmitted (3.26) electric fields. We omit the details of this procedure since one may find them in Publication I, Publication II, and Publication IV for different special cases. We next present the results for the general procedure of parameter retrieval suitable for both sets of characteristic parameters: collective polarizability and effective susceptibility tensors.

3.5 General methodology

So far, we have obtained the transversal components of the reflected and transmitted fields $\mathbf{E}_t^r$ and $\mathbf{E}_t^t$ in terms of the incident/average field $\mathbf{E}_t^i/\mathbf{E}_t^{ave}$. In this section, we present the general algorithm manifesting the advantages of our method of metasurface characterization. As we have already discussed, we emphasize that the presented formulas are suitable for the general case of an arbitrary polarized incident wave and arbitrary optical contrast between the medium of incidence and medium of transmission. Moreover, our metasurface may be bianisotropic with arbitrary anisotropy of electric, magnetic, and magneto-electric coupling tensors. Some special cases are studied in Publication I, Publication II, Publication III, Publication IV, Publication V, and Publication VI. For simplicity, we adopt below the notations of the ST approach. However, one may choose also the HK notations as we did in Publication I and Publication II. The step-by-step algorithm to characterize the metasurfaces, therefore, reads as:

1. We assume that the metasurface may be characterized by collective polarizabilities (electric: $\bar{\bar{\alpha}}^{\mathrm{ee}}$, magnetic: $\bar{\bar{\alpha}}^{\mathrm{mm}}$, magneto-electric: $\bar{\bar{\alpha}}^{\mathrm{em}}$, and electro-magnetic: $\bar{\bar{\alpha}}^{\mathrm{me}}$). These parameters relate the surface polarizations $\bar{\mathcal{P}}$ and $\bar{\mathcal{M}}$ to the incident transversal electric field as in (3.39). We may briefly describe these equations in the following form:

$$\bar{\mathcal{P}}, \bar{\mathcal{M}} = f(\hat{\bar{\bar{\alpha}}}, \mathbf{k}_t, \mathbf{E}_t^i). \tag{3.42}$$

Here $f(\cdot)$ means a function.

2. Then we use our generalized sheet boundary conditions (3.13) and relate the reflected and transmitted fields to the incident field and the surface polarizations $\bar{\mathcal{P}}$ and $\bar{\mathcal{M}}$ as in (3.25) and (3.26). The simple representation of these relations may be presented as:

$$E_t^r, E_t^t = g(\mathbf{E}_t^i, \bar{\mathcal{P}}, \bar{\mathcal{M}}). \tag{3.43}$$

Here $g(\cdot)$ denotes another function.

3. Next, combining the first two items, one finds the reflection and transmission dyadics $\bar{\bar{r}}$ and $\bar{\bar{t}}$ as functions of the polarizability tensors and the vectorial operator $\mathbf{k}_t$; i.e.;

$$E_t^r, E_t^t = h(\hat{\bar{\bar{\alpha}}}, \mathbf{k}_t) \cdot \mathbf{E}_t^i, \qquad \text{or} \qquad \bar{\bar{r}}, \bar{\bar{t}} = h(\hat{\bar{\bar{\alpha}}}, \mathbf{k}_t) \tag{3.44}$$

Notice, as we have mentioned earlier, in the plane wave representation $\nabla_t = -j\mathbf{k}_t$. This implies that in the normal illumination this dependence vanishes while in the oblique incidence, reflection and transmission dyadics are functions of the incident angle "θ_i".

4. To characterize the metasurface, we have to present the characteristic parameters $\hat{\bar{\bar{\alpha}}}$ through reflection and transmission dyadics, inverting equation (3.44). It is not so simple because each polarizability tensor is a three-dimensional matrix which has generally 9 components, and we generally need to determine 36 complex scalars. However, we may have only 4 equations for each of the two-dimensional tensors $\bar{\bar{r}}$ and $\bar{\bar{t}}$. Therefore, with one incidence case we may totally have only 8 equations for 36 unknowns. Nevertheless, we may do the same experiment for different incident angles, say for 5 angles, and obtain 40 numerical equations to reliably solve for all 36 polarizability components which keep the same for all incidence angles. Yet, in many practical cases, depending on the physical shape of the metasurface elements and the excitation polarization, many of these scalar polarizabilities are either negligibly small or can be related to one another by the reciprocity conditions or due to the symmetry of the structure. Therefore, we rarely need to solve 36 unknowns. For most important functional metasurfaces used for opti-

cal applications (e.g. see Publication I, Publication II, Publication III, Publication IV, Publication V, and Publication VI) we only need to solve for 3 or 4 components from 36. Therefore, we only need to know the reflection/transmission coefficients for 2 or 3 incident angles. Finally, the solution to the characteristic parameters $\bar{\bar{\alpha}}$ read as:

$$\hat{\bar{\bar{\alpha}}} = h^{-1}(\bar{\bar{r}}(\theta), \bar{\bar{t}}(\theta), \mathbf{k}_t) \tag{3.45}$$

Here $h^{-1}(\cdot)$ represents the inverse of the function $h(\cdot)$. Two-dimensional tensors $\bar{\bar{r}}(\theta)$ and $\bar{\bar{t}}(\theta)$ stand for the transversal reflection and transmission dyadics for an arbitrary incident angle θ.

5. The final step of the algorithm is to validate the solution. One may put the retrieved polarizabilities from (3.45) into (3.44) in order to find the reflection/transmission coefficients for other incident angles (different from those we have used for our retrieval in (3.45)) and compare it with reflection and transmission coefficients numerically simulated or experimentally measured for these test angles.

Before going to the next chapter, it is worth to note here that we have also developed a circuit model for substrated metasurfaces in Publication III. The drawback of the model from Publication III is its suitability for only one-direction modeling (different circuits for the illumination in the forward and in the backward directions). The equivalent circuit of Publication III is Γ-shaped; i.e., comprises only two equivalent lumped impedances, whereas the general circuit model applicable for both illumination cases is either the T-shaped or Π-shaped schemes comprising 3 lumped impedances [47]. The general idea is to use the concept of voltages and currents instead of the transversal electric and magnetic fields. Besides, effective polarizabilities/susceptibilities must be replaced by the effective sheet impedances and/or admittances. This may simplify the study especially when we deal with finite-thickness substrates or with piece-wise homogeneous (step inhomogeneity) metasurfaces.

In the next chapter, we consider some examples and show the applicability of the proposed characterization technique. The examples correspond to optical frequencies where the need in this technique is especially keen. We only present final results and perform some physical discussions about them. For detailed discussions one may refer to Publication I, Publication II, Publication III, Publication IV, Publication V, and Publication VI.

4. Practical Examples

In the previous chapter, we presented a general approach to the characterization of metasurfaces. However, solving equation (3.45) to find the metasurface characteristic parameters (collective polarizabilities or surface susceptibilities) in the general case, is very complicated and rarely needed. It is reasonable to reduce the problem and simplify its solution. In the upcoming sections, we present different examples and show how a priori knowledge of the problem may simplify the study. In these examples we have adopted the HK model.

4.1 A planar array of plasmonic nano-spheres: a periodic metasurface

Let us consider a dense planar periodic array of *non-bianisotropic* plasmonic nano-spheres located in free space at $z = 0$ as in Fig. 4.1(a). This array may be considered as a metasurface since the particles and the period of the array are enough smaller than the operational wavelength; that is, $D = 0.1\lambda_0$ and $a = 0.2\lambda_0$, where λ_0 is the central operational wavelength in the host medium (here, free space). Moreover, the response of this composite is in the frequency band of its inclusions' resonances which implies a metasurface.

According to the geometry of the problem, the general susceptibility tensors may be written as:

$$\hat{\bar{\bar{\chi}}}^{\mathrm{ee}} = \begin{pmatrix} \hat{\bar{\bar{\chi}}}^{\mathrm{ee}}_{tt} & \hat{\bar{\chi}}^{\mathrm{ee}}_{tn} \\ \hat{\bar{\chi}}^{\mathrm{ee}}_{nt} & \hat{\chi}^{\mathrm{ee}}_{nn} \end{pmatrix} = \begin{pmatrix} \hat{\chi}^{\mathrm{ee}}_{xx} & \hat{\chi}^{\mathrm{ee}}_{xy} & \hat{\chi}^{\mathrm{ee}}_{xz} \\ \hat{\chi}^{\mathrm{ee}}_{yx} & \hat{\chi}^{\mathrm{ee}}_{yy} & \hat{\chi}^{\mathrm{ee}}_{yz} \\ \hat{\chi}^{\mathrm{ee}}_{zx} & \hat{\chi}^{\mathrm{ee}}_{zy} & \hat{\chi}^{\mathrm{ee}}_{zz} \end{pmatrix}, \tag{4.1}$$

$$\hat{\bar{\bar{\chi}}}^{\mathrm{em}} = \begin{pmatrix} \hat{\bar{\bar{\chi}}}^{\mathrm{em}}_{tt} & \hat{\bar{\chi}}^{\mathrm{em}}_{tn} \\ \hat{\bar{\chi}}^{\mathrm{em}}_{nt} & \hat{\chi}^{\mathrm{em}}_{nn} \end{pmatrix} = \begin{pmatrix} \hat{\chi}^{\mathrm{em}}_{xx} & \hat{\chi}^{\mathrm{em}}_{xy} & \hat{\chi}^{\mathrm{em}}_{xz} \\ \hat{\chi}^{\mathrm{em}}_{yx} & \hat{\chi}^{\mathrm{em}}_{yy} & \hat{\chi}^{\mathrm{em}}_{yz} \\ \hat{\chi}^{\mathrm{em}}_{zx} & \hat{\chi}^{\mathrm{em}}_{zy} & \hat{\chi}^{\mathrm{em}}_{zz} \end{pmatrix}, \tag{4.2}$$

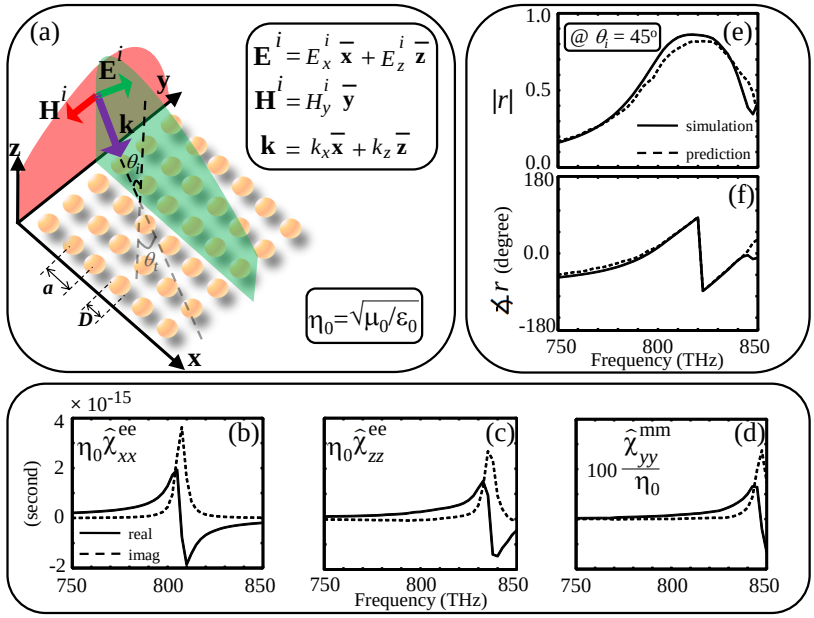

Figure 4.1. (a) A planar periodic array of silver plasmonic nano-spheres positioned at the **xy**–plane in free space, where ϵ_0 and μ_0 are the permittivity and permeability of the free space, respectively. The array is excited by a TM-polarized electromagnetic plane wave. The diameter of each sphere is $D = 40$ nm while the cell size is $a = 80$ nm. (b) Tangential electric (c) Normal electric and (d) Tangential magnetic effective susceptibility components of the metasurface retrieved from the reflection and transmission data at $\theta_i = 0$ and 10°. (e) Predicted and simulated results for the amplitude of the reflection coefficient of the proposed metasurface for an incidence of $\theta_i = 45^\circ$. (f) The same plot as in (e) for the phase of the reflection coefficient. The material data for silver is taken from [48]. Notice, the time dependence is assumed to be $\exp(-i\omega t)$ in these calculations.

$$\hat{\bar{\chi}}^{\text{me}} = \begin{pmatrix} \hat{\bar{\chi}}^{\text{me}}_{tt} & \hat{\chi}^{\text{me}}_{tn} \\ \hat{\chi}^{\text{me}}_{nt} & \hat{\chi}^{\text{me}}_{nn} \end{pmatrix} = \begin{pmatrix} \hat{\chi}^{\text{me}}_{xx} & \hat{\chi}^{\text{me}}_{xy} & \hat{\chi}^{\text{me}}_{xz} \\ \hat{\chi}^{\text{me}}_{yx} & \hat{\chi}^{\text{me}}_{yy} & \hat{\chi}^{\text{me}}_{yz} \\ \hat{\chi}^{\text{me}}_{zx} & \hat{\chi}^{\text{me}}_{zy} & \hat{\chi}^{\text{me}}_{zz} \end{pmatrix}, \tag{4.3}$$

and

$$\hat{\bar{\chi}}^{\text{mm}} = \begin{pmatrix} \hat{\bar{\chi}}^{\text{mm}}_{tt} & \hat{\chi}^{\text{mm}}_{tn} \\ \hat{\chi}^{\text{mm}}_{nt} & \hat{\chi}^{\text{mm}}_{nn} \end{pmatrix} = \begin{pmatrix} \hat{\chi}^{\text{mm}}_{xx} & \hat{\chi}^{\text{mm}}_{xy} & \hat{\chi}^{\text{mm}}_{xz} \\ \hat{\chi}^{\text{mm}}_{yx} & \hat{\chi}^{\text{mm}}_{yy} & \hat{\chi}^{\text{mm}}_{yz} \\ \hat{\chi}^{\text{mm}}_{zx} & \hat{\chi}^{\text{mm}}_{zy} & \hat{\chi}^{\text{mm}}_{zz} \end{pmatrix}. \tag{4.4}$$

However, as we mentioned earlier, there are some physical insights which may help to reduce the problem complexities. At this point, we discuss these issues based on our prior knowledge about the proposed problem:

1. We are going to analyze the metasurface in the resonance band of its constituent elements; i.e., spheres. The particles are assumed to be

made of silver which implies strong electric resonance. Therefore, the magnetic resonance is negligible compared to the electric one; that is $\hat{\bar{\chi}}^{\mathrm{mm}} \approx 0$. However, we do not neglect the magnetic resonance to prove this issue. Nevertheless, neglecting this magnetic resonance causes a much easier solution.

2. There is no reason for bianisotropy in the structure. Therefore, both bianisotropic tensors $\hat{\bar{\chi}}^{\mathrm{em}}$ and $\hat{\bar{\chi}}^{\mathrm{me}}$ must vanish.

3. The particles do not have any possibility to rotate the polarization of the incident fields. This means that all cross components of the electric and magnetic susceptibility tensors $\hat{\bar{\chi}}^{\mathrm{ee}}$ and $\hat{\bar{\chi}}^{\mathrm{mm}}$ are zero; i.e., $\hat{\chi}^{\mathrm{ee}}_{tn} = \hat{\chi}^{\mathrm{mm}}_{tn} = \hat{\chi}^{\mathrm{ee}}_{nt} = \hat{\chi}^{\mathrm{mm}}_{nt} = \hat{\chi}^{\mathrm{ee}}_{xy} = \hat{\chi}^{\mathrm{mm}}_{xy} = \hat{\chi}^{\mathrm{ee}}_{yx} = \hat{\chi}^{\mathrm{mm}}_{yx} = 0$. As a result, the cross components of reflection and transmission tensors are also zero; that is $r_{xy} = r_{yx} = t_{xy} = t_{yx} = 0$.

4. The geometry of the structure and its excitation imposes some other conditions on the susceptibilities. With the TM-polarization of the incident field, there is no way to have nonzero **y**–directed electric components and **x**/**z**–directed magnetic components of the susceptibility tensors. This means that $\hat{\chi}^{\mathrm{ee}}_{yy}$, $\hat{\chi}^{\mathrm{mm}}_{xx}$, and $\hat{\chi}^{\mathrm{mm}}_{zz}$ must be zero. To have these components nonzero, one may use a TE-polarized wave as the incident field.

5. Finally, the susceptibility components, which may arise in the case of the TM-wave incidence, are only 3: $\hat{\chi}^{\mathrm{ee}}_{xx}$, $\hat{\chi}^{\mathrm{ee}}_{zz}$, and $\hat{\chi}^{\mathrm{mm}}_{yy}$. In general, it is not enough since we need also $\hat{\chi}^{\mathrm{ee}}_{yy}$ and $\hat{\chi}^{\mathrm{mm}}_{xx}$. However, the particles have spherical symmetry and being arranged in a square array in the **xy**-plane, possess an in-plane isotropic response. As a result, we need to find only 3 components $\hat{\chi}^{\mathrm{ee}}_{xx} = \hat{\chi}^{\mathrm{ee}}_{yy}$, $\hat{\chi}^{\mathrm{mm}}_{yy} = \hat{\chi}^{\mathrm{mm}}_{xx}$, and $\hat{\chi}^{\mathrm{mm}}_{zz}$. Two first ones can be found from the study of the normal incidence. The third susceptibility $\hat{\chi}^{\mathrm{mm}}_{zz}$ may be found applying an oblique TE incidence under arbitrary angle.

Considering the above hints, one may reduce the complex vectorial form of the equations (3.25), (3.26) and (3.39) to a scalar problem. Therefore, the inverse problem of equation (3.45) may even be solved analytically as we did in Publication I and Publication VI for the general case when a metasurface is placed at the interface of two media with different permit-

tivities. For a special case when the two surrounding media are the same, the results read as:

$$r = \frac{-\frac{i\omega}{2\cos\theta}[\eta_0\hat{\chi}^{\mathrm{ee}}_{xx}\cos^2\theta - \eta_0\hat{\chi}^{\mathrm{ee}}_{zz}\sin^2\theta - \hat{\chi}^{\mathrm{mm}}_{yy}/\eta_0]}{1-(\frac{\omega}{2})^2[\hat{\chi}^{\mathrm{ee}}_{xx}\hat{\chi}^{\mathrm{mm}}_{yy} + \eta_0^2\hat{\chi}^{\mathrm{ee}}_{xx}\hat{\chi}^{\mathrm{ee}}_{zz}\sin^2\theta] - \frac{i\omega}{2\cos\theta}[\eta_0\hat{\chi}^{\mathrm{ee}}_{xx}\cos^2\theta + \eta_0\hat{\chi}^{\mathrm{ee}}_{zz}\sin^2\theta + \hat{\chi}^{\mathrm{mm}}_{yy}/\eta_0]}, \tag{4.5a}$$

$$t = \frac{1+(\frac{\omega}{2})^2[\hat{\chi}^{\mathrm{ee}}_{xx}\hat{\chi}^{\mathrm{mm}}_{yy} + \eta_0^2\hat{\chi}^{\mathrm{ee}}_{xx}\hat{\chi}^{\mathrm{ee}}_{zz}\sin^2\theta]}{1-(\frac{\omega}{2})^2[\hat{\chi}^{\mathrm{ee}}_{xx}\hat{\chi}^{\mathrm{mm}}_{yy} + \eta_0^2\hat{\chi}^{\mathrm{ee}}_{xx}\hat{\chi}^{\mathrm{ee}}_{zz}\sin^2\theta] - \frac{i\omega}{2\cos\theta}[\eta_0\hat{\chi}^{\mathrm{ee}}_{xx}\cos^2\theta + \eta_0\hat{\chi}^{\mathrm{ee}}_{zz}\sin^2\theta + \hat{\chi}^{\mathrm{mm}}_{yy}/\eta_0]}, \tag{4.5b}$$

and the retrieval formulas are as follows:

$$\eta_0\hat{\chi}^{\mathrm{ee}}_{xx} = \frac{-2i}{\omega}\frac{r_0+t_0-1}{r_0+t_0+1}, \tag{4.6a}$$

$$\frac{\hat{\chi}^{\mathrm{mm}}_{yy}}{\eta_0} = \frac{-2i}{\omega}\frac{r_0-t_0+1}{r_0-t_0-1}, \tag{4.6b}$$

$$\sin^2\theta\eta_0\hat{\chi}^{\mathrm{ee}}_{zz} = \frac{\hat{\chi}^{\mathrm{mm}}_{yy}}{\eta_0} - \frac{2i}{\omega}\frac{r_\theta-t_\theta+1}{r_\theta-t_\theta-1}\cos\theta. \tag{4.6c}$$

Notice, in the above formulas the time dependence is assumed to be $\exp(-i\omega t)$. Also, $r_{0,\theta}$ and $t_{0,\theta}$ are, respectively, the reflection and transmission coefficients for $\theta_i = 0, \theta$. The susceptibilities are retrieved from exactly simulated reflection and transmission data for two incident angles $\theta_i = 0, 10^\circ$. The susceptibility components are then plotted in Fig. 4.1(b, c, d). As it is clear from the plots, the resonance amplitude of the magnetic susceptibility is two orders of magnitude smaller than those of the electric susceptibilities. It is in agreement with what we have expected, since there is no significant source for magnetic polarization in the metasurface. In order to examine whether these parameters are characteristic or not, the reflection amplitude and phase are plotted in Fig. 4.1(e, f) for a different incident angle ($\theta_i = 45^\circ$) using the retrieved susceptibilities from analytical formulas in (4.5) and (4.6). It is evident that the numerical results using HFSS simulation tool [49] are very well matched with the predicted results from our retrieval. Moreover, the retrieved susceptibilities respect the constraints of causality and passivity [50]; that is, the real parts of the susceptibility components are growing functions of frequency far from resonance and the sign of their imaginary parts do not change with the frequency and regarding to our assumption of the time dependence are always positive. The causal and passive behavior of the susceptibilities together with the correct prediction of reflection and transmission (not shown here) prove the applicability of our characterization model as well as its effectiveness.

Another important point is that although the particles are spherical and we may expect the normal and tangential susceptibility components (i.e., $\hat{\chi}_{zz}^{\mathrm{ee}}$ and $\hat{\chi}_{xx}^{\mathrm{ee}}$) to be the same, they are not. This is true for both their resonance frequencies and amplitudes. The reason is that these susceptibilities are the effective ones and they account also for the interaction effects between the particles in the array. Really, each sphere may be replaced by a vertical and a horizontal dipole. Therefore, since the cumulative effect of normal and horizontal dipoles are different, then it respectively influences on the effective susceptibility components. Generally, in our formalism, the effective susceptibilities may be written as:

$$\hat{\chi} = f(\alpha, \beta), \tag{4.7}$$

where $\hat{\chi}$ and α stand for the effective susceptibility and individual polarizability, respectively, while β stands for the effective interaction constant of the other elements in the array on the individual element under study. Therefore, while α_{xx} and α_{zz} are equal for all elements, the interactions are different for horizontally or vertically oriented dipoles. It implies different effective susceptibilities for different orientations of the dipoles in the array. One may refer to [10] and Publication III for more discussion on the interaction effects in arrays. We discuss this issue in the last section of the next chapter where we present the differences between amorphous and periodic metasurfaces.

So far, we successfully performed the characterization for a periodic metasurface. In the next section, however, we show that our characterization model is not restricted to periodic metasurfaces. This model even works for metasurfaces with disordered arrangement of the inclusions. In general, the applicability of our retrieval algorithm for disordered arrays keeps as long as the arrangement of particles is optically dense everywhere (all interparticle distances in the random metasurface are sufficiently smaller than the operational wavelength, see Sections 2.1.1 and 2.2 for more discussion).

4.2 A planar array of coupled plasmonic nano-patches: a disordered metasurface

In this section we present a different example of a metasurface: now it is composed of pairs of mutually coupled plasmonic nano-patches and the arrangement of these inclusions in the array is disordered. Figure 4.2(a)

demonstrates the geometry of such an array. One may refer to [51] to

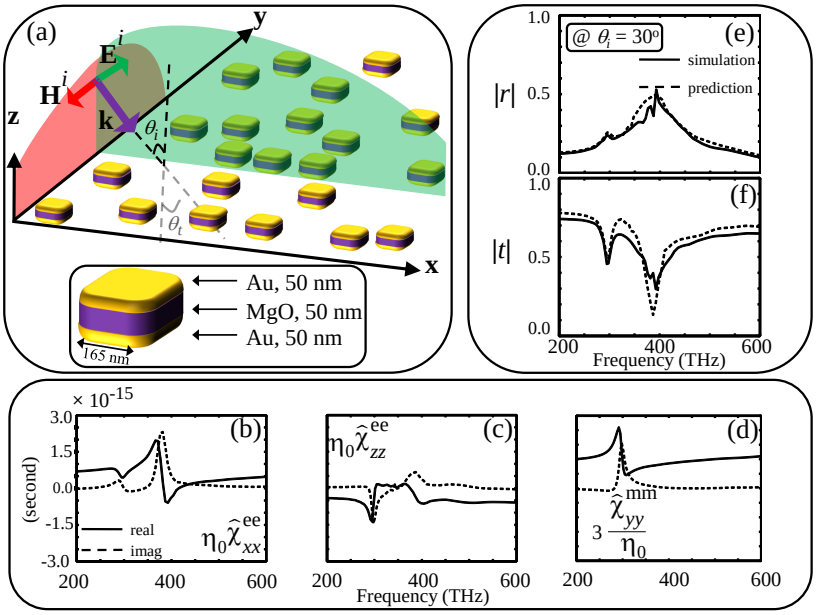

Figure 4.2. (a) A planar disordered array of gold plasmonic coupled nano-patches located at the **xy**–plane on top of a fused silica substrate with the refractive index of $n = 1.5$. The patches are separated by a dielectric spacer of MgO with the refractive index of $n = 1.72$. The array is excited by a TM-polarized electromagnetic plane wave. (b) Tangential electric (c) Normal electric and (d) Tangential magnetic effective susceptibility components of the metasurface retrieved from the reflection and transmission data at $\theta_i = 0$ and 45° from numerical Finite Difference Time Domain method [52, 53]. (e) Predicted and simulated results for the amplitude of the reflection coefficient of the proposed metasurface for an incidence of $\theta_i = 30^\circ$. (f) The same plot as in (e) for the amplitude of the transmission coefficient. The average unit cell size of the array is 510 nm. The material data for gold is taken from [48]. Notice, the time dependence is assumed to be $\exp(-i\omega t)$ in these calculations.

understand how the positional disorder is generated (when the disorder parameters varies from 0 to ∞ the array transits from strictly regular to amorphous one). The effective susceptibilities are retrieved using the same approach as in the previous example and are plotted in Fig.4.2(b, c, d). This plot corresponds to an explicit value of the disorder parameter corresponding to a quite strong randomness (adequately illustrated by the drawing). Due to the different type of inclusions, in contrast with the previous example, the magnetic response [Fig.4.2(d)] is comparable with the electric response [Fig.4.2(b, c)]. We will see later that the effective electric response is much more vulnerable to the positioning disorder compared to the magnetic response and the values of $\hat{\chi}^{\mathrm{ee}}_{xx}$ are noticeably different from those which were retrieved for a periodic analogue of this metasurface.

Figures 4.2(e) and (f) show the prediction for the reflection and transmission coefficients for and incident angle of $\theta_i = 30^\circ$ obtained through the retrieved characteristic parameters and directly by simulations. Indeed, the predicted results are in quite good agreement with the numerical results [52, 53] which demonstrates the predictive power of our approach in the characterization of disordered metasurfaces.

An important point is the anti-resonance behavior observed in the normal component of the electric susceptibility ($\hat{\chi}^{\mathrm{ee}}_{zz}$) at the frequency range of the magnetic resonance (~ 300 THz). This may be understood by recalling the averaged unit cell size of the array which is 510 nm at this frequency; i.e., $a/\lambda \approx 0.5$. The anti-resonant feature is also slightly manifested in $\hat{\chi}^{\mathrm{ee}}_{xx}$ at this frequency. To avoid the anti-resonance the high-order evanescent modes of the array must be included into the model which are out of the scope of our locally quasi-static study. More interesting is that at higher frequency ranges – that of the electric resonance (~ 400 THz), the array acts as a homogeneous metasurface. That is, the passivity and causality constraints hold while the correct prediction of the reflection and transmission are also obtained. It is not very surprising, though the effective homogeneity is respected at even higher frequencies. The condition $a/\lambda \approx 0.5$ which holds at the magnetic resonance is, in fact, that of the spatial resonance of our array. At the corresponding frequencies the features of strong spatial dispersion are obviously enhanced. These features are non-Foster behavior of the real part and wrong sign of the imaginary part of the retrieved material parameters. At the frequency of the electric resonance ($a/\lambda \approx 0.7$), the structure again becomes effectively homogeneous for the waves propagating under small angles to the normal. Beyond the lattice resonance and before condition of high-order propagating modes ($a/\lambda \geq 1$) holds, the strong spatial dispersion maybe only because of the noticeable phase shift per unit cell. However, we retrieved our characteristic parameters from data for $\theta \leq 45^\circ$ and this shift is still sufficiently small.

With these two examples, we showed the correctness and capability of our approach for the characterization of metasurfaces. In the next chapter, we characterize and discuss metasurfaces with different functionalities. These functionalities include resonant magnetic response, resonant bianisotropy, extraordinary absorption and high local field enhancement. Moreover, in some of these examples the effect of the substrate becomes crucial for the correct characterization of metasurfaces. Disordered ar-

rangements of particles are also considered in more details. Notice, in the following chapter the goal is not to prove the correctness of our homogenization approach but to illustrate some observable effects using our characterization method.

5. Functional Metasurfaces

In this chapter we present metasurfaces with differen features. These features may be physically explained using our characterization model. There are wide ranges of applications for this class of surfaces and, as we mentioned earlier, the applications of metasurfaces are rapidly developing due to their versatility. Correct understanding of these structures, results in taking more advantages out of them. With this aim, we unveil some functionalities of metasurfaces utilizing our characterization model in the following sections.

5.1 Metasurfaces with resonant magnetic response

If we apply an external electromagnetic field to a known natural atom, then the interaction between the magnetic dipole moment of that atom and the magnetic component of the external field is much weaker than the interaction of its electric dipole moment [54] with the electric component of the same field. This effect is increasing with the frequency and lead to the absence of magnetic material in the optical frequencies for known natural materials. However, magnetic materials could have many potential applications if they would exist in optics. Faster data transmission, higher storage capacity, and device miniaturization are only a few of them. Therefore, there are many attempts to obtain artificial magnetic materials at this frequency range. In the last section of the previous chapter, we presented an example of such composites with resonant magnetic response using coupled plasmonic nano-patches. An alternative solution may be the use of split-ring resonators [18]. The idea in all of these solutions is to create an electric circulating current which has a magnetic moment. We may put many of these elements together in an array to get an effective magnetic response. To show that these two solutions may

present effective magnetic response, we characterize two different periodic metasurfaces; one composed of coupled plasmonic patches and the other composed of split-ring resonators.

Figure 5.1(a) demonstrates an array of the same coupled plasmonic nano-patches as in the previous example. However, the inclusions in this case

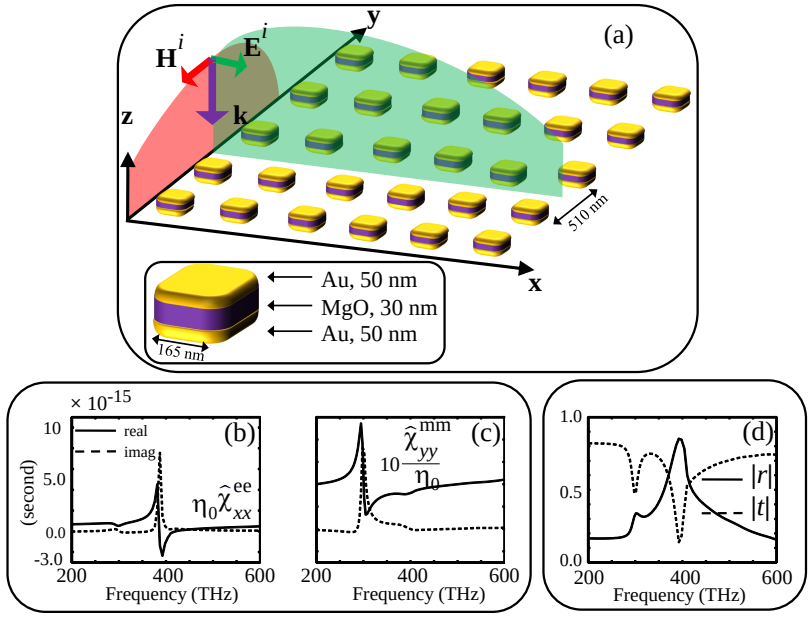

Figure 5.1. (a) A planar periodic array of gold plasmonic coupled nano-patches at the **xy**–plane at free space. The array is excited by a normally-polarized electromagnetic plane wave. (b) Tangential electric and (c) Magnetic effective susceptibility components of the metasurface retrieved from the reflection and transmission data. (d) Simulated results for the amplitude of the reflection and transmission coefficients of the proposed metasurface. The material data for gold is taken from [48]. Notice, the time dependence is assumed to be $\exp(-i\omega t)$ in these calculations.

are arranged regularly to create a periodic metasurface. Moreover, with the goal of problem simplification, we have excited this array normally rather than obliquely. This will be enough to show that the proposed metasurface has an effective magnetic response. The tangential electric and magnetic susceptibilities are calculated from the reflection and transmission data using (4.6) and then plotted in Figs. 5.1(b, c). The magnetic resonance at ~ 300 THz is obvious. Two resonances are observable from the reflection and transmission spectra shown in Fig. 5.1(d). However, it is not possible to grasp the nature of these resonances using only its reflection/transmission data without characterization. With our characterization model, we demonstrate the type of each resonance; that is, electric resonance at ~ 400 THz and magnetic resonance at ~ 300 THz.

The next example of a metasurface which demonstrates the magnetic response is sketched in Fig. 5.2(a). The metasurface is composed of split-

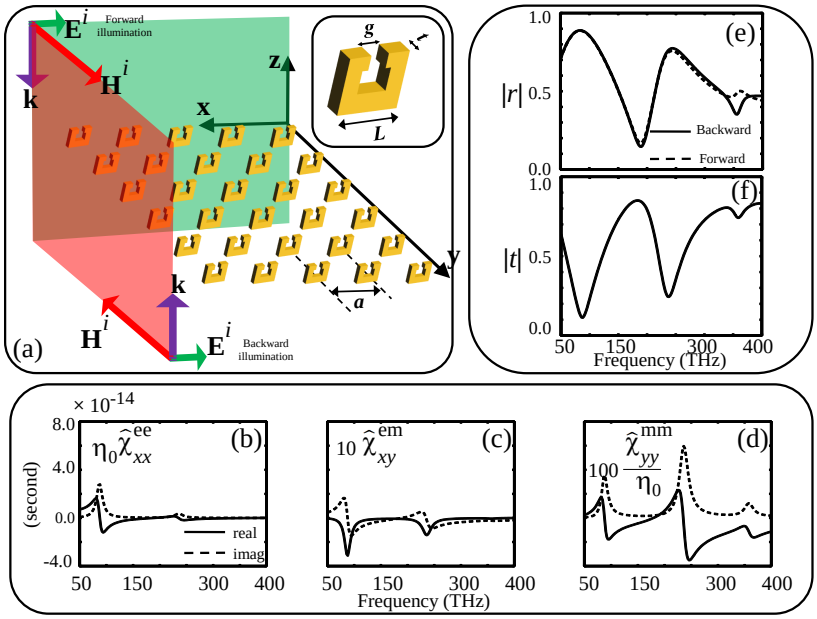

Figure 5.2. (a) A planar periodic array of gold plasmonic split-rings at the **xy**–plane put in free space. The array is excited by a normally-polarized electromagnetic plane wave. (b) Tangential electric (c) Magneto-electric and (d) Magnetic effective susceptibility components of the metasurface retrieved from the reflection and transmission data. (e) Simulated results for the amplitude of the reflection coefficients of the proposed metasurface for forward and backward directions. (f) Simulated result for the amplitude of the transmission coefficient. The unit cell size of the array is $a = 175$ nm. Other geometrical dimensions of each inclusion are: $g = 80$ nm, $t = 30$ nm, and $L = 170$ nm. The material data for gold is taken from [55]. Notice the factors 10 and 100 in front of magneto-electric and magnetic susceptibilities, respectively. Time dependence is $\exp(-i\omega t)$.

ring resonators. It is normally excited through an electromagnetic wave with its magnetic field vector $\mathbf{H}^i$ along the ring axis. This excitation, creates a circulating current which in turn produces a net magnetic moment that causes a magnetic resonance response. Again, to reduce the complexities of the problem and with the aim to prove the magnetic response we have excited this array normally. An important point in this example is the presence of magneto-electric coupling which produces a bianisotropic magneto-electric response [$\hat{\chi}^{\text{em}}_{xy}$ in Fig. 5.2(c)]. Bianisotropic metasurfaces are discussed in the next section and the retrieval formulas for this problem are given there. Here, the goal is only to show the magnetic polarization and it is obviously resonant and is mainly resulting from the magneto-electric susceptibility which is by one order of magni-

tude higher than the magnetic one (normalized to η_0) [see Fig. 5.2(c, d)]. Again, one may not explicitly claim a magneto-electric and magnetic response from only the reflection or transmission data in Fig. 5.2(e) or (f). The magnetic and magneto-electric responses are not distinguishable a priori. To understand which of them is dominating one needs to correctly characterize the metasurface. And this tool is given by our characterization method. It turns out that the magnetic susceptibility of the array of SRRs is pretty small. This result fits the known theoretical models which show the saturation of the magnetic response of metal rings in the optical range due to the high kinetic inductance of the Drude electron gas (see e.g. in [2]). However, the important and new thing is that the biansiotropy of the split-ring results in a non-negligible magnetization of the metasurface (by electric field). On the contrary, an array of dual patches does not possess bianisotropy and its magnetic response has the resonance magnitude much closer to that of the electric one (only five times smaller than the latter normalized to η_0^2).

Another issue regards the asymmetric reflection for the illumination from forward and backward directions [Fig. 5.2(e)]. It will be discussed in the next section. In the present case, when the optically contrast substrate is absent, this asymmetry is related to the bianisotropy in the metasurface.

The last important issue is the difference between the resonances of coupled patches and split-rings. The electric, bianisotropic and magnetic resonances in the split-ring have the same resonance frequencies while for the coupled patches the electric and magnetic ones are detached. Figure 5.3 schematically demonstrates what is happening for an individual particle in these two designs when the particles are excited as in Fig. 5.1 and 5.2. Indeed, the different resonant behavior in the two cases corresponds to the difference in the creation of the electric currents in these two examples. In the split-ring, the electrical length ($\propto L_{\mathrm{SRR}}$) of the current which is responsible for the electric and magnetic resonances f_{e} and f_{m} are the same and are proportional to its total length [Fig. 5.3(a,c)]. However, in the coupled patches, the electrical length for the magnetic resonance ($\propto 2L_{\mathrm{patch}}$) is roughly proportional to two times of that for the electric resonance ($\propto L_{\mathrm{patch}}$) [Fig. 5.3(b,d)]. This is why in the coupled patch metasurface example, the magnetic resonance frequency f_{m} is roughly one half of its electric resonance frequency f_{e} [Fig. 5.1(b, c) and Fig. 5.2(b, d)].

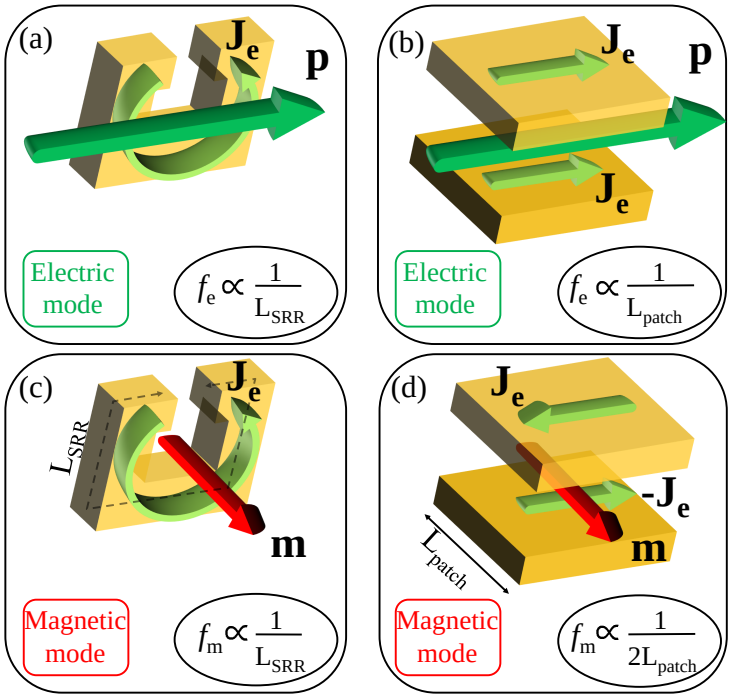

Figure 5.3. Schematic representation for the (a, b) electric and (c, d) magnetic modes for an individual split-ring resonator of Fig. 5.2(a) and a single coupled patch element of the array in Fig. 5.1(a). The total average length of the split-ring resonator is demonstrated by L_{SRR} and the length of each patch is denoted by L_{patch}.

As we promised, the next section is devoted to bianisotropic metasurfaces where an array of split-rings will be revisited as realizing a specific type of bianisotropy; i.e., omega-type bianisotropy. We then continue with two design examples which mimic the bianisotropic response in metasurfaces. After that, we present an important result of metasurfaces supported by a highly-refractive dielectric substrate. Therein, the effect of *substrate-induced bianisotropy* is discussed. Finally, we conclude the section with discussing an important advantage of this class of metasurfaces; that is, perfect absorbance. In the whole upcoming process, our characterization model shows off in the proof of the bianisotropy in metasurfaces under study.

5.2 Bianisotropic metasurfaces

As it is defined in the literature [26] and was mentioned in Section 2.2, bianisotropy is briefly defined as the electric response of a material to

a magnetic excitation field and, vice versa, its magnetic response to an electric excitation field. This concept is formulated in equations (3.29) and (3.30) as electro-magnetic and magneto electric effective polarizability ($\hat{\bar{\alpha}}^{\rm me}$ and $\hat{\bar{\alpha}}^{\rm em}$) or susceptibility ($\hat{\bar{\chi}}^{\rm me}$ and $\hat{\bar{\chi}}^{\rm em}$) tensors as the characteristic parameters of metasurfaces, respectively. Bianisotropic metasurfaces may have many potential applications including wave polarizers, absorbers, Huygens surfaces, non-reciprocal surfaces, and planar antennas, to name only a few. Therefore, their analysis would be very important and the milestone is to correctly characterize them in order to have a perfect design. According to [26], there are four general types of bianisotropy in materials; that is, reciprocal omega, reciprocal chiral, non-reciprocal Tellegen, and non-reciprocal "moving". There are also many approaches to design different type of bianisotropic elements and metasurfaces [56, 57]. However, in the present work we present one of these four classes which is much easier to implement in optics; that is, reciprocal omega-type bianisotropy. In the tensor formalism, an omega-type bianisotropy should have the following specifications [26]:

- The diagonal terms in $\hat{\bar{\chi}}^{\rm me}$ and $\hat{\bar{\chi}}^{\rm em}$ must be zero.

- If we decompose tensors $\hat{\bar{\chi}}^{\rm me}$ and $\hat{\bar{\chi}}^{\rm em}$ into symmetric and antisymmetric parts; i.e., $\hat{\bar{\chi}}_{\rm sym} = (\hat{\bar{\chi}} + \hat{\bar{\bar{\chi}}})/2$ and $\hat{\bar{\chi}}_{\rm asym} = (\hat{\bar{\chi}} - \hat{\bar{\bar{\chi}}})/2$, then the symmetric part must be zero.

- For reciprocal media, in general, we have: $\hat{\bar{\chi}}^{\rm me} = -\hat{\bar{\chi}}^{\rm em}$.

Physically, for an omega-type bianisotropic metasurface, it means that the orientation of the magnetic moment which is induced by the electric field is orthogonal to the induced electric moment by the same electric field. For example, the split-ring resonators [Fig. 5.2(a)] have an omega-type bianisotropy, since the induced magnetic polarization $\mathcal{M}_y$ and electric polarization $\mathcal{P}_x$ are orthogonal.

5.2.1 Split-ring resonators make an omega-type bianisotropic metasurface

We may consider all 36 susceptibility parameters to fully and correctly characterize our metasurface of omega-type array of split-ring resonators. However, this would be very complicated and make the problem diffi-

cult to solve. Therefore, we make use of all our a priori knowledge in making the problem as simple as possible with least unknown characteristic parameters. According to the discussion in Section 4.1, the only nonzero susceptibility terms associated with the specific excitation shown in Fig. 5.2(a) would be $\hat{\chi}_{\mathrm{xx}}^{\mathrm{ee}}$, $\hat{\chi}_{\mathrm{yy}}^{\mathrm{mm}}$, and $\hat{\chi}_{\mathrm{xy}}^{\mathrm{em}} = -\hat{\chi}_{\mathrm{yx}}^{\mathrm{me}}$. In the mentioned example of split-ring resonators and all of the other examples we are going to present from now on, we put our particles in a way that we get the same nonzero terms. Using our homogenization model, we may solve the problem for normal incidence to get the reflection and transmission coefficients as:

$$r_{\pm} = \frac{-\frac{i\omega}{2}[\eta_0\hat{\chi}_{xx}^{\mathrm{ee}} \pm (\hat{\chi}_{yx}^{\mathrm{me}} - \hat{\chi}_{xy}^{\mathrm{em}}) - \hat{\chi}_{yy}^{\mathrm{mm}}/\eta_0]}{1 - (\frac{\omega}{2})^2[\hat{\chi}_{xx}^{\mathrm{ee}}\hat{\chi}_{yy}^{\mathrm{mm}} - \hat{\chi}_{yx}^{\mathrm{me}}\hat{\chi}_{xy}^{\mathrm{em}}] - \frac{i\omega}{2}[\eta_0\hat{\chi}_{xx}^{\mathrm{ee}} + \hat{\chi}_{yy}^{\mathrm{mm}}/\eta_0]}, \tag{5.1a}$$

$$t = \frac{1 + (\frac{\omega}{2})^2[\hat{\chi}_{xx}^{\mathrm{ee}}\hat{\chi}_{yy}^{\mathrm{mm}} - \hat{\chi}_{yx}^{\mathrm{me}}\hat{\chi}_{xy}^{\mathrm{em}}]}{1 - (\frac{\omega}{2})^2[\hat{\chi}_{xx}^{\mathrm{ee}}\hat{\chi}_{yy}^{\mathrm{mm}} - \hat{\chi}_{yx}^{\mathrm{me}}\hat{\chi}_{xy}^{\mathrm{em}}] - \frac{i\omega}{2}[\eta_0\hat{\chi}_{xx}^{\mathrm{ee}} + \hat{\chi}_{yy}^{\mathrm{mm}}/\eta_0]}, \tag{5.1b}$$

Note that r_+ and r_- stand for the reflection from the forward and backward directions, respectively, and t is the transmission coefficient. Also, for our reciprocal omega-type bianisotropy $\hat{\chi}_{yx}^{\mathrm{me}} = -\hat{\chi}_{xy}^{\mathrm{em}}$. Also, due to the geometrical asymmetry, the reflection coefficients are different when the metasurface is illuminated from the forward and backward directions. However, if we carelessly do not consider this asymmetry, then we may neglect an important factor in the correct characterization. For example, if we use the same characterization model as we did in the first example of the previous section (identical coupled nano-patches), then we may obtain nonphysical characteristic parameters. Moreover, even if we get physical retrieved parameters from the forward data, they would not correctly predict the reflection of the metasurface for the backward direction [58]. Therefore, we must add the bianisotropic terms $\hat{\chi}_{\mathrm{xy}}^{\mathrm{em}}$ and $\hat{\chi}_{\mathrm{yx}}^{\mathrm{me}}$ in our characterization model in order to achieve physical results. Solving equations (5.1) for the susceptibility components leads to:

$$\eta_0\hat{\chi}_{xx}^{\mathrm{ee}} = -\frac{2i}{\omega}\left[1 - \Delta\left(1 + t - \frac{r_+ + r_-}{2}\right)\right], \tag{5.2a}$$

$$\frac{\hat{\chi}_{yy}^{\mathrm{mm}}}{\eta_0} = -\frac{2i}{\omega}\left[1 - \Delta\left(1 + t + \frac{r_+ + r_-}{2}\right)\right], \tag{5.2b}$$

$$\hat{\chi}_{xy}^{\mathrm{em}} = -\hat{\chi}_{yx}^{\mathrm{me}} = -\frac{2i}{\omega}\Delta\left(\frac{r_+ - r_-}{2}\right). \tag{5.2c}$$

In the above equations

$$\Delta = \frac{2}{(1+t)^2 + \left(\frac{r_+ - r_-}{2}\right)^2 - \left(\frac{r_+ + r_-}{2}\right)^2}. \tag{5.3}$$

The retrieved susceptibility components for an array of split–ring resonators are given in Fig. 5.2(b, c, d). Notice, $\hat{\chi}^{\mathrm{em}}_{xy} = -\hat{\chi}^{\mathrm{me}}_{yx}$. The presence of the bianisotropic response is obvious from Fig. 5.2(c). Moreover, the magnetic response in the present metasurface is mainly due to this bianisotropic term. This is becaues the magnetic susceptibility $\hat{\chi}^{\mathrm{mm}}_{yy}$ [Fig. 5.2(d)] is two orders of magnitude smaller than the electric susceptibility $\hat{\chi}^{\mathrm{ee}}_{xx}$ [Fig. 5.2(b)] and an order of magnitude smaller than the magneo-electric susceptibility component $\hat{\chi}^{\mathrm{em}}_{xy}$ [Fig. 5.2(c)].

An alternative design solution, for a bianisotropic metasurface, which is more convenient for implementation in optics, is the topic of the next section. More advantages associated with this design will be discussed later in Section 5.3.

5.2.2 Nonidentical coupled plasmonic nano-patches: an omega-type bianisotropic metasurface

Another topology which has the omega-type bianisotropy in metasurfaces is shown in Fig. 5.4(a). Each element in the metasurface is composed of two gold nano-patches with different lateral dimensions W_1 and W_2. Notice that a similar topology was presented in Sections 4.2 and 5.1 in Figs. 4.2(a) and 5.1(a). However, in those examples, the two coupled nano-patches were identical. Therefore, although those metasurfaces resulted in magnetic response, they could not offer bianisotropic response. The asymmetry in the present geometry obviously results in asymmetric reflection coefficients for the forward and backward directions [Fig. 5.4(e)]. This is correctly characterized through a magneto-electric susceptibility shown in Fig. 5.4(c). Again, note that in the present example in contrast with the split-ring resonator [Fig. 5.2], the electric and magnetic resonance modes are detached. This is, as discussed before, due to the different resonant lengths of these two modes in this structure. Beside its easier implementation in optics, the present topology is capable of gifting a perfect absorbance which is going to be discussed in Section 5.3. Furthermore, the proposed absorber is not fully reflective out of its resonance band from the opposite direction; that is, $|r_-| \neq 1$ while the absorbance is nearly perfect in the forward illumination direction. This is in contrast with reflector-backed absorbers.

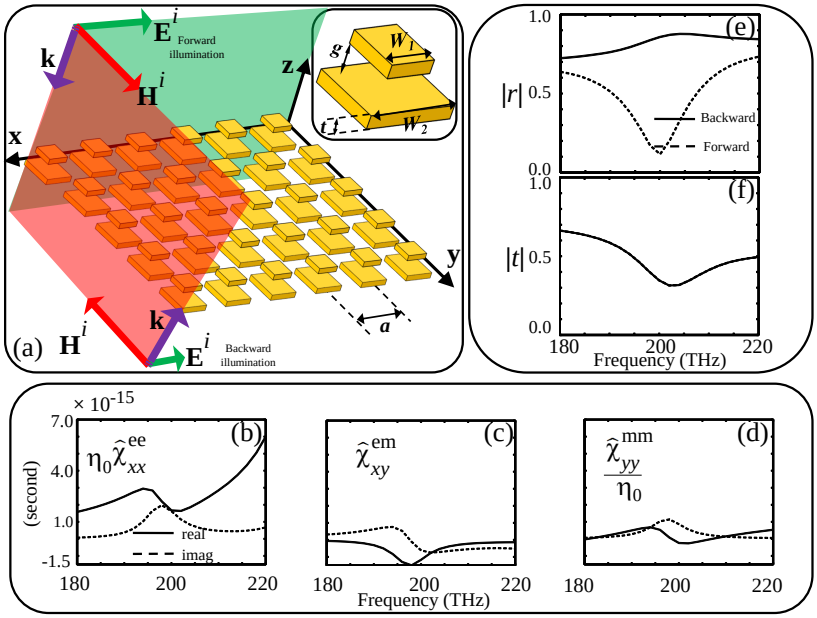

Figure 5.4. (a) A planar periodic array of coupled plasmonic nano-patches of gold positioned in the **xy**–plane at free space. The array is excited by a normally-polarized electromagnetic plane wave. (b) Tangential electric (c) Magneto-electric and (d) Magnetic effective susceptibility components of the metasurface retrieved from the reflection and transmission data using equations (5.2). (e) Simulated results for the amplitude of the reflection coefficients of the proposed metasurface for forward and backward directions. (f) Simulated result for the amplitude of the transmission coefficient. The unit cell size of the array is $a = 300$ nm. Other geometrical parameters of each inclusion are: $g = 8$ nm, $t = 50$ nm, $W_1 = 175$ nm, and $W_2 = 250$ nm. The material data for gold is taken from [48]. Notice, the time dependence is assumed to be $\exp(-i\omega t)$ in these calculations.

Before continuing the discussion on the absorbance, we first unveil an important result of correct characterization of metasurfaces which deals with bianisotropy. That is, *substrate-induced bianisotropy* which is a result of the contrast between the two media in which our metasurfaces may be positioned in between. More discussions are going to be presented in the following section.

5.2.3 Substrate-induced bianisotropy in metasurfaces

Metasurfaces including metafilms and metascreens (see Section 2.1.4) are very thin sheets of resonant structures. As a result, for mechanical reasons they need to be supported by bulk substrates or superstrates in order to be practically applicable. However, refractive dielectric substrates certainly modify the properties of these resonant surfaces.

The problem of finding the reflection/transmssion of an electrically dense

array of resonant dipoles located on a dielectric interface dates back to nearly a century. The attempts to solve the problem in the quasi-static regime started by Strachan in 1930s [36] and then completed by Sivukhin in 1950s [59, 60]. Later, other researchers [61, 62, 63, 64, 65, 66, 67, 68, 69, 70] have tried to develop previous works. However, none of them succeeded to be satisfactory due to incomplete approaches by the authors. A complete overview of the problem may be found in Publication I and Publication II. To sum up, the presented approaches either were not suitable for resonant grids or they could not correctly predict the reflection coefficient. More importantly, none of them were appropriate for substrates with a high index of refraction.

The reason for unsuccessful attempts was neglecting the bianisotropy associated with metasurfaces when supported by substrates. Indeed, all metasurfaces independent of their type; that is, either bianisotropic or non-bianisotropic ones, when put at the interface of two different media would present a bianisotropic response. This is due to the contrast between the two media which surround the metasurface on its both sides. This results in breaking the symmetry and, hence, introducing bianisotropy. This implies a different characterization model. We refer this effect as *substrate-induced bianisotropy* since it is an outcome of the modulation of a resonant metasurface with a refractive substrate. This would not happen if one of these two factors are absent; that is, metasurface or substrate. But, what is really happening in the microscopic level?

Consider a plasmonic nano-particle on top of a refractive substrate with the relative permittivity ϵ_r as in Fig. 5.5(a). Now, we apply an external electromagnetic field to this particle. We assume that the particle size is enough smaller than the wavelength of the applied field in the surrounding media. As it is well known [71], an electric polarization current $\mathbf{J}_\mathrm{e}$ is induced on this particle that creates a dipole moment $\mathbf{p}$. However, this is not the whole story in the presence of a substrate. If we carefully look at the local fields [see in Publication I] in the vicinity of the particle, a field concentration is clearly observable partially in the particle, and to some extent beneath the particle, in the substrate [Fig. 5.5(a)]. This concentration is often called hot spot. Therefore, in addition to the induced $\mathbf{J}_\mathrm{e}$ in the particle, an electric current $\mathbf{J}'_\mathrm{e}$ is induced in the substrate. If the moduli of the permittivity of the particle and the substrate are in the same order then these two currents are comparable in amplitude. There is a frequency range in which these two currents are in-phase. This is the

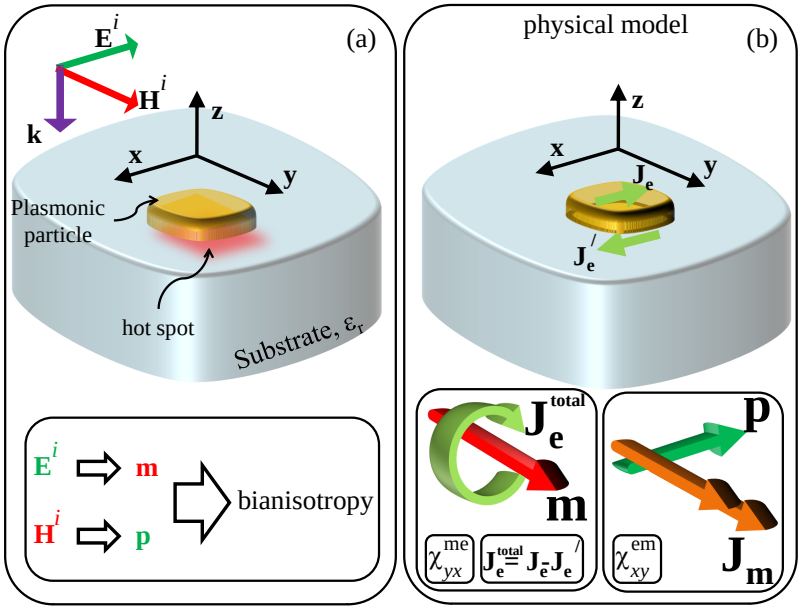

Figure 5.5. (a) The creation of the hot spot for a plasmonic particle on top of a substrate with refractive index $n = \sqrt{\epsilon_r}$ which is exposed by an electromagnetic wave $\{E^i, H^i, k\}$. (b) The physical model which explains the bianisotropy induced by the substrate for the proposed plasmonic particle in (a).

ordinary known electric mode region and the characterization leads to an electric susceptibility χ_{xx}^{ee} for an array of such particles.

However, there are some frequencies at which the induced electric currents $\mathbf{J}_\text{e}$ and $\mathbf{J}_\text{e}'$ are out of phase and comparable in the amplitude; that is, $\mathbf{J}_\text{e} \approx -\mathbf{J}_\text{e}'$. Notice, they would not be equal. This implies a nonsymmetric circulating current $\mathbf{J}_\text{e}^{\text{total}}$ that creates a magnetic dipole moment $\mathbf{m}$. However, due to the asymmetric origination of this current, an array of such particles must be characterized by a bianisotropic response χ_{yx}^{me}. A dual scenario is true for the magnetic field $\mathbf{H}^i$ and the birth of the induced electric dipole moment $\mathbf{p}$ which results in χ_{xy}^{em}. Also, since the induced magnetic moment $\mathbf{m}$ and the applied electric field $\mathbf{E}^i$ are orthogonal, this results in an omega-type bianisotropy. Therefore, the same characterization model as in omega-type bianisotropic metasurfaces of Section 5.2.1 is applicable in this case. However, the formulation must be modified to consider the effect of substrate. To elaborate the discussion, we present the example of a planar array of plasmonic nano-spheres of Section 4.1 in the following section. However, we put the proposed array on top a dielectric substrate.

A substrated metasurface of plasmonic nano-spheres

Let us consider the metasurface example of Section 4.1 at the interface of two different media with the permittivity $\epsilon_{\pm}$ ($+$ for $z>0$ and $-$ for $z<0$). According to our last discussions, this metasurface may be considered as an omega-type metasurface. Applying our homogenization methodology in Section 3.5 for the average field concept, the reflection and transmission coefficients for the TM polarization in Fig. 4.1 read as:

$$r_{\pm} = \frac{N_r}{\Delta}, \tag{5.4a}$$

$$\frac{t_{\pm}}{\cos\theta_{\pm}\sqrt{\epsilon_{+}\epsilon_{-}}} = \frac{1+\left(\frac{\omega}{2}\right)^2\left[\hat{\chi}^{\mathsf{ee}}_{xx}\hat{\chi}^{\mathsf{mm}}_{yy}-\hat{\chi}^{\mathsf{em}}_{xy}\hat{\chi}^{\mathsf{me}}_{yx}\right]+\frac{\eta^2}{\epsilon_{\pm}}\sin^2\theta\hat{\chi}^{\mathsf{ee}}_{xx}\hat{\chi}^{\mathsf{ee}}_{zz}}{\Delta}, \tag{5.4b}$$

where

$$\begin{aligned}
N_{r_{\pm}} &= \left[\epsilon_{\pm}\cos\theta_{\mp}-\epsilon_{\mp}\cos\theta_{\pm}\right] \\
&\quad +i\omega\left[\cos\theta_{+}\cos\theta_{-}\eta\hat{\chi}^{\mathsf{ee}}_{xx}-\frac{\epsilon_{+}+\epsilon_{-}}{2}\sin^2\theta\eta\hat{\chi}^{\mathsf{ee}}_{zz}\right. \\
&\qquad \left.-\epsilon_{+}\epsilon_{-}\frac{\hat{\chi}^{\mathsf{mm}}_{yy}}{\eta}\mp\left(\epsilon_{+}\cos\theta_{-}+\epsilon_{-}\cos\theta_{+}\right)\hat{\chi}^{\mathsf{em}}_{xy}\right] \\
&\quad -\left(\frac{\omega}{2}\right)^2\left[\left(\epsilon_{\pm}\cos\theta_{\mp}-\epsilon_{\mp}\cos\theta_{\pm}\right)\left(\hat{\chi}^{\mathsf{ee}}_{xx}\hat{\chi}^{\mathsf{mm}}_{yy}-\hat{\chi}^{\mathsf{em}}_{xy}\hat{\chi}^{\mathsf{me}}_{yx}\right)\right. \\
&\qquad \left.-\sin^2\theta\eta\hat{\chi}^{\mathsf{ee}}_{zz}\{\left(\cos\theta_{\pm}-\cos\theta_{\mp}\right)\eta\hat{\chi}^{\mathsf{ee}}_{xx}-\left(\epsilon_{\pm}-\epsilon_{\mp}\right)\hat{\chi}^{\mathsf{em}}_{xy}\}\right],
\end{aligned}$$

and

$$\begin{aligned}
\Delta &= \left[\epsilon_{+}\cos\theta_{-}+\epsilon_{-}\cos\theta_{+}\right] \\
&\quad -i\omega\left[\cos\theta_{+}\cos\theta_{-}\eta\hat{\chi}^{\mathsf{ee}}_{xx}+\frac{\epsilon_{+}+\epsilon_{-}}{2}\sin^2\theta\eta\hat{\chi}^{\mathsf{ee}}_{zz}\right. \\
&\qquad \left.+\epsilon_{+}\epsilon_{-}\frac{\hat{\chi}^{\mathsf{mm}}_{yy}}{\eta}+\left(\epsilon_{+}\cos\theta_{-}-\epsilon_{-}\cos\theta_{+}\right)\hat{\chi}^{\mathsf{em}}_{xy}\right] \\
&\quad -\left(\frac{\omega}{2}\right)^2\left[\left(\epsilon_{+}\cos\theta_{-}+\epsilon_{-}\cos\theta_{+}\right)\left(\hat{\chi}^{\mathsf{ee}}_{xx}\hat{\chi}^{\mathsf{mm}}_{yy}-\hat{\chi}^{\mathsf{em}}_{xy}\hat{\chi}^{\mathsf{me}}_{yx}\right)\right. \\
&\qquad \left.-\sin^2\theta\eta\hat{\chi}^{\mathsf{ee}}_{zz}\{\left(\cos\theta_{+}+\cos\theta_{-}\right)\eta\hat{\chi}^{\mathsf{ee}}_{xx}+\left(\epsilon_{+}-\epsilon_{-}\right)\hat{\chi}^{\mathsf{em}}_{xy}\}\right],
\end{aligned}$$

In the above equations, $\begin{smallmatrix}\mathsf{top}\\ \mathsf{bottom}\end{smallmatrix}$ sign refers to the illumination from $\begin{smallmatrix}\mathsf{forward},\, z>0\\ \mathsf{backward},\, z<0\end{smallmatrix}$ (see in Fig. 4.1) direction. Also, θ denotes the incidence angle, and $\cos\theta_{\pm}=\sqrt{\epsilon_{\pm}-\sin^2\theta}$. Notice, η is the characteristic impedance of the medium in which we assume that the metasurface is put in. It would be not η_{+} nor η_{-}. Also note that the definition for the reflection/transmission is based on the fields and not power; this is why $t_{+}\cos\theta_{-}=t_{-}\cos\theta_{+}$. Another important point is that equations (5.4) transit to our previous examples: that is, in the case of a uniform host medium and when bianisotropy is absent ($\hat{\chi}^{\mathsf{em}}_{xy}=0$), equations (5.4) and (4.5) are equal. Moreover, for the case

of the normal incidence and uniform host medium and in the presence of bianisotropy, equations (5.4) transit to (5.1).

Solving (5.4) for the susceptibility components in the general case is cumbersome. However, we have suggested an algorithm in Publication I to numerically solve these equations for the susceptibility components using two sets of reflection and transmission data for two different incident angles. One may perform another simplification for a plasmonic grid of nano-spheres. It is appropriate to neglect $\hat{\chi}_{yy}^{\mathrm{mm}}$, since we proved in Section 4.1 that its resonance amplitude is two orders of magnitude smaller than those of the electric susceptibilities $\hat{\chi}_{xx}^{\mathrm{ee}}$ and $\hat{\chi}_{zz}^{\mathrm{ee}}$ [Fig.4.1(b, c, d)].

Next, we put the proposed metasurface on top of two different dielectric substrates; one with $\epsilon_- = \epsilon_r = 2$ and the other with $\epsilon_- = \epsilon_r = 12.8$. Notice, for both cases $\epsilon_+ = 1$, since it is assumed to be free space. The most pronounced susceptibility components $\hat{\chi}_{xy}^{\mathrm{em}}$, $\hat{\chi}_{xx}^{\mathrm{ee}}$ and $\hat{\chi}_{zz}^{\mathrm{ee}}$ are retrieved from two sets of reflection/transmission data at $\theta = 0$ and 10° and then the results are plotted in Fig. 5.6. As it is obvious from Fig. 5.6(e, f), both cases represent a bianisotropic response in addition to their tangential electric [Fig. 5.6(a, b)] and normal electric [Fig. 5.6(c, d)] responses, in their effective characterization modeling. However, this response is two times stronger for the case of the higher permittivity substrate. It is reasonable, since the bianisotropy effect is associated with the asymmetry in the structure; that is, a more asymmetric structure (here the contrast between the two surrounding media) results in a stronger effective bianisotropic response. This conclusion is more elaborated in Fig. 5.7 by predicting the reflection amplitude and phase for the incident angle of $\theta = 45^\circ$. As it is clear from the plots of this figure, the predicted reflection coefficient is much more deviated from the simulated results when we neglect the effective bianisotropy response (dashed lines) for $\epsilon_r = 12.8$ than for $\epsilon_r = 2$. This proves that the bianisotropy should always be considered when a metasurface is supported by a substrate which is different from the superstrate. However, it may be neglected when the substrate permittivity is not very high and should be certainly considered when the contrast between the substrate and the superstrate is high. This is why the works by Yamaguchi *et al.* [68, 69, 70] and others [61, 62, 63, 64, 65, 66] could not correctly predict the reflection/transmission behavior of plasmonic arrays when supported by a highly refractive substrate.

There are also other situations when the effective bianisotropic response may be neglected. For example, a plasmonic metasurface which is very

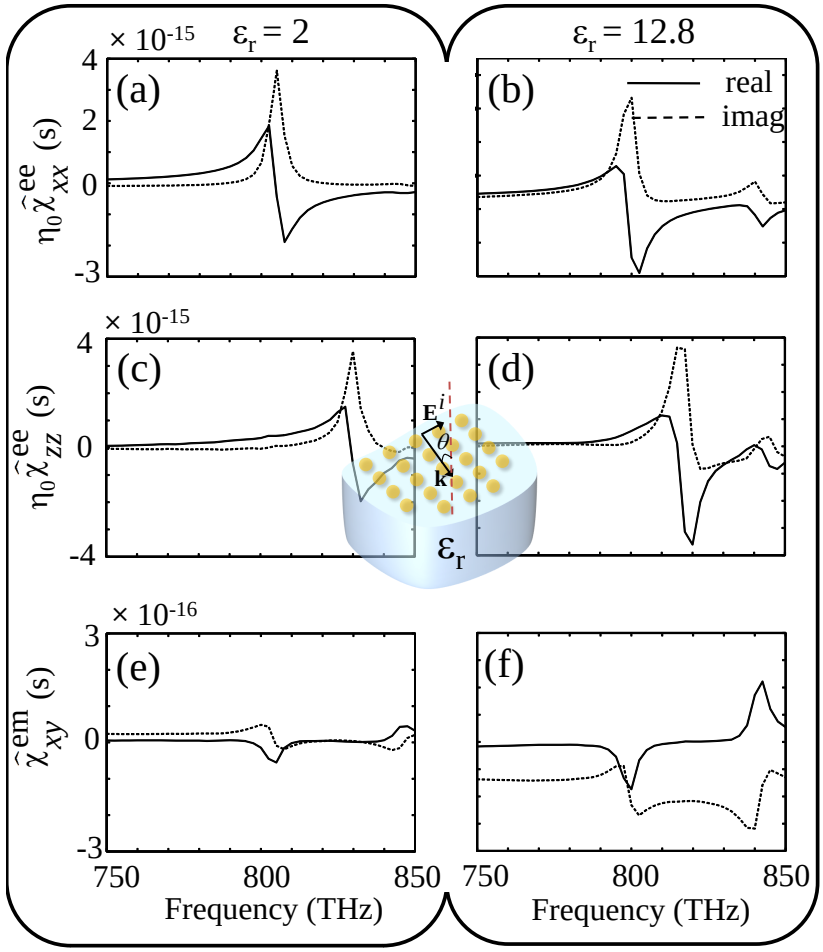

Figure 5.6. Retrieved (a) tangential electric (c) normal electric and (e) tangential magneto-electric effective susceptibility components of the metasurface in the example of Section 4.1 [Fig. 4.1] when supported by a substrate with the relative permittivity $\epsilon_r = 2$. (b), (d), (f) similar plots for the case when the substrate relative permittivity is $\epsilon_r = 2$.

thin compared to the skin depth of the material which is used in the metasurface. Also, it is possible to cancel the intrinsic bianisotropy of a metasurface using *substrate-induced bianisotropy* concept. Indeed, adding the substrate may reduce or increase the intrinsic bianisotropy in a general bianisotropic metasurface, depending on the design. However, we do not discuss this issue here. One may refer to [58] for more discussions on this concept.

In the next section, however, we are going to take the advantage of bianisotropy concept (both intrinsic and substrate-induced) in order to get an important regime called “perfect absorbance”. In this regime, no electromagnetic field may be transmitted through or reflected back from the

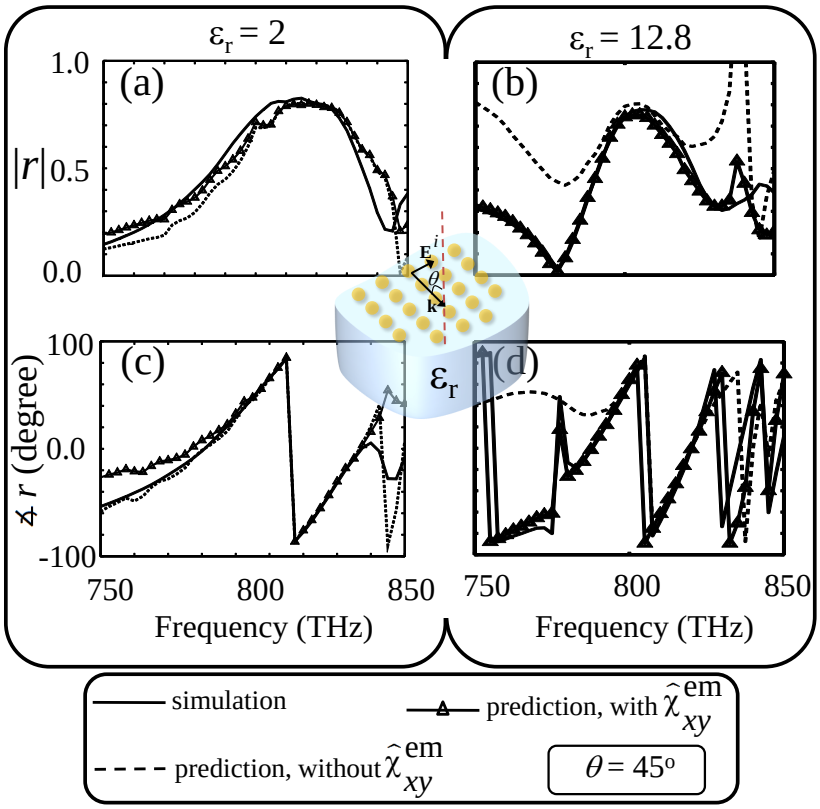

Figure 5.7. Predicted and simulated results for an incidence of $\theta_i = 45°$, considering (triangular-marked lines) and neglecting (dashed lines) the effect of bianisotropy for the (a) amplitude and (c) phase of the reflection coefficient of the proposed metasurface located on a substrate with $\epsilon_r = 2$. (b), (d) Corresponding results for as in (a) and (c) when the substrate relative permittivity is $\epsilon_r = 12.8$.

metasurface. Instead, it will be locally concentrated within and/or around the metasurface. There are many works devoted to this class of metasurfaces [9, 72, 73, 74, 75, 76, 77, 78, 79, 80]. Our contribution is to introduce two design solutions for omega-type bianisotropic perfect absorbers. The advantage of our bianisotropic metasurface is to provide an asymmetric reflection for illumination from different directions. Moreover, in contrast to the reflector backed metasurface absorbers, our proposal, does not reflect the whole incident waves out of the metasurface resonance band from the opposite direction. This is very useful for applications where we have many transmitting/recieving systems and we still need to use an absorber for a particular frequency band without prohibiting the operation of other systems.

5.3 Perfect metasurface absorbers with bianisotropic responses

It is well known that the perfect absorbance regime ($r = t = 0$) in metasurfaces may happen if both the electric and magnetic polarization currents associated with the metasurface are excited together [81] when illuminated by an electromagnetic wave. Notice, these two polarization currents must be orthogonal to each other in reciprocal metasurfaces in order to be capable of a perfect absorbance [46, 82]. The simplest metasurface design, capable of achieving such a regime, is one which may be characterized by two effective electric $\hat{\chi}^{\mathrm{ee}}_{xx}$ and magnetic $\hat{\chi}^{\mathrm{mm}}_{yy}$ susceptibilities in our formalism. Notice, we assumed that the metasurface is located in the **xy**–plane and is illuminated normally by an x-polarized plane electromagnetic wave [see e.g. Fig. 5.8 and Fig. 5.10]. As it is shown in Publication IV, the condition for perfect absorbance at normal incidence in terms of these two susceptibilities read as:

$$\eta\hat{\chi}^{\mathrm{ee}}_{xx} = \frac{\hat{\chi}^{\mathrm{mm}}_{yy}}{\eta} = \frac{2i}{\omega}, \tag{5.5}$$

where η is the characteristic impedance of the host medium surrounding the metasurface. This condition is called "*balance condition*" for a metasurface without bianisotropy which is illuminated at normal incidence. This insures zero reflection and transmission from the metasurface of isolated particles (metafilm) for the illumination from both directions. However, we aim at bianisotropic metasurfaces with an additional degree of freedom. Therefore, we need to add the extra term $\hat{\chi}^{\mathrm{em}}_{xy}$ to our calculations. Notice, we are interested in omega-type bianisotropy which is the only option in reciprocal metasurfaces that are capable of being perfect absorbers. For a discussion on different types of bianisotropy and the perfect absorbance one may refer to [46, 82]. Since we are dealing with a bianisotropic metasurface, then it is important to distinguish between the perfect absorbance from forward ($r_+ = t = 0$, $r_- \neq 0$ in equations (5.1)) or backward ($r_- = t = 0$, $r_+ \neq 0$ in equations (5.1)) direction. Note that for the reciprocal metasurface absorbers, the transmission coefficient must be zero for both illumination directions. As a result, for an omega-type bianisotropic metasurface located in a uniform host medium when illuminated normally, the balance conditions according to equations (5.1), read

as:

$$\eta\hat{\chi}_{xx}^{\mathrm{ee}} = \frac{2i}{\omega}\,\left[1 \mp (\frac{\omega}{2i})\,\hat{\chi}_{xy}^{\mathrm{em}}\right], \tag{5.6a}$$

$$\frac{\hat{\chi}_{yy}^{\mathrm{mm}}}{\eta} = \frac{2i}{\omega}\,\left[1 \pm (\frac{\omega}{2i})\,\hat{\chi}_{xy}^{\mathrm{em}}\right], \tag{5.6b}$$

$$\hat{\chi}_{xy}^{\mathrm{em}} = \pm\frac{2i}{\omega} r_{\mp}. \tag{5.6c}$$

Notice, the $\substack{\text{top}\\\text{bottom}}$ sign refers to the case of perfect absorbance for the illumination from $\substack{\text{forward}\\\text{backward}}$ direction. These equations reduce to:

$$\eta\hat{\chi}_{xx}^{\mathrm{ee}} = \left(\frac{1 \mp (\frac{\omega}{2i})\,\hat{\chi}_{xy}^{\mathrm{em}}}{1 \pm (\frac{\omega}{2i})\,\hat{\chi}_{xy}^{\mathrm{em}}}\right)\,\frac{\hat{\chi}_{yy}^{\mathrm{mm}}}{\eta}, \tag{5.7a}$$

$$\hat{\chi}_{xy}^{\mathrm{em}} = \pm\frac{2i}{\omega} r_{\mp}. \tag{5.7b}$$

in term of the magneto-electric term $\hat{\chi}_{xy}^{\mathrm{em}}$. It is very instructive to see that parameter $\kappa = \left(\frac{1\mp(\frac{\omega}{2i})\,\hat{\chi}_{xy}^{\mathrm{em}}}{1\pm(\frac{\omega}{2i})\,\hat{\chi}_{xy}^{\mathrm{em}}}\right)$ may be considered as the correction factor to the equation (5.5) for bianisotropic metasurfaces. This is an additional degree of freedom in omega-type bianisotropic metasurfaces which offers the possibility to have both regimes of perfect absorbance and asymmetric resonant reflectance[1] together.

At the next step, we present two different design solutions of nearly perfect bianisotropic absorbers. One of them is based on the intrinsic bianisotropy associated with the metasurface itself and approximately satisfies the balance conditions (5.7). On the other hand, the second one is built up with the concept of *substrate-induced bianisotropy* which is imposed extrinsically to a non-bianisotropic metasurface through a refractive substrate.

5.3.1 Perfect absorber: an intrinsically bianisotropic metasurface

Consider the same example as in Section 5.2.2. There, we had presented a bianisotropic metasurface using non-identical coupled nano-patches with different lateral dimensions of its coupled patches. Figure 5.8(a) shows the same structure as in Fig. 5.4(a). However, we demonstrate here, that optimizing the same structure presents the perfect absorbance regime. This is possible by judiciously taking the advantage of the concept of bianisotropy. As we may see from the balance condition (5.7a), the bianisotropic term $\hat{\chi}_{xy}^{\mathrm{em}}$ is the key parameter. Therefore, we might justify this

[1]Absorbance is referred to the amplitude of the reflection coefficient in the current text.

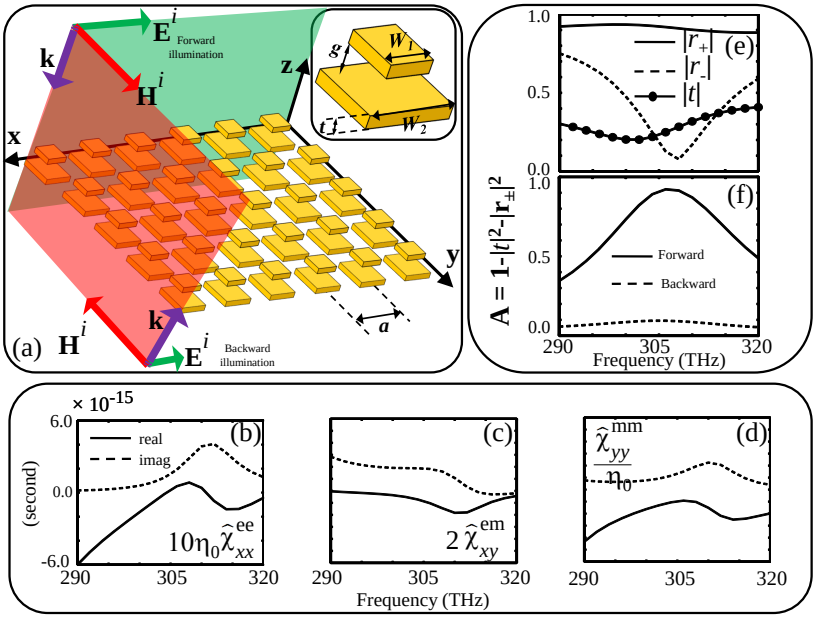

Figure 5.8. (a) The schematic of the same array as in Fig. 5.4(a). (b) Tangential electric (c) Magneto-electric and (d) Magnetic effective susceptibility components of the metasurface retrieved from the reflection and transmission data using equations (5.2). (e) Simulated results for the amplitude of the reflection/transmission coefficients of the proposed metasurface for forward and backward directions. (f) Simulated result for the amplitude of the absorbance coefficient for two illumination directions. $W_1 = 100$ nm $= 0.4\ W_2$ and other geometrical and material parameters are the same as in Fig. 5.4.

term to achieve the absorbance regime. Now, since we know that symmetry breaking is the seminal condition to create bianisotropy, we may play with the asymmetry part of this structure. The asymmetry in this structure is presented by the difference between the lateral lengths of the two patches [$W_1 \neq W_2$ in Fig. 5.8(a)]. We have studied different cases and ended up with $W_1 = 0.4W_2$ which gives the maximum absorbance of $A = 92\%$ in the proposed geometry for the illumination from forward direction [see in Fig. 5.8(a),(f)]. Notice, the absorbance from the opposite direction of illumination is only 9%. Also, note that the effective susceptibility components clearly show a bianisotropic response [Fig. 5.8(c)]. Moreover, the effective electric susceptibility in this case is one order of magnitude smaller than those of magneto-electric and magnetic effective susceptibilities. As it is obvious from Fig. 5.8(e), (f), both reflectance and absorbance are asymmetric with respect to the illumination direction.

To examine the correspondence of the susceptibilities to the balance conditions (5.6) one may refer to Table 5.1. This table shows the values of the electric and magnetic susceptibilities in term of the magneto-electric one

Table 5.1. Comparison between the desired and obtained effective surface susceptibilities for the frequency of maximum absorbance (308 THz). For the desired values in term of $\hat{\chi}^{\text{em}}_{xy}$, we have taken the data of Fig. 5.8(c) [$\hat{\chi}^{\text{em}}_{xy}(@308\text{THz}) = (-7.27 + i\ 8.04) \times 10^{-16} s$] and then have substituted it into the equations (5.6a) and (5.6b). The obtained values are taken from Fig. 5.8(b), (d).

Susceptibility (second)	Desired $\times 10^{-16}$	Obtained $\times 10^{-16}$
$\eta\hat{\chi}^{\text{ee}}_{xx}$	$7.27 + i\ 2.30$	$0.84 + i\ 2.86$
$\hat{\chi}^{\text{mm}}_{yy}/\eta$	$-7.27 + i\ 18.37$	$-10.22 + i\ 19.33$

which are calculated using equations (5.6a) and (5.6b). As it is clear, the imaginary parts are in quite good agreement while the real parts specially for the electric susceptibility are far from ideal and that is why we could not get a 100% absorbance from this topology.

Next, before going to the second example, it is worth discussing a very important issue at this point. According to equation (5.1b) for omega-type bianisotropic metasurfaces, if

$$\hat{\chi}^{\text{ee}}_{xx}\hat{\chi}^{\text{mm}}_{yy} - \hat{\chi}^{\text{me}}_{yx}\hat{\chi}^{\text{em}}_{xy} = 0, \tag{5.8}$$

the transmission coefficient never becomes zero and the total absorbance regime is not possible. This relation holds for those classes of omega-type metasurfaces in which the current distributions are continuous and simple [84]. An example of this type of metasurfaces is given in Section 5.2.1 as a metasurface composed of split-ring resonators. Fig. 5.9 demonstrates the difference between the two values $\hat{\chi}^{\text{ee}}_{xx}\hat{\chi}^{\text{mm}}_{yy}$ and $\hat{\chi}^{\text{me}}_{yx}\hat{\chi}^{\text{em}}_{xy}$ for two different cases. In one case, the condition (5.8) holds; that is, $[\hat{\chi}^{\text{ee}}_{xx}\hat{\chi}^{\text{mm}}_{yy} = \hat{\chi}^{\text{me}}_{yx}\hat{\chi}^{\text{em}}_{xy}]$ while in the other case, the condition (5.8) is violated; that is, $[\hat{\chi}^{\text{ee}}_{xx}\hat{\chi}^{\text{mm}}_{yy} \neq \hat{\chi}^{\text{me}}_{yx}\hat{\chi}^{\text{em}}_{xy}]$. While the former corresponds to the metasurface of split-ring resonators, the later regards to the metasurface with non-identical coupled plasmonic nano-patches. In conclusion, Figs. 5.9(a),(c), show that condition (5.8) clearly holds for the metasurface of split-ring resonators while it is obviously violated for nonidentical coupled plasmonic nano-patches [Fig. 5.9(b),(d)]. Therefore, it is not possible to achieve the total absorbance using a metasurface composed of split-ring resonators.

With the above discussion we continue to present the second example solution which can provide perfect absorbance. This is feasible using the concept of *substrate-induced bianisotropy*.

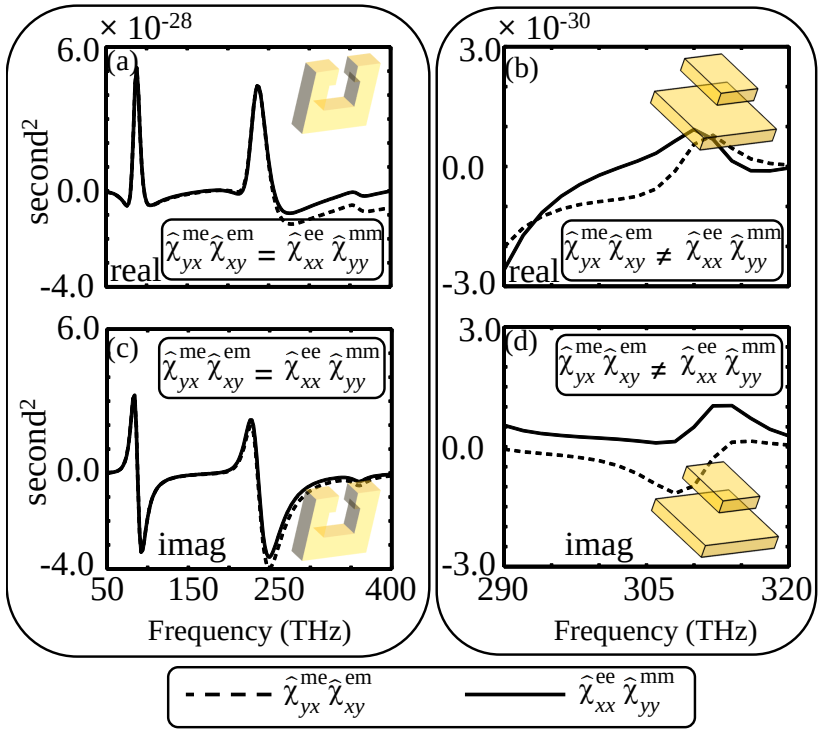

Figure 5.9. Comparison for the (a), (b) real and (c), (d) imaginary parts of $\hat{\chi}^{\mathrm{ee}}_{xx}\hat{\chi}^{\mathrm{mm}}_{yy}$ (solid lines) and $\hat{\chi}^{\mathrm{me}}_{yx}\hat{\chi}^{\mathrm{em}}_{xy}$ (dashed lines) for two different metasurfaces. One composed of split-ring resonators (righ plots) and the other composed of non-identical coupled nano-patches (left plots). For the geometrical and material parameters refer to Figs. 5.2 and 5.8, respectively.

5.3.2 Perfect absorber: an extrinsically bianisotropic metasurface

As we mentioned earlier in Section 5.3, the key prerequisite to achieve perfect absorbance at normal illumination is the simultaneous induction of the electric and magnetic currents which are relaxed with the balance condition (5.5) for non-bianisotropic and (5.7) for reciprocal bianisotropic metasurfaces. In the example of this section, in contrast with the previous section, we use the concept of *substrate-induced bianisotropy* to provide the magnetic response for the metasurface and, hence, achieve the perfect absorbance regime. Therefore, since the bianisotropy is induced by a substrate and is not provided intrinsically by the metasurface inclusions, then we refer to this type as "*extrinsic*" bianisotropy. Fig. 5.10(a) demonstrates such a solution. Indeed, in the present case, the effective magnetic susceptibility $\hat{\chi}^{\mathrm{mm}}_{yy}$ is negligible [see sections 4.1 and 5.2.3]. Therefore, the metasurface may be characterized using only two components of effective

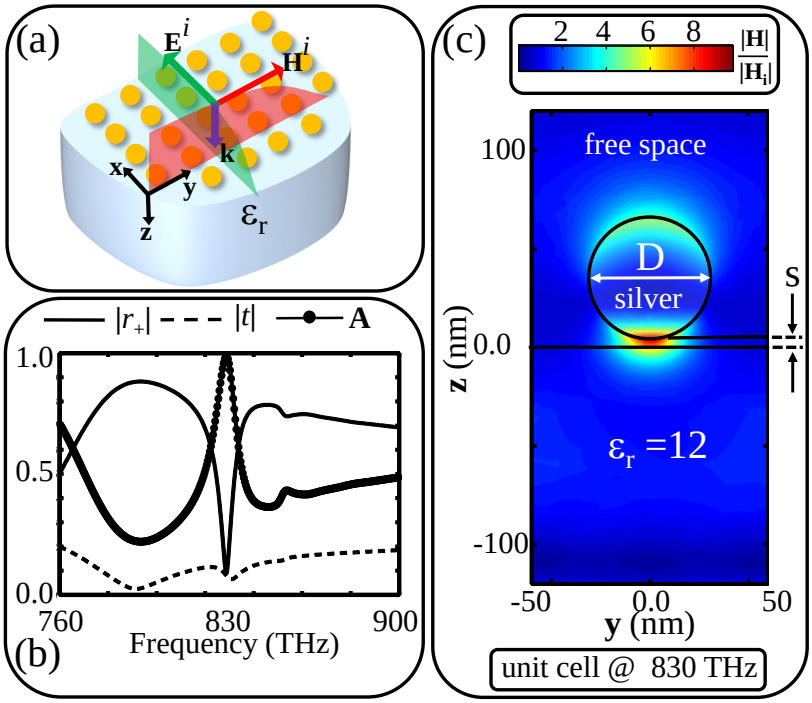

Figure 5.10. (a) A planar periodic array of silver nano-spheres located on top of a silicon substrate. (b) The amplitude of the reflection (from forward direction) and transmission coefficients and the absorbance. (c) Normalized field distribution in one unit cell at the central frequency of the absorbance. The gap between the metasurface and the substrate is $s = 4$ nm, each silver diameter is $D = 60$ nm, and the array period is $a = 120$ nm. The data for silver is taken from [48] and the substrate is amorphous silicon with the relative permittivity $\epsilon_r = 12.8 + i0.1$ in the resonance band.

susceptibility dyadics; that is, $\hat{\chi}^{\mathrm{ee}}_{xx}$ and $\hat{\chi}^{\mathrm{em}}_{xy}$ (notice, $\hat{\chi}^{\mathrm{em}}_{xy} = -\hat{\chi}^{\mathrm{me}}_{yx}$ for omega-type bianisotropy). As a result, the retrieved effective parameters for the forward direction read as in Publication IV:

$$\eta\hat{\chi}^{\mathrm{ee}}_{xx} = \frac{4i}{\omega}\,\frac{1-r^2-nt^2}{(1+r+t)^2}, \tag{5.9a}$$

$$\hat{\chi}^{\mathrm{em}}_{xy} = \frac{2i}{\omega}\,\frac{1+r-t}{(1+r+t)}, \tag{5.9b}$$

where $n = \sqrt{\epsilon_r}$. As a result, the condition for the perfect absorbance is:

$$\eta\hat{\chi}^{\mathrm{ee}}_{xx} = 2\,\hat{\chi}^{\mathrm{em}}_{xy} = \frac{4i}{\omega}, \tag{5.10}$$

Clearly, the above susceptibilities are idealized and hard to achieve. However, we may approach this limit by optimizing the proposed metasurface of plasmonic silver spheres. After optimization at 830 THz, the obtained values for the optimized metasurface with nearly perfect absorbance are

Table 5.2. Comparison between the desired and obtained effective surface susceptibilities for the frequency of maximum absorbance (830 THz).

Susceptibility (second)	Desired $\times 10^{-16}$	Obtained $\times 10^{-16}$
$\eta\hat{\chi}_{xx}^{\mathrm{ee}}$	$7.7\ (0+i)$	$11.2\ (0.20+i)$
$\hat{\chi}_{xy}^{\mathrm{em}}$	$3.84\ (0+i)$	$4.52\ (0.26+i)$

given in Table 5.2. A maximum absorbance of $A \sim 99\%$ is achieved as shown in Fig. 5.10(b). This absorbance is accompanied by a local field enhancement. In Fig. 5.10(c) we show the color map of the horizontal magnetic field. For its amplitude, the enhancement in the hot spot attains one order of magnitude. For the electric field (also horizontal component) the enhancement is several times higher: the electric energy density is increased by 3 orders [see e.g. in Publication IV]. The birth of this hot spot is obviously linked to the bianisotropy offered by the substrate as discussed before in Section 5.2.3. Strong field enhancement may find applications in SERS and other schemes of modern optical sensing. More detailed analysis about these issues may be found in Publication IV.

Now, we finish with the bianisotropy and revisit the random metasurfaces. The last part of this chapter is dedicated to a discussion on disordered arrangements of inclusions and amorphous metasurfaces representing an important class of surface materials. We compare their responses to the plane electromagnetic waves with that of periodic metasurfaces.

5.4 Amorphous versus periodic arrangements in metasurfaces

At the end of this section we will see how a correct view on phenomena will help to understand the true physics behind that. Let us first consider a metasurface with a periodic arrangement of its inclusions. Moreover, we assume that the array may potentially provide both electric and magnetic dipolar resonant modes in response to a plane electromagnetic wave. This is feasible, for instance, with coupled plasmonic nano-patches [see e.g. Section 5.1, Fig.5.1]. Recently, it was experimentally observed that in transition from periodic to amorphous positioning of inclusions in the proposed metasurface, the resonant responses would be broaden and damped [51]. However, this observation was different for different resonant modes. It is not possible to understand the reason using only a macroscopic homogenized model which does not provide any information

about the interaction of the inclusions. Therefore, a complete understanding is feasible only by probing into the microscopic behavior of the local fields in the vicinity of inclusions. Here, we do not much go to the details of the analysis, however, we supply some important prerequisites to make the discussion understandable. More detailed discussion is provided in Publication IV and [10].

As we briefly discussed in Section 4.1, an effective (macroscopic) susceptibility/polarizability component ($\hat{\chi}/\hat{\alpha}$) may be presented in terms of an individual (microscopic) susceptibility/polarizability (χ/α) and an *interaction constant* (β) [see equation (4.7)]. Indeed, the interaction constant measures the contributions of the fields created by all other particles of the array into the local field; i.e.,

$$\mathbf{E}^{loc} = \mathbf{E}^{i} + \beta \mathbf{p}, \tag{5.11}$$

that excite each polarizable particle. $\mathbf{p}$ is the induced electric dipole moment in each particle and $\mathbf{E}^{i}$ is the incident electric field. The dual relation holds for the magnetic fields $\{\mathbf{H}^{loc}, \mathbf{H}^{i}\}$ and magnetic dipole moment $\mathbf{m}$. We are interested in normal illumination, since it is the simplest case providing enough information to understand the issue. Therefore, we may go back to our example of coupled plasmonic nano-patches at normal incidence [Section 5.1, Fig.5.1]. It is shown in Publication IV that the reflection and transmission coefficients in a dense periodic array of electrically small resonant inclusions at normal illumination (as in our example [Fig.5.1]), read as:

$$r_{\mathrm{e}} = \frac{ik_0 a}{2} \frac{1}{\frac{\epsilon_0 a^3}{\alpha^{\mathrm{ee}}_{xx}} - \epsilon_0 a^3 \beta}, \tag{5.12}$$

$$r_{\mathrm{m}} = -\frac{ik_0 a}{2} \frac{1}{\frac{\mu_0 a^3}{\alpha^{\mathrm{mm}}_{yy}} - \mu_0 a^3 \beta}, \tag{5.13}$$

$$r = r_{\mathrm{e}} + r_{\mathrm{m}}, \qquad t = 1 + r_{\mathrm{e}} - r_{\mathrm{m}}. \tag{5.14}$$

Notice, the particles may be both electrically and magnetically polarizable. Here, $\alpha^{\mathrm{ee}}_{xx}$ and $\alpha^{\mathrm{mm}}_{yy}$ are, respectively, the *individual* electric and magnetic polarizability of each element when separated from other elements in the array, a is the unit cell size, and $k_0 = \omega\sqrt{\epsilon_0 \mu_0}$ is the wave number in the surrounding space. The two partial reflection coefficients r_{e} and r_{m} correspond to the fields created by the induced electric and magnetic currents, respectively. The normalized interaction constants are the same for both electric and magnetic particles, and denoted as β:

$$\epsilon_0 a^3 \beta^{\mathrm{ee}} = \mu_0 a^3 \beta^{\mathrm{mm}} = \beta. \tag{5.15}$$

Moreover, the individual electric and magnetic polarizability components are written as:

$$\frac{\epsilon_0 a^3}{\alpha_{xx}^{\mathrm{ee}}} = \left(\frac{A_{\mathrm{e}}}{\omega_{0\mathrm{e}}^2 - \omega^2 + j\omega\Gamma_{\mathrm{e}}} \right)^{-1} + j\frac{k_0^3 a^3}{6\pi}, \tag{5.16}$$

$$\frac{\mu_0 a^3}{\alpha_{yy}^{\mathrm{mm}}} = \left(\frac{A_{\mathrm{m}}}{\omega_{0\mathrm{m}}^2 - \omega^2 + j\omega\Gamma_{\mathrm{m}}} \right)^{-1} + j\frac{k_0^3 a^3}{6\pi}. \tag{5.17}$$

In these relations a simple Lorentz-type resonant response model of individual particles is assumed. This type of resonant response is very common and approximates very well the particles response near their resonances. Therefore, $\Gamma_{\mathrm{e,m}}$ model the dissipation losses in the particle (in respective modes), while the last imaginary term is due to the scattering (re-radiation of power) loss [10].

In the case of a periodic array and when the array period is smaller than the operational wavelength λ, the scattering loss of the individual particles is suppressed by the interaction between the particles in the array. Indeed, the imaginary part of the interaction constant contains a term proportional to k_0 which compensates the corresponding term in the polarizabilities [10]:

$$\beta_{\mathrm{periodic}} = \mathrm{Re}(\beta) + j\frac{k_0^3 a^3}{6\pi} - j\frac{k_0 a}{2}. \tag{5.18}$$

The other imaginary term corresponds to the plane waves created by the surface-averaged currents. In case of amorphous (on the wavelength scale) arrays particles scatter individually, and there is no corresponding term in the interaction constants, that is:

$$\beta_{\mathrm{amorph}} = \mathrm{Re}(\beta) - j\frac{k_0 a}{2}. \tag{5.19}$$

We note that in the quasi-static limit $\mathrm{Re}(\beta) \approx 0.36$. If we now substitute the interaction constants (5.18) and (5.19) for periodic and amorphous arrays both with the Lorentz-model of the individual polarizabilities (5.16) and (5.17) into the partial reflection coefficients (5.12) and (5.13), we end up with the resonant curve widths:

$$2\Delta\omega_{\mathrm{e,m\,periodic}} = \Gamma_{\mathrm{e,m}} + \frac{k_0 a}{2}\frac{A_{\mathrm{e,m}}}{\tilde{\omega}_{0\mathrm{e,m}}} \tag{5.20}$$

for periodic arrays and

$$2\Delta\omega_{\mathrm{e,m\,amorph}} = \Gamma_{\mathrm{e,m}} + k_0^3 a^3 \frac{A_{\mathrm{e,m}}}{\tilde{\omega}_{0\mathrm{e,m}}} + \frac{k_0 a}{2}\frac{A_{\mathrm{e,m}}}{\tilde{\omega}_{0\mathrm{e,m}}} \tag{5.21}$$

for amorphous arrays. Here $\tilde{\omega}_0$ denotes the resonant frequency shifted due to the interactions between the particles in the array. Notice, we assumed the case when electric and magnetic resonances occur at different

frequencies. Now, it is easy to see from the comparison of (5.20) and (5.21) that if

$$\tilde{\omega}_{0\mathrm{e,m}}\frac{\Gamma_{\mathrm{e,m}}}{A_{\mathrm{e,m}}}+\frac{k_0 a}{2}\gg\frac{k_0^3 a^3}{r\pi} \tag{5.22}$$

is satisfied, near the corresponding resonant frequency $\tilde{\omega}_{0\mathrm{e,m}}$, the effect of inclusion position randomness is negligible, and the responses of periodic and amorphous structures are nearly the same. The above condition shows that this is the case of high losses and low resonance strength. Also we can note that the condition is easier to satisfy at low frequencies, when the scattering amplitude proportional to k_0^3 is smaller. From these results we can conclude that the effect of strong widening of the resonant curve of the electric-dipole mode and hardly any effect of array randomness on the magnetic mode can be due to two reasons:

1. At the frequency of the magnetic resonance the array is practically homogeneous on the wavelength scale ("totally random[2]"). Then the scattering term cancels out just like for periodical arrays, and there is no difference in the resonant curve widths for periodic and amorphous metasurfaces.

2. At the magnetic resonance the particles are considerably more lossy and weaker excited than at the electric resonance, that is, (5.22) is satisfied near the magnetic resonance but not satisfied near the electric-mode resonance. In this case the effect of additional scattering loss is negligible in one of the modes but can be relatively significant in the other.

In order to observe what really happens for the reflection and transmission in transition from periodic to amorphous arrangements, we may introduce a disorder parameter r_{n} to the different term between (5.20) and (5.21); i.e.:

$$\beta=\Re\{\beta\}+r_{\mathrm{n}}\frac{jk_0^3 a^3}{6\pi}-\frac{jk_0 a}{2}. \tag{5.23}$$

Here $0\leq r_{\mathrm{n}}\leq 1$, where unity corresponds to the case where the scattering loss is completely compensated *(periodic array)* and $r_{\mathrm{n}}=0$ means that the scattering loss is not compensated at all *(amorphous array, each inclusion scatters individually)*.

[2]Totally random means a structure which appears uniform at the wavelength scale.

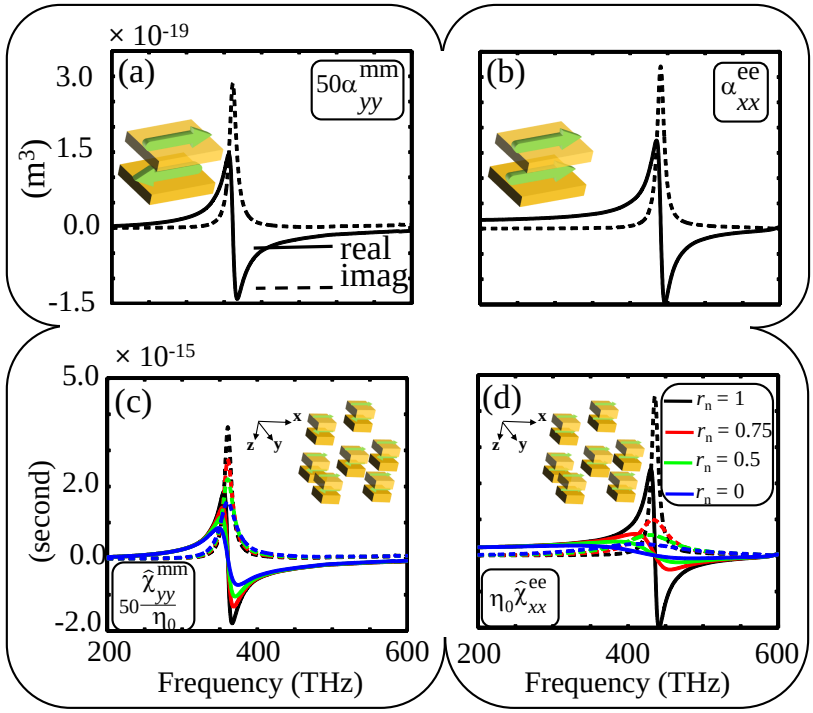

Figure 5.11. Individual (a) magnetic (b) electric polarizability for the coupled plasmonic nano-patches shown in Fig. 5.12(a). (c) Effective magnetic susceptibility for different arrays composed of the proposed coupled plasmonic nano-patches with different disorder parameter r_{n}. (d) Effective electric susceptibility for the same situation as in (c). Notice, all the dashed lines are the imaginary parts while the solid lines are the real parts.

Let us present a practical example to visualize the concept. Consider an array of coupled plasmonic gold nano-patches [see e.g. Fig. 5.12(a)]. The array may be periodic ($r_{\mathrm{n}} = 1$) or amorphous ($r_{\mathrm{n}} \neq 1$). In the periodic case, the period of the array is $a = 512$ nm while in the amorphous state the *average distance* between two inclusions is $a = 512$ nm. As we have seen in a similar example in Section 5.1, both electric and magnetic polarization currents may be induced in such an array. Moreover, the resonances are similar to Lorentz-type resonance. One may now find the individual polarizabilities of an element of this array (two coupled patches) using different methods [see e.g. in Ref. [85, 82, 83]. The individual polarizabilities are obtained from induced electric and magnetic dipole moments $\mathbf{p}$ and $\mathbf{m}$; i.e.,

$$\mathbf{p} = \int_{\mathrm{V}} \mathbf{r}\rho(\mathbf{r})\, dv, \qquad \mathbf{m} = \tfrac{1}{2}\int_{\mathrm{V}} \mathbf{r} \times \mathbf{J}(\mathbf{r})\, dv, \tag{5.24}$$

respectively. In (5.24), the induced charge and current densities inside

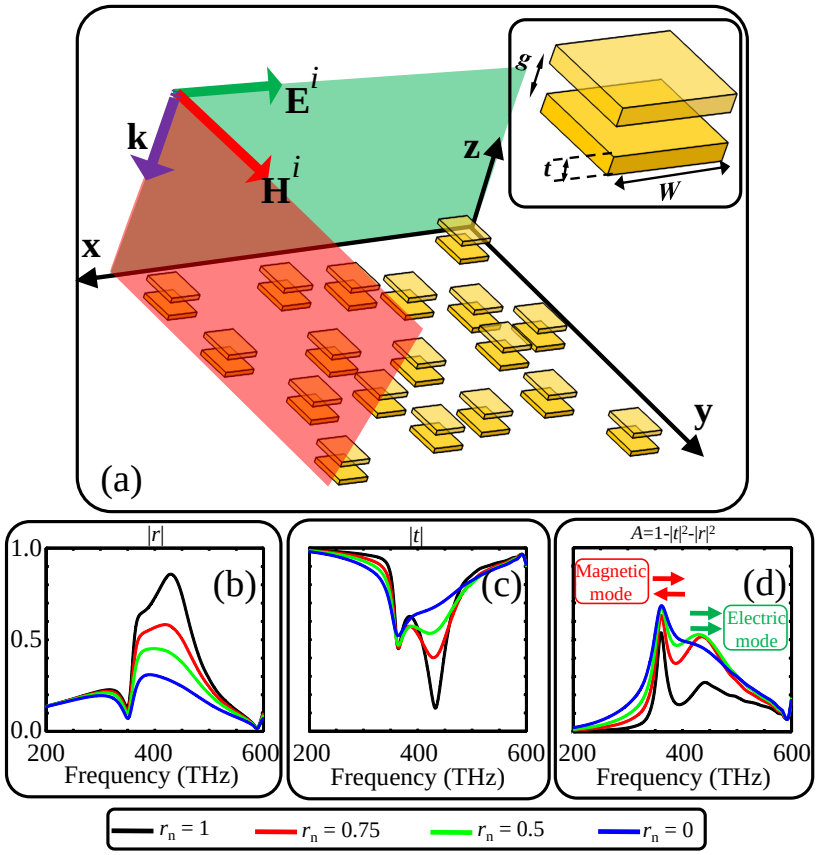

Figure 5.12. (a) A planar array of gold plasmonic nano-patches located in free space with: $g = 30$ nm, $t = 45$ nm, and $W = 180$ nm. (b) The amplitude of the reflection coefficients for different disorder parameter r_{n}. (c) The amplitude of the transmission coefficients corresponding to the same reflection coefficients as in (b). () The same plots for the amplitude of the absorbance coefficient.

an infinitesimal volume element dv are denoted by $\rho(\mathbf{r})$ and $\mathbf{J}(\mathbf{r})$, where $\mathbf{r}$ is the position vector of dv with respect to the Cartesian coordinate system[3] and V is the volume of the induced charge (current) distribution. Using these definitions for the moments, one may numerically calculate the individual polarizability components $\alpha_{yy}^{\mathrm{mm}}$ and $\alpha_{xx}^{\mathrm{ee}}$ [86] as shown in Figs. 5.11(a),(b).

In the next step, we apply our proposed model to arrays with different arrangements of their inclusions. We first find the *effective* susceptibilities in terms of *individual* polarizabilities and the interaction constant β. To

[3]The particle is assumed to be positioned in the center of the Cartesian coordinate system in a way that the upper patch is positioned at $g/2$ and the lower one is positioned at $-g/2$

do this, it is easy to show from (5.1) that:

$$r = -\frac{1}{1-\frac{i\omega}{2}\eta_0\hat{\chi}^{\mathrm{ee}}_{xx}} + \frac{1}{1-\frac{i\omega}{2}\frac{\hat{\chi}^{\mathrm{mm}}_{yy}}{\eta_0}} = r_{\mathrm{e}} + r_{\mathrm{m}}, \tag{5.25}$$

when $\hat{\chi}^{\mathrm{em}}_{xy} = \hat{\chi}^{\mathrm{me}}_{yx} = 0$. Now, comparing (5.25) with (5.12) and (5.13) results in:

$$\eta_0\hat{\chi}^{\mathrm{ee}}_{xx} = -\frac{2i}{\omega}\left[1 - \frac{2i}{k_0 a}\left(\frac{\epsilon_0 a^3}{\alpha^{\mathrm{ee}}_{xx}} - \beta\right)\right], \tag{5.26a}$$

$$\frac{\hat{\chi}^{\mathrm{mm}}_{yy}}{\eta_0} = -\frac{2i}{\omega}\left[1 - \frac{2i}{k_0 a}\left(\frac{\mu_0 a^3}{\alpha^{\mathrm{mm}}_{yy}} - \beta\right)\right]. \tag{5.26b}$$

Therefore, one may calculate the effective susceptibilities from known individual polarizabilities and the proposed model for the interaction constant β in (5.23) for different disorder parameters r_{n}. The results are shown in Figs. 5.11(c),(d). As it is evident from these plots, both resonances bear a broadening and damping in transition from periodic to amorphous states. However, the change in the electric resonance mode [Fig. 5.11(d)] is much more severe than in the magnetic resonance mode [Fig. 5.11(c)]. This is, as we discussed before, due to the lower resonance strength of the magnetic mode compared to the electric one ($A_{\mathrm{m}} < A_{\mathrm{e}}$). Indeed, condition (5.22) is satisfied for the magnetic resonance while it is not satisfied for the electric one. This effect is observable in both the reflection and transmission coefficients which are shown in Figs. 5.12(b),(c). Moreover, Fig. 5.12(d) shows the absorbance coefficient of the proposed metasurface. It demonstrates higher losses at the magnetic resonance than at the electric one; that is, $\Gamma_{\mathrm{m}} > \Gamma_{\mathrm{e}}$ in condition (5.22). This is again another reason of the different behavior between different resonant modes in transition from periodic to amorphous arrangements. These results nicely confirm the previous experimentally observed behavior in amorphous arrays [51]. Therefore, they prove our correct modeling for amorphous metasurfaces. Notice, in this last example we were not able to explain the behavior of amorphous arrays without probing the metasurface at the microscopic level. That is, calculating the individual polarizabilities and their relations to the effective susceptibilities through the interaction constant.

We finally conclude this section with the following statement: “Not always the correct characterization models help to grasp the naturae of some phenomena in metasurfaces. But, we should sometimes dig deeper into the microscopic level in order to get enough information for analysis and correct explanation of the metasurfaces operations.”

6. Conclusions

This thesis starts from the definition of the term *electromagnetic characterization of metamaterials*. A history of the metamaterials' research field is briefly presented. After that, *characterization* is explained. Next, the general concept of metamaterials and the place of metasurfaces are presented in connection to the bigger categories of metamaterials and ordinary materials. A brief history of electromagnetic characterization of materials is then given and the chapter is finished by the explanation of the whole concept of *electromagnetic characterization of metasurfaces*.

Thereafter, we have reproduced the known criticism for the application of the traditional bulk media retrieval procedures used for the characterization of metasurfaces. We have commented on two alternative approaches: that based on the so-called Generalized Sheet Transition Conditions and that based on the collective effects in arrays of electrically resonant inclusions. Further, we have shown that both these approaches are similar and mathematically equivalent. We have then given a generalized formalism for characterization of a broad spectrum of metasurfaces in terms of either surface susceptibilities or collective polarizabilities.

We have actually obtained the most general boundary conditions for a general bianisotropic metasurface located at the interface of two different media. We have next shown how the reflected/transmitted field vectors are related to the incident/average fields through the effective polarizability/susceptibility tensors and hence what would be the two-dimensional reflection/transmission dyadics. Finally, we have developed a general algorithm for the retrieval of the effective polarizability/susceptibility tensors as the characteristic parameters of the metasurface under study.

We have studied several explicit examples of plasmonic metasurfaces. Unlike previous studies, our generalized model covers bianisotropic metasurfaces, substrated metasurfaces, metasurfaces illuminated from two

sides, and metasurfaces with disordered arrangements of inclusions. We have studied all these types of metasurfaces as explicit examples. We have also explained the differences between the magnetic resonant modes in metasurfaces formed by solid scatterers (split-ring resonators) and coupled nano-patches of plasmonic metals.

Indeed, we have considered a novel and interesting topic of bianisotropic metasurfaces. As two important illustrations, we have presented metasurfaces composed of split-ring resonators and of non-identical pairs of plasmonic nano-patches. We have then discussed the important differences between these two types.

Using our model, we have revealed an important phenomena of *substrate–induced bianisotropy*. With both intrinsically bianisotropic and substrate–induced bianisotropic metasurfaces, we have presented an important functionality such as the perfect absorbance in metasurfaces. It is important to note that the bianisotropic absorbers have the advantageous of asymmetric reflectance. Moreover, they provide a weakly reflective surface out of the resonance band. We have presented two different examples in order to demonstrate a nearly perfect absorbance regime.

In the last part, we have discussed an important class of metasurfaces – random and amorphous metasurfaces. There, we have explained what is happening at the microscopic level. We have explained the differences in the electric and magnetic interactions of inclusions in both periodic and disordered metasurfaces. We have finalized our study by demonstrating different resonant behavior of the electric and magnetic modes in transition from periodic to amorphous states.

With all of the above discussions, we are pleased to say that we have significantly contributed to the characterization of a so popular class of metamaterials; that is, metasurfaces. The recognition of this class of metamaterials is rapidly increasing and the correct understanding is strongly needed for developing the effective designs. Of course, although we did our best in this stream, there are still many unsolved challenges.

References

[1] Y. Leng, *Materials characterization: introduction to microscopic and spectroscopic methods,* Singapore, John Wiley & Sons (Asia), 2008.

[2] D. R. Smith and N. Kroll, "Negative refractive index in left-handed materials," *Physcal Review Letters*, vol. 85, no. 14, pp. 2933–2936, 2000.

[3] R. A. Shelby, D. R. Smith, and S. Schultz, "Experimental verification of a negative index of refraction," *Science*, vol. 292, no. 5514, pp. 79–81, 2001.

[4] F. Capolino (ed), *Metamaterials Handook: vol 1, Theory and phenomena of metamaterials*. Boca Raton, FL: CRC Press, 2009.

[5] F. Capolino (ed), *Metamaterials Handook: vol 2, Applications of metamaterials*. Boca Raton, FL: CRC Press, 2009.

[6] R. S. Anantha and T. Grzegorczyk, *Physics and applications of negative-index materials*. Boca Raton, FL: CRC Press, 2008.

[7] C. R. Simovski, "On electromagnetic characterization and homogenization of nanostructured metamaterials", *J. Opt.*, vol. 13, no. 1, pp. 013001–22, 2011.

[8] E. F. Kuester, M. A. Mohamed, M. Piket-May and C. L. Holloway, "Averaged transition conditions for electromagnetic fields at a metafilm", *IEEE Transactions on Antennas and Propagation*, vol. 51, no. 10, pp. 2641–2651, Oct. 2003.

[9] C. L. Holloway, A. Dienstfrey, E. F. Kuester, J. F. O'Hara, A. K. Azad and A. J. Taylor, "A discussion on the interpretation and characterization of metafilms/metasurfaces: The two-dimensional equivalent

of metamaterials", *Metamaterials*, vol. 3, no. .2, pp. 100–112, Oct. 2009.

[10] S.A. Tretyakov, *Analytical modeling in applied electromagnetics,* Norwood, MA: Artech House, 2003.

[11] S. H. Lee, C. M. Park, Y. M. Seo, Z. G. Wang and C. K. Kim, "Acoustic metamaterial with negative modulus", *Journal of Physics: Condensed Matter*, vol. 21, no. 17, pp. 175704(1-4), April 2009.

[12] S. H. Lee, C. M. Park, Y. M. Seo, Z. G. Wang and C. K. Kim, "Acoustic metamaterial with negative density", *Physics Letters A*, vol. 373, no. 48, pp. 4464–4469, Dec. 2009.

[13] Z. Yang, J. Mei, M. Yang, N. Chan and P. Sheng, "Membrane-type acoustic metamaterial with negative dynamic mass", *Physical Review Letters*, vol. 101, no. 20, pp. 204301(1-4), Nov. 2008.

[14] Y. Ding, Z. Liu, C. Qiu, and J. Shi, "Metamaterial with simultaneously negative bulk modulus and mass density", *Physical Review Letters*, vol. 99, no. 9, pp. 093904(1-4), Aug. 2007.

[15] S. H. Lee, C. M. Park, Y. M. Seo, Z. G. Wang and C. K. Kim, "Composite acoustic medium with simultaneously negative density and modulus", *Physical Review Letters*, vol. 104, no. 5, pp. 054301(1-4), Feb. 2010.

[16] H. G. Liddell and R. Scott, *A Greek-English Lexicon,* on Perseus Digital Library.

[17] S. M. Walker, *Matter (Early Bird Energy)*, Lerner Publications Company, Minneapolis, MN, USA, 2006.

[18] D. R. Smith, W. J. Padilla, D. C. Vier, S. C. Nemat-Nasser and S. Schultz, "Composite medium with simultaneously negative permeability and permittivity", *Physical Review Letters*, vol. 84, no. 18, pp. 4184–4187, May 2000.

[19] J. B. Pendry, "Negative refraction makes a perfect lens", *Physical Review Letters*, vol. 85, no. 18, pp. 3966–3969 Oct. 2000.

[20] A. Sihvola, "Metamaterials in electromagnetics", *Metamaterials*, vol. 1, no. 1, pp. 2–11, March 2007.

[21] `http://global.britannica.com/EBchecked/topic/125898/colloid`

[22] http://www.metamorphose-vi.org/index.php/metamaterials

[23] M. Lapine and S. Tretyakov, “Contemporary notes on metamaterials”, *Microwaves, Antennas & Propagation, IET*, vol. 1, no. 1, pp. 3–11, Feb. 2007.

[24] R. Grimberg, “Electromagnetic metamaterials”, *Materials Science and Engineering: B*, vol. 178, no. 19, pp. 1285–1295, Nov. 2013.

[25] J. Daintith (ed), *Oxford, a dictionary of science,* 5th edition, Oxford University Press, USA, 2005.

[26] A. N. Serdyukov, I. V. Semchenko, S. A. Tretyakov, and A. Sihvola, *Electromagnetics of bi-anisotropic materials: Theory and applications*, Amsterdam, The Netherlands: Gordon and Breach, 2001.

[27] D. R. Smith, S. Schultz, P. Markos and C. M. Soukoulis, “Determination of effective permittivity and permeability of metamaterials from reflection and transmission coefficients”, *Physical Review B*, vol. 65, no.19, pp. 195104(1-5), Apr. 2002.

[28] X. Chen, T. M. Grzegorczyk, B.-I. Wu, J. J. Pacheco and J. A. Kong, “Robust method to retrieve the constitutive effective parameters of metamaterials”, *Physical Review E*, vol. 70. no. 1, pp. 016608(1-7), July 2004.

[29] A. D. Scher and E. F. Kuester, “Extracting the bulk effective parameters of a metamaterial via the scattering from a single planar array of particles”, *Metamaterials*, vol. 3, no .1, pp. 44–55, March 2009.

[30] E. Shamonina and L. Solymar, “Metamaterials: How the subject started”, *Metamaterials*, vol. 1, no. 1, pp. 12–18, March 2007.

[31] C. J. F. Böttcher, *Theory of electric polarization*, Elsevier, Amsterdam, second edition, 1973.

[32] C. L. Holloway, E. F. Kuester, J. A. Gordon, J. O’Hara, J. Booth and David R. Smith, “An overview of the theory and applications of metasurfaces: the two-dimensional equivalents of metamaterials”, *IEEE Antennas and Propagation Magazine*, vol. 54, no. 2, pp. 10–35, April 2012.

[33] A. R. Von Hippel, *Dielectric materials and applications*, Technology Press of M.I.T and John Wiely & Sons, Inc., New York, 1954.

[34] A. M. Nicolson and G. F. Ross, “Measurement of the intrinsic properties of materials by time-domain techniques”, *IEEE Transactions on Instrumentation and Measurement*, vol. 19, no.4, pp. 377–382, Nov. 1970.

[35] W. B. Weir, “Automatic measurement of complex dielectric constant and permeability at microwave frequencies”, *Proceedings of the IEEE*, vol. 62, no.1, pp. 33–36, Jan. 1974.

[36] C. Strachan,“The reflection of light at a surface covered by a monmolecular film”, *in Proc. Camb. Phil. Soc.*, vol. 29, pp. 116–130, 1933.

[37] T. B. A. Senior, *Combined resistive and conductive sheets*, *IEEE Transactions on Antennas and Propagation*, vol. 33, no. 5, pp. 577–579, May 1985.

[38] T. B. A. Senior and J. L. Volakis, *Approximate boundary conditions in electromagnetics*, The Institute of Electrical Engineers, London, UK, 1995.

[39] P. A. Belov, C. R. Simovski and M. S. Kondratjev, “Problem of the local field for plane grids with bi-anisotropic particles”, *5th Annual International Symposium on Smart Structures and Materials, International Society for Optics and Photonics*, pp. 680–691, June 1997.

[40] M. S. Kondratjev, C. R. Simovski and P. A. Belov, “Reflection and transmission of plane waves in bianisotropic planar grids”, *5th Annual International Symposium on Smart Structures and Materials, International Society for Optics and Photonics*, pp. 669–678, 1998.

[41] P. A. Belov, C. R. Simovski and M. S. Kondratjev, “Analytical-numerical study of electromagnetic interaction in two-dimensional bianisotropic arrays”, *5th Annual International Symposium on Smart Structures and Materials, International Society for Optics and Photonics*, pp. 679–690, 1998.

[42] C. R. Simovski, M. S. Kondratjev, P. A. Belov and S. A. Tretyakov, “Interaction effects in two-dimensional bianisotropic arrays”, *IEEE Transactions on Antennas and Propagation*, vol. 47, no. 9, pp. 1429–1439, Sept. 1999.

[43] S. I. Maslovski and S. A. Tretyakov, “Full-wave interaction field in twodimensional arrays of dipole scatterers” *International Jour-*

nal of Electronics and Comunications, Arch. Elek. Übertragungstech. (AEÜ), vol. 53, no. 3, pp. 135–139, 1999.

[44] S. A. Tretyakov, A. J. Viitanen, S. I. Maslovski and I. E. Saarela, "Impedance boundary conditions for regular dense arrays of dipole scatterers", *IEEE Transactions on Antennas and Propagation*, vol. 51, no. 8, pp. 2073–2078, August 2003.

[45] V. V. Yatsenko, S. I. Maslovski, S. A. Tretyakov, S. L. Prosvirnin and S. Zouhdi, "Plane-wave reflection from double arrays of small magnetoelectric scatterers", *IEEE Transactions on Antennas and Propagation*, vol. 51, no. 1, pp. 2–11, Jan. 2003.

[46] Y. Ra'di, V. S. Asadchy and S. A. Tretyakov, "Total absorption of electromagnetic waves in ultimately thin layers", *IEEE Transactions on Antennas and Propagation*, vol. 61, no. 9, , pp. 4606–4614, Sept. 2013.

[47] Y. Ra'di, C. R. Simovski, and S. A. Tretyakov, "Thin perfect absorbers for electromagnetic waves: Theory, design, and realizations", *Phys. Rev. Applied*, in print.

[48] P. B. Johnson and R. W. Christy, "Optical constants of the noble metals", *Physical Review B*, vol. 6, no. 12, p. 4370, Dec. 1972.

[49] `http://www.ansys.com/Products/Simulation+Technology/Electronics/Signal+Integrity/ANSYS+HFSS`

[50] C. R. Simovski S. A. Tretyakov, "Local constitutive parameters of metamaterials from an effective-medium perspective", *Physical Review B*, vol. 75, no .19, p. 195111, May 2007.

[51] C. Helgert, C. Rockstuhl, C. Etrich, C. Menzel, E-B. Kley, A. Tünnermann, F. Lederer, and T. Pertsch. "Effective properties of amorphous metamaterials", *Physical Review B*, vol. 79, no. 23, p. 233107, June 2009.

[52] A. Taflove and S. Hagness, *Computational electrodynamics: The finite-difference time-domain method*, [Taflove, A. & Hagness, S. (eds.)] (Artech House, Boston,3rd edition, 2005.

[53] R. Esteban, R. Vogelgesang, J. Dorfmuller, A. Dmitriev, C. Rockstuhl, C. Etrich and K. Kern, "Direct near-field optical imaging of higher

order plasmonic resonances", *Nano Letters*, vol. 8, no. 10, pp. 3155–3159, Sept. 2008.

[54] L. D. Landau and E. M. Lifchits, *Course of theoretical physics: Electrodynamics of continuous media*, Pergamon Press, 1960.

[55] A. D. Rakic, A. B. Djurišic, J. M. Elazar, and M. L. Majewski, "Optical properties of metallic films for vertical-cavity optoelectronic devices", *Applied optics*, vol. 37, no. 22, pp. 5271–5283, August 1998.

[56] T. Niemi, A. Karilainen, and S. Tretyakov, "Synthesis of polarization transformers", *IEEE Transactions on Antennas and Propagation*, vol. 61, no. 6, pp. 3102–3111, June 2013.

[57] M. S. Mirmoosa, Y. Ra'di, V. S. Asadchy, C. R. Simovski and S. A. Tretyakov, "Polarizabilities of nonreciprocal bianisotropic particles", *Physical Review Applied*, vol. 1. no. 3, p. 034005, April 2014.

[58] M. Albooyeh, R. Alaee, C. Rockstuhl and C. R. Simovski, "Revisiting substrate-induced bianisotropy in metasurfaces", *under review*.

[59] D.V. Sivukhin, "Molecular theory of the reflection and refraction of light", *Zhurnal Eksperimentalnoi i Teoreticheskoi Fiziki*, vol. 18, 976, 1948, in Russian.

[60] D.V. Sivukhin, "Theory of elliptic polarization of light reflected from isotropic media", *Sov. Phys. JETP*, vol. 3, p. 269, 1957.

[61] V.A. Kizel, "Spectroscopy of liquids", *Sov. Phys. JETP*, vol. 2, p. 533, 1956.

[62] V.A. Kizel, "Modern status of the theory of light reflection", *Sov. Phys. Uspekhi*, vol. 10, p. 485, 1968.

[63] O.S. Heavens, *Optical properties of thin solid films*, Dover, New York, 1991.

[64] O.N. Gadomski and S.V. Sukhov, "Microscopic theory of a transition layer on the ideal surface of semiinfinite dielectric media and the near-field effect", *Optics and Spectroscopy*, vol. 89, no. 2, pp. 261–267, August 2000.

[65] D. Bedeaux, J. Vlieger, "A statistical theory of the dielectric properties of thin island films: I. The surface material coefficients", *Physica*, vol. 73, no. 2, pp. 287–311, April 1974.

[66] M.M. Wind, J. Vlieger, D. Bedeaux,“ The polarizability of a truncated sphere on a substrate”, *Physica A*, vol. 141, no. 1, pp. 33–57, Feb. 1987.

[67] D.C. Langreth, “Macroscopic approach to the theory of surface reflectivity”, *Physcal Review B*, vol. 39, no. 14, p. 10020–10027, May 1989.

[68] T. Yamaguchi,S. Yoshida and A. Kinbara, “Anomalous optical absorption of aggregated silver films Thin Solid Films”, vol. 18, no. 1, pp. 63–70, May 1973.

[69] T. Yamaguchi, S. Yoshida and A. Kinbara, “Optical effect of the substrate on the anomalous absorption of aggregated silver films”, *Thin Solid Films*, vol. 21, no. 1, pp. 173–187, March 1974.

[70] T. Yamaguchi, S. Yoshida and A. Kinbara, “Effect of retarded dipole-dipole interactions between island particles on the optical plasma-resonance absorption of a silver-island film”, Jornal of the Optical Society of America, vol. 64, no. 11, pp. 1563–1568, Nov. 1974.

[71] L. Novotny, “Effective wavelength scaling for optical antennas”, *Physical Review Letters*, vol. 98, no. 26, p. 266802, June 2007.

[72] N. I. Landy, S. Sajuyigbe, J. J. Mock, D. R. Smith, and W. J. Padilla, “Perfect metamaterial absorber”, *Physcal Review Letters*, vol. 100, no. 20, pp. 207402(1–4), May 2008.

[73] N. Liu, M. Mesch, T. Weiss, M. Hentschel, and H. Giessen, Harald, “Infrared perfect absorber and its application as plasmonic sensor”, *Nano letters*, vol. 10, no. 7, pp. 2342–2348, June 2010.

[74] F. Costa, A. Monorchio, and G. Manara, “Analysis and design of ultra thin electromagnetic absorbers comprising resistively loaded high impedance surfaces”, *IEEE Transactions on Antennas and Propagation*, vol. 58, no. 5, pp. 1551–1558, May 2010.

[75] J. A. Mason, S. Smith, and D. Wasserman, “Strong absorption and selective thermal emission from a midinfrared metamaterial”, *Applied Physics Letters*, vol. 98., no. 24, pp. 241105(1–3), June 2011.

[76] ref.12 : (Correction)H. Tao, C. M. Bingham, A. C. Strikwerda, D. Pilon, D. Shrekenhamer, N. I. Landy, K. Fan, X. Zhang, W. J. Padilla, and R. D. Averitt, “Highly flexible wide angle of incidence terahertz

metamaterial absorber: Design, fabrication, and characterization", *Physical Review B*, vol. 78, no. 24, pp. 241103(1–4), Dec. 2008.

[77] H. Li, L. H. Yuan, B. Zhou, X. P. Shen, Q. Cheng and T. J. Cui, "Ultra-thin multiband gigahertz metamaterial absorbers", *Jornal of Applied Physics*, vol. 110, no. 1, pp. 014909(1–4), July 2011.

[78] Y. Ma, Q. Chen, J. Grant, S. C. Saha, A. Khalid, and D. R. S. Cumming, "A terahertz polarization insensitive dual band metamaterial absorber", *Optics Letters*, vol. 36, no.6 , pp. 945–947, March 2011.

[79] J. Lee and S. Lim, "Bandwidth-enhanced and polarisation-insensitive metamaterial absorber using double resonance", *Electronic Letters*, vol. 47, no. 1, pp. 8–9, Jan. 2011.

[80] H. T. Chen, "Interference theory of metamaterial perfect absorbers", *Optics Express*, vol. 20, no. 7, pp. 7165–7172, March 2012.

[81] D.-H. Kwon and D.M. Pozar, "Optimal characteristics of an arbitrary receive antenna", *IEEE Transactions on Antennas and Propagation*„ vol. 57, no. 12, pp. 3720–3727, Dec. 2009.

[82] M. Yazdi, M. Albooyeh, R. Alaee, V. Asadchy, N. Komjani, C. Rockstuhl, C. R. Simovski and S. Tretyakov, "A bianisotropic metasurface with resonant asymmetric absorption", *under review*.

[83] R. Alaee, M. Albooyeh, M. Yazdi, N. Komjani, C. R. Simovski, F. Lederer and C. Rockstuhl, "Magneto-electric coupling in non-identical plasmonic nanoparticles: Theory and applications", *under review*.

[84] S. A. Tretyakov, C. R. Simovski, and A. A. Sochava, "The relation between co-and cross-polarizabilities of small conductive bi-anisotropic particles", *Advances in Complex Electromagnetic Materials, Springer Netherlands*, vol. 28, pp. 271–280, 1997.

[85] V. S. Asadchy, I. A. Faniayeu, Y. Ra'di and S. A. Tretyakov, "Determining polarizability tensors for an arbitrary small electromagnetic scatterer", *Photon. Nanostruct.: Fundam. Appl.,* `http://dx.doi.org/10.1016/j.photonics.2014.04.004,2014.`

[86] Y. E. Terekhov, A. V. Zhuravlev, and G. V. Belokopytov, "The polarizability matrix of split-ring resonators", *Moscow University Physics Bulletin*, vol. 66, no. 3, pp. 254–259, July 2011.

Electromagnetic characterization of metasurfaces, electrically thin sheet metamaterials, is the subject of the current thesis. Briefly, a metamaterial is a composite material with unusual electromagnetic properties offered by specific response of its constituents and their arrangement. The main goal in this thesis is to attribute some macroscopic parameters to metasurfaces. The basic definitions are discussed. A heuristic homogenization model of metasurfaces located on a dielectric interface is introduced. The general boundary conditions invariant on the polarization of the excitation field are derived and a general algorithm to retrieve the macroscopic characteristic parameters through two-dimensional reflection and transmission dyadics is presented next. A plenty of examples of metasurfaces are given in order to prove the applicability of the presented theory. Novel physical effects: such as *substrate-induced* bianisotropy, magnetic response, and the difference between periodic and amorphous metasurfaces are theoretically revealed.

ISBN 978-952-60-6210-5 (printed)
ISBN 978-952-60-6209-9 (pdf)
ISSN-L 1799-4934
ISSN 1799-4934 (printed)
ISSN 1799-4942 (pdf)

Aalto University
School of Electrical Engineering
Department of Radio Science and Engineering
www.aalto.fi

BUSINESS + ECONOMY

ART + DESIGN + ARCHITECTURE

SCIENCE + TECHNOLOGY

CROSSOVER

DOCTORAL DISSERTATIONS

Aalto-DD 70/2015